Universidade Federal de São Carlos
Centro de Ciências Exatas e Tecnologia
Programa de Pós-Graduação em Engenharia Química

“Compreendendo a reação ‘step-wise’ de conversão de metano a metanol usando zeólitas trocadas ionicamente com Cobre”

Understanding trends in step-wise methane to methanol conversion using Cu-exchanged zeolites

Stefanie Caroline Mayumi Mizuno
Orientador: Prof. Dr. José Maria Corrêa Bueno

São Carlos
2020

Universidade Federal de São Carlos
Centro de Ciências Exatas e Tecnologia
Programa de Pós-Graduação em Engenharia Química

Understanding trends in step-wise methane to methanol conversion using Cu-exchanged zeolites

Stefanie Caroline Mayumi Mizuno

Tese apresentada no curso de Pós-Graduação em Engenharia Química da Universidade Federal de São Carlos como exigência parcial para obtenção do título de Doutora em Engenharia Química, área de concentração: Pesquisa e Desenvolvimento de Processos Químicos.

Orientador: Prof. Dr. José Maria Corrêa Bueno

São Carlos
2020

Mizuno, Stefanie Caroline Mayumi

Compreendendo a reação ‘step-wise’ de conversão de metano a metanol usando zeólitas trocadas ionicamente com Cobre / Stefanie Caroline Mayumi Mizuno -- 2020.
121f.

Tese de Doutorado - Universidade Federal de São Carlos, campus São Carlos, São Carlos
Orientador (a): José Maria Corrêa Bueno
Banca Examinadora: Diogo Paschoalini Volanti, Leandro Martins, Alejandro Lopez Castillo, João Batista Oliveira dos Santos
Bibliografia

1. Engenharia química. 2. Processos da engenharia química. 3. Catálise heterogênea. I. Mizuno, Stefanie Caroline Mayumi. II. Título.

Ficha catalográfica desenvolvida pela Secretaria Geral de Informática (SIn)

DADOS FORNECIDOS PELO AUTOR

Bibliotecário responsável: Ronildo Santos Prado - CRB/8 7325

MEMBROS DA BANCA EXAMINADORA DA DEFESA DE TESE DE STEFANIE CAROLINE MAYUMI MIZUNO APRESENTADA AO PROGRAMA DE PÓS-GRADUAÇÃO EM ENGENHARIA QUÍMICA DA UNIVERSIDADE FEDERAL DE SÃO CARLOS, EM 06 DE MARÇO DE 2020.

BANCA EXAMINADORA:

José Maria Corrêa Bueno
Orientador, UFSCar

Diogo Paschoalini Volanti
UNESP

Leandro Martins
UNESP

Alejandro López Castillo
UFSCar

João Batista Oliveira dos Santos
UFSCar

Ao meu amado esposo Henry.

A família e amigos queridos.

“Eben-Ezer, pois disse: “Até aqui nos socorreu o Senhor.”

(1 Samuel 7:12b)

AGRADECIMENTOS

Agradeço primeiramente a Deus, por ter me capacitado e dado esta oportunidade de aprendizado e evolução. Obrigada Deus pela graça e misericórdia derramada sobre minha vida.

Aos professores:

Ao professor José Maria, pela orientação, oportunidade única de obter ricos conhecimentos e por me ensinar a ter paciência. Muito obrigada por me atender todas as (muitas) vezes que bati em sua porta e por se tornar meu exemplo de profissional dedicado e pessoa humilde que demonstra respeito ao próximo. Obrigada por todo o apoio que me deu na decisão de ir para o exterior e por se preocupar a cada vez que fiquei doente, rs.

Ao professor Jeroen Anton van Bokhoven por me orientar e dar suporte durante meu estágio em seu grupo de pesquisa, sempre apoiando minhas ideias e acreditando em meu potencial.

Ao professor João Batista, por sempre me ouvir e aconselhar, sempre disposto a oferecer ajuda e uma palavra amiga.

Ao professor e amigo Jean Marcel Gallo, pela contribuição com a compra de materiais para minha pesquisa e carne para churrasco! Obrigada pelos momentos de descontração e por sua amizade.

A professora e amiga Clélia pela amizade, conselhos e longas conversas.

Ao professor Leandro Martins e Alejandro Castillo, por todas as contribuições no exame de qualificação para que este trabalho se concluisse com êxito.

A família:

Aos meus pais Adriana e Carlos que me educaram para me tornar uma mulher honesta que sempre batalha pelos seus sonhos. Obrigada por todos os ensinamentos e puxões de orelha, espero que meus filhos sintam tanto orgulho de mim quanto eu sinto dos senhores. Amo muito vocês.

Ao meu amado esposo Henry, que SEMPRE esteve ao meu lado ao longo de toda jornada acadêmica de pós-graduação me dando todo o suporte que precisei. Obrigada por sempre me apoiar em todas as decisões de forma tão paciente e amorosa. Mesmo durante meu estágio no exterior você sempre se fez presente, as vezes não fisicamente, mas sempre em pensamento e coração. Obrigada por tudo, pelas conversas, conselhos, companheirismo, amor e compreensão. Te amo muito por você ser do jeitinho que você é...amoroso, companheiro e maravilhoso, te amo meu 'mozi'.

A minha madrinha Clarice que mesmo de longe sempre me apoiou orgulhosa por tudo que conquistei. Saiba que esta conquista é nossa, te amo.

Aos meus irmãos Geisa, Anderson, Carlos e Maysa por todo o carinho e apoio. Saibam que os amo muito.

Aos meus sobrinhos Arthur, Jenniffer, Miguel e Daniel. Obrigada por tanta alegria, a alegria de vocês me ajudou nos momentos pesados desta jornada deixando-os muito mais leves. Titia ama.

A toda minha família. Sogra, sogro, cunhados, primos, tios e tias e avós...obrigada pela compreensão nos momentos de ausência para estudar e ficar no laboratório e principalmente durante meu estágio no exterior. Obrigada.

Aos amigos e colegas de trabalho:

A todos os meus amigos *(eles sabem quem são)* que sempre me apoiaram e entenderam os momentos de ausência para estudar e pesquisar.

Ao Voleitão, por todos os momentos de alegria e suporte. Em especial às minhas Masters (Rolê Master das Masters). Amo vocês. Voa voleitão.

Ao Voleiball Brugg Club - VBC Brugg. Amo vocês. "Danke für alles, go go go Brugg. *Liebi grüess zämme."*

A todos os colegas de grupo: Alan, Thais, Thiago, Tassia, Jussara, Breno e Siriwan. Aos ex-colegas de grupo, Taynara, Priscila, Lais, Paula, Camila e Adriano.

Em especial Taynara, Alan, Thiago e Thais por me ajudarem durante o tempo de feixe no LNLS. Gratidão.

Aos meus colegas do Labcat – Ufscar. Obrigada pelos momentos de descontração, companhia para almoçar no RU e cafezinhos.

Aos colegas de grupo na Suíça que participaram ativamente na minha tese: Amy, Jie, Vitaly, Mark e Dennis. E aos colegas de escritório, Patrick, Li, Arik, Julian, Xang.

A Dohris Büller por toda ajuda.

A colegas especiais do LSK – Laboratory of Sustainable Chemistry do Paul Scherrer Institut, Villigen, Suíça e do The van Bokhoven group – ETH Zurich.

Aos colegas especiais do Greencat – Ufscar.

Meus amigos Patrik Zimmermann e Patric Zimmermann, os dois tem o mesmo nome e um lugar no meu coração. Obrigada por me ajudarem tanto durante meu estágio na Suíça.

Ao Dr. Thiago Faheina Chaves por toda a ajuda no inicio deste projeto deste doutorado.

Ao Dr. Santiago Figueroa pela ajuda durante o tempo de feixe no LNLS.

Peter e Margret Haudenchild por me disponbilizarem um quarto em sua casa e aos colegas de casa, Francesco, Ysuan Li, Cristiane e Adriana.

Ao suporte técnico:

Ao Ademir e Oscar, por sempre me ajudarem com tudo que precisei desde equipamentos até uma xícara de café.

Ao Rômulo, Eudoro, Biscoito e Alexandra. Obrigada.

Thomas Rohrbach e Frank Krumeich. Obrigada por tudo.

Obrigada Junior por me ajudar durante o tempo de feixe na XAFS2.

A todos que de alguma forma contriburiam com este trabalho.

Ao leitor desta tese.

RESUMO

O metano (CH_4) é uma molécula estável abundantemente encontrada no nosso planeta possuindo reservas ainda maiores do que as de petróleo bruto. Devido à sua alta disponibilidade e impactos ambientais causados pela sua emissão exacerbada na atmosfera, o desenvolvimento de processos para sua conversão em produtos de alto valor agregado está em ascenção. A conversão direta de CH_4 a metanol mostra-se vantajosa já que este processo converte CH_4 a baixas temperaturas (<300^oC) através da reação 'step-wise' de oxidação parcial direta do metano (OPDM). Intenso estudo científico tem sido realizado sobre esta reação e todos eles convergem para a utilização de materiais baseados em metais trocados ionicamente com zeólitas, especialmente cobre. Apesar de o CH_4 ser facilmente ativado sobre esses materiais, controlar a oxidação total dos intermediários de reação a CO_x ainda é um desafio e um limitante para o rendimento de metanol. Além disso, sabe-se que apenas uma fração do Cu participa efetivamente da reação o que faz com que o rendimento de metanol também seja limitado a mais este fator. Diferentes estruturas de Cu podem ser formadas em zeólitas pelo método de troca iônica, tais como: $([Cu_3(\mu\text{-}O)_3]^{2+}$, $([Cu_2(\mu\text{-}O)_2]^{2+}$, $([Cu_2(\mu\text{-}O)]^{2+}$, e CuO, além disso, ainda existem questões fundamentais a serem respondidas para maior entendimento desta reação como, por exemplo, o efeito da estrutura zeolítica na formação das espécies de Cu e como maximizar a sua partipação na reação. Neste trabalho, realizamos um estudo criterioso de diferentes materiais zeolíticos trocados ionicamente com cobre variando diversos parâmetros de síntese e reação, relacionando a atividade com a estrutura do sítio ativo. Nossos resultados sugerem que altas cargas de Cu e baixa razão Si/Al são desfavoráveis e o contra-íon afeta a performance da zeólita mazzita em reação. Com esses resultados, buscamos contribuir em aspectos importantes para uma possível implementação deste processo em escala industrial.

Palavras chave: oxidação parcial, metano, zeólita, metanol, cobre.

ABSTRACT

Methane (CH_4) is a stable molecule abundantly found on our planet with reserves even greater than crude oil. Due to its high availability and environmental impacts caused by its emission into the atmosphere, the development of processes for its conversion into high value-added products is highly desired. Direct conversion of CH_4 to methanol is advantageous as this process converts CH_4 at low temperatures (<300 ° C) through the step-wise methane to methanol direct conversion (MMet). Intense scientific studies have been conducted on this reaction and all of them converged to the use of metal ion-exchanged zeolites, especially copper. Although CH_4 is easily activated on these materials, controlling methane total oxidation to CO_x is still a challenge and a limiting for methanol yield. In addition, only a fraction of Cu species actually participates in the reaction, which means that methanol yield is also limited to this factor. Since different Cu structures can be formed in zeolites by copper exchanged method, such as $[Cu_3(\mu\text{-}O)_3]^{2+}$, $[Cu_2(\mu\text{-}O)_2]^{2+}$, $[Cu_2(\mu\text{-}O)]^{2+}$, and CuO, there are still fundamental questions to be answered for a better understanding of this reaction, such as the effect of zeolite structure on the formation of Cu species and how to maximize its participation in the reaction. We herein carried out a careful study of different copper-exchanged zeolite materials varying several synthesis/reaction parameters and related the activity to the structure of the Cu species. Our results suggested that high Cu content and low Si/Al ratio were unfavorable and the counter ion affects the performance of mazzite zeolite on MMet reaction. With this study, we hope to contribute with important aspects that might help in a future process scale-up.

Keywords: partial oxidation; methane; zeolite; methanol; copper.

LIST OF FIGURES

LIST OF ABBREVIATIONS AND ACRONYMS

AAS – Atomic Absorption Spectroscopy

BET – Brunauer, Emmett, and Teller

CFCs - Chlorofluorocarbons

CHA – Chabazite

DFT - Density Functional Theory

DMTM – Direct methane to methanol conversion

DRIFTS – Diffuse Reflectance Infrared Fourier Transformed Spectroscopy

(DR) UV-Vis - Diffuse Reflectance UV-Visible Spectroscopy

EFAl – Extraframework Aluminum

EXAFS – Extended X-Ray Absorption Fine Structure

FER – Ferrierite

FTIR – Fourier-transform infrared spectroscopy

GC – Gas Chromatography

GME – Gmelinite

ICP-OES – Inductively Coupled Plasma Optical Emission Spectrometry

LCA – Linear Combination Analysis

LMCT – Ligand-to-metal charge transfer

LNLS – Laboratório Nacional de Luz Síncroton

MAS – Magical Angle Spinning

MAZ – Mazzite

MCT – Mercury cadmium telluride

MMet – Step-wise methane to methanol direct conversion

MMO – Monooxygenase

MOR – Mordenite

MR – Membered Ring

MS – Mass Spectroscopy

NMR – Nuclear magnetic resonance

pMMO – Particulate Monooxygenase

sMMO – Soluble Monooxygenase

SOD - Sodalite

TGA – Thermogravimetric Analysis

UV-Vis-NIR – Ultraviolet-Visible-Near Infrared Spectroscopy

XANES – X-Ray absorption near edge structure

XAS – X-Ray Absorption Spectroscopy

XRD – X-Ray Diffraction

CONTENTS

CHAPTER 1 - GENERAL INTRODUCTION AND OBJECTIVES

1.1 Introduction

With the substantial increase in the world population, consequently, the increase of human activity and energy demand, the development of new processes to supply the energy matrix is highly desired. The use of some energy sources such as fossil fuels is responsible for the emission of harmful gases into the atmosphere contributing to global warming. Methane (CH_4), carbon dioxide (CO_2), nitrous oxide (N_2O) and chlorofluorocarbons (CFCs) are mainly responsible for this effect (ZAKARIA; KAMARUDIN, 2016a).

Natural gas, constituted mainly by methane (CH_4), is abundantly found on our planet and has even greater reserves than crude oil. Although CH_4 has potential as a fuel, the troubles related to its transportation and storage classifies CH_4 as ‘underestimated feedstock’. Thereby, the conversion of CH_4 to add-value liquid chemicals, easier to store and transport, might be one of the methods to reduce greenhouse gases flaring by natural gas refining processes (HAN BAOZHAI, YANG, YANG, XU, YANYAN, U. J. ETIM, QIAO, KE, XU, BENJING, YAN, 2016).

However, CH_4 is a very stable symmetric molecule and its C-H bonds have strong binding energy (407 kJ / mol). The CH_4 molecule also does not have functional groups that facilitate chemical attacks allowing its disruption. Thus, CH_4 activation by non-catalytic pathways is not economically viable since high temperatures or the use of strong oxidants are required (HOLMEN, 2009).

Figure 1.1 presents an overview of different routes for CH_4 valorization. Between the CH_4 conversion routes shown in Figure 1.1, the conversion of CH_4 to methanol currently used by industry involves catalytic reactions with high energy consumption, through ‘indirect route’ with synthesis gas ($CO + H_2$) as the reaction intermediate, followed by hydrogenation of CO under high pressures (REDDY; KIM; SONG, 2013).

Options such as step-wise methane to methanol direct conversion (MMet) is gaining attention because methanol, as a liquid fuel, could be a viable raw material alternative to petroleum (GROOTHAERT et al., 2005a) and this reaction occurs at low temperatures, different from the current industrial process that requires high energy consumption and several

processes up to the final product (REDDY; KIM; SONG, 2013).

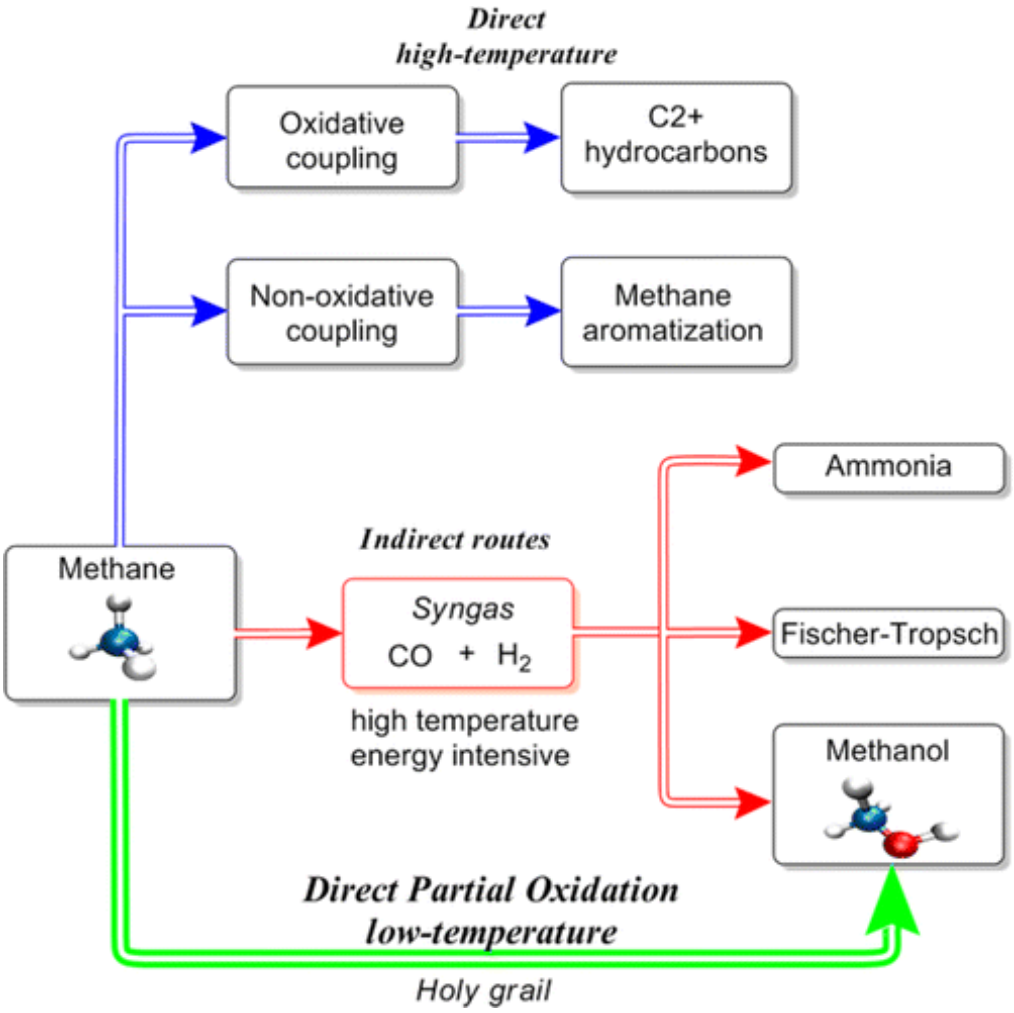

Figure 1. 1 Overview of the different routes for methane valorization. Source: Adapted from (OLIVOS-SUAREZ et al., 2016).

Although MMet is attractive and promising, because of C-H bond strength of CH_4, selective MMet reaction is relatively challenging since the reaction intermediates are more reactive then CH_4, leading to form secondary products or total oxidation to CO_x (TAIFAN;

BALTRUSAITIS, 2016).

Enzymes can be active materials for selective methane conversion to methanol at low temperatures. Characterization of *soluble methane monooxygenase* (sMMO) enzymes revealed that inorganic active sites for MMet reaction are based on iron-oxygen clusters, while *particulate methane monooxygenase* (pMMO) displays copper-oxygen sites (BALASUBRAMANIAN et al., 2010; CHAN et al., 2013; OLIVOS-SUAREZ et al., 2016).

Learning from *methane monooxygenase* enzymes allowed the development of inorganic materials based on ion-exchanged zeolites with copper and iron, for instance, so-called Cu/Fe-exchanged zeolites for MMet reaction, especially copper has shown interesting results for MMet reaction (GRUNDNER et al., 2015; HAMMOND et al., 2012a; TAIFAN; BALTRUSAITIS, 2016).

Focusing on Cu-exchanged zeolites, an intense study has been made about possible active Cu species and this assumption still under warm discussion among the scientific community(PALAGIN et al., 2017). According to different zeolite structures, Cu species such as $[Cu_3(\mu\text{-}O)_3]^{2+}$, $[Cu_2(\mu\text{-}O)]^{2+}$ and CuO, with different Cu-O-Cu angles can be formed, leading to different performances towards MMet reaction (MAHYUDDIN et al., 2017; MARKOVITS et al., 2016).

Grundner et al. (GRUNDNER et al., 2015) synthesized isolated Cu trinuclear sites in MOR and suggested that equal site distribution over the zeolite structure allowed a high conversion of CH_4 to methanol. Markovits et al. (MARKOVITS et al., 2016) studied Cu-exchanged with ZSM-5 for MMet reaction and reported that the type of Cu site formed depends directly on the zeolite Si/Al ratio and distance of two or more Al atoms in the structure. They further claimed that the Cu active species in zeolite always consist of more than one Cu atom (Figure 1.2).

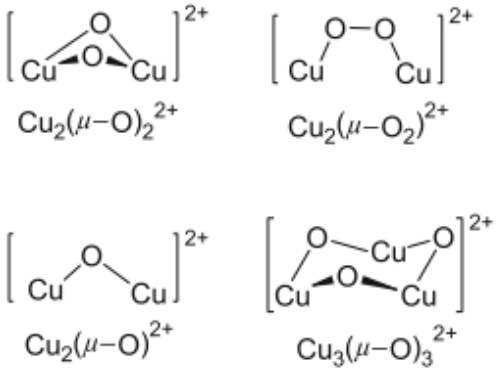

Figure 1. 2 Cu species proposed as active sites for methane activation in ZSM-5 with a high content of silica. Source: Adapted from (MARKOVITS et al., 2016).

Density Functional Theory (DFT) calculations could help to predict active sites for MMet reaction. Mahyuddin et al. (MAHYUDDIN et al., 2018) studied active sites for MMet reaction in Cu-exchanged MOR and Mazzite (MAZ) zeolite and proposed two distinct $[Cu_2O]^{2+}$ structures and a $[Cu_3O_3]^{2+}$ species (Figure 1.3). They concluded that the MOR Al pair, that host $[Cu_2O]^{2+}$ species, influenced sites stability during MMet reaction.

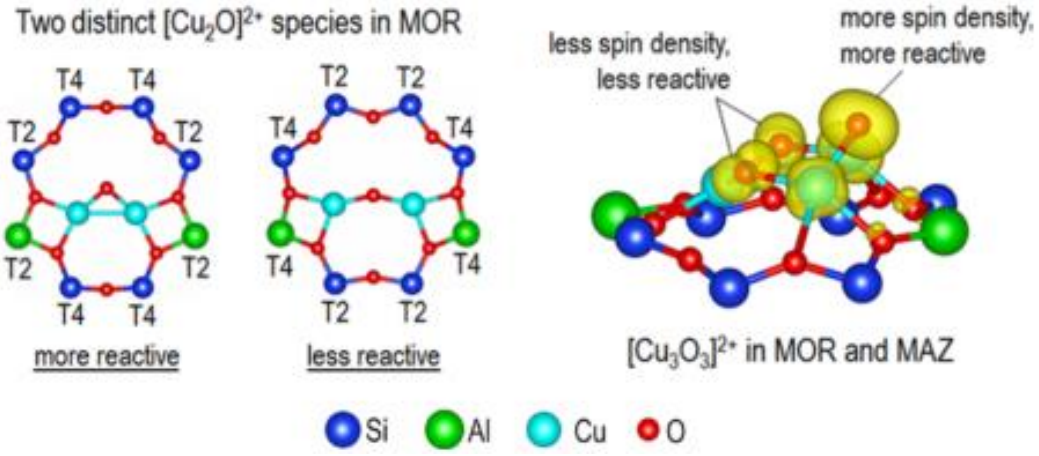

Figure 1. 3 Active sites in Cu-exchanged MOR and MAZ zeolites proposed by Mahyuddin et al. for MMet reaction. Source: Adapted from (MAHYUDDIN et al., 2018).

Conversantly, Alayon et al. (ALAYON et al., 2015a) proposed as active sites for MMet reaction in Cu-exchanged MOR the mono(m-oxo) and bis (m-oxo)dicopper species (Figure 1.4). They suggested through DFT calculations that constraints of MOR framework disfavor bis(m-oxo) formation and contribute to the relative stabilization of mono(m-oxo)dicopper species.

It is clear that different Cu species can be formed in Cu-exchanged zeolites, such as ($[Cu_3(\mu\text{-}O)_3]^{2+}$, $[Cu_2(\mu\text{-}O)]^{2+}$, and CuO (MARKOVITS et al., 2016). However, it is not clear how the zeolite structure can affect the catalytic activity and how changes in the oxidation state of Cu species during methane activation influence other properties such as zeolite stability during reaction.

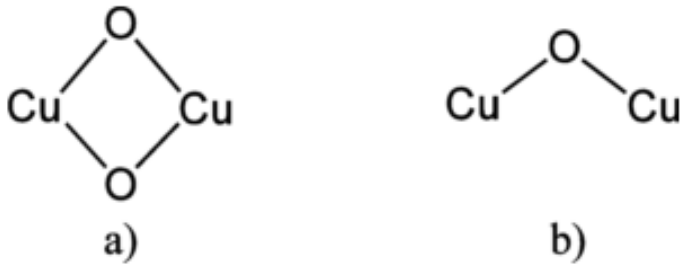

Figure 1. 4 Structures of the (a)bis(m-oxo)dicopperII and (b)mono(m-oxo)dicopperII clusters in copper-zeolites, proposed active for methane activation. Source: Adapted from (ALAYON et al., 2015a).

We herein performed step-wise MMet reaction using Cu-exchanged zeolites. Aspects such as preparation method, Si/Al ratio, zeolite counter-ions, Cu content and its relation with Cu species it was evaluated.

1.2 Objectives

The main purpose of this work is to study CH_4 functionalization through MMet reaction using Cu-exchanged zeolites and to study the influence of synthesis method, Si/Al ratio and Cu content on the material properties, specifically the activity and stability during reaction.

As specific objectives we highlight:

- To study how the zeolite structure (MAZ, MOR) and copper loading affects the material performance on MMet reaction;
- To study the effect of the counter ion in the material;
- Analysis of materials performance in different MMet reaction conditions;
- To investigate post-synthesis acidic treatments and how this affects the Cu sites formation.

CHAPTER 2: STATE OF THE ART

2.1 Direct methane to methanol conversion (DMTM)

From the 1900's to the late 70's direct methane to methanol conversion (DMTM) was widely studied and despite the scientific efforts, the methanol yield was limited and the reaction conditions boiled down to high pressure and temperature or strongly acid medium. (RAVI; RANOCCHIARI; VAN BOKHOVEN, 2017) Table 2.1 summarized some scientific contributions on methane oxidation up to 1975.

Table 2.1: Timeline summarizing some of the most significant research on methane oxidation up to 1975. Adapted from (RAVI; RANOCCHIARI; VAN BOKHOVEN, 2017).

Year	Catalyst	Significance	Conclusions
1905(LANCE; ELWORTHY, 1905)	$FeSO_4$	one of the first patents in methane oxidation	products: methanol, formaldehyde, formic acid
1934(WIEZEVICH; FROLICH, 1934)	Ni, Al, Fe	the first use of catalysts in high-pressure systems	Up to 35% by weight methanol in the liquid product
1937(BOOMER; THOMAS, 1937)	electrolytic copper	study of parameters which affect product yield of catalytic high-pressure systems	higher methanol yield with lower oxygen concentration and higher feed flow rates
1947(BOOMER; NALDRETT, 1947)	Ag-, Zn-, Ni-based	use of metal oxides for high-pressure methane oxidation	nickel-based catalyst emerged as the most promising catalyst
1961 (ANDERSON et al., 161AD)	supported oxides of Pd,Co,Cu, Mn, Ce,V, Fe,Ti	screening of up to 30 catalysts in a micro catalytic reactor	performance of catalysts for methane oxidation characterized by Arrhenius plots
1970 (CULLIS; KEENE; TRIMM, 1970)	palladium on thorium dioxide	reported use of additives to increase product yield by inhibiting deep oxidation to carbon dioxide	Addition of dichloromethane increased formaldehyde yield by inhibiting subsequent oxidation
1975 (H. J. F. STROUD, 1975)	molybdenum/copper oxide	one of the first reports of two-component unsupported oxide systems	maximal oxygenate yield of 490 g $(kg_{cat})^{-1}$ h^{-1} at 758K

As observed in Table 2.1, in the last hundred years the partial methane oxidation at high temperatures has been widely discussed in the scientific field as an alternative to avoid methane wasting. Firstly, transition metal oxides catalysts were studied, mainly molybdenum and iron-based compounds(HAN et al., 2016). Bañares et al. (BAÑARES; FIERRO; MOFFAT, 1993) reported silica-supported MoO_3 as an active catalyst for methane oxidation to formaldehyde using molecular oxygen as oxidant. Barbaux et al. (BARBAUX et al., 1988) also described that Mo/SiO_2 catalysts prepared by the impregnation method were active for methane oxidation to formaldehyde and the total methane oxidation to carbon dioxide occurs preferably over molybdenum surface.

Despite the continuous research and the claim that MoO_3 successfully converted methane into methanol, the operation conditions were harshly drastic with high pressures and temperatures. Also, the successive oxidation to methanol was difficult and the formation of byproducts such as carbon dioxide was observed (LIU, H. F. ; LIU, R. S. ; JOHNSON, R. E. ; LUNSFORD, 1984; SPENCER, 1988). Concomitantly to molybdenum catalysts, iron-based compounds were also studied for methane oxidation to methanol (HAN et al., 2016).

Wiezevich et al. (WIEZEVICH; FROLICH, 1934) reported hydrocarbon oxidation over transition metal catalysts using a high-pressure procedure. The authors described that for methane to methanol conversion the procedure was not effective even using a combined high-pressure and temperature system since a considerable amount of the reacting methane suffered side reactions such as dehydrogenation, cracking, and polymerization.

Figure 2.1.1 shows the main events for methane oxidation from the 1900s to nowadays. At the beginning of 21st century, a ‘new’ reaction promised to cause a revolution on the methane conversion technology: the so-called ‘step-wise methane conversion to methanol at low temperature’ (MMet), that uses metal-centers ion-exchanged in zeolite structures ‘mimicking’ the methane monooxygenase (MMO) enzyme to convert methane into methanol at relatively low temperatures (RAVI; RANOCCHIARI; VAN BOKHOVEN, 2017).

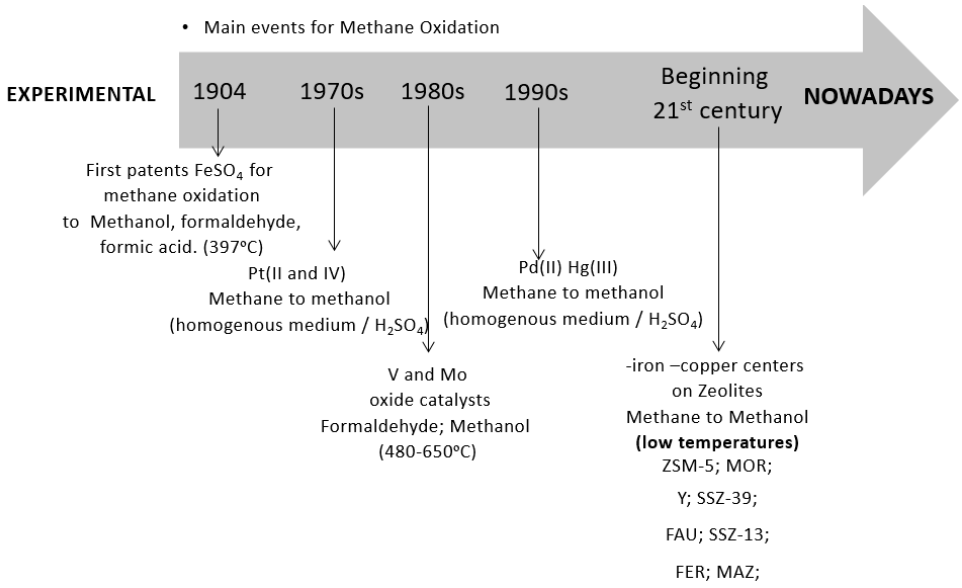

Figure 2. 1 - A brief timeline of the main events for methane oxidation. Adapted from (HUERTAS-MIRANDA; MARTINEZ-IÑESTA, 2010; PERIANA et al., 1993; RAVI; RANOCCHIARI; VAN BOKHOVEN, 2017; SHILOV; SHUL, 1997).

Methane monooxygenase is an enzyme contained on methanotrophic bacteria which is capable to use methane as a source of energy converting it into methanol through its metabolic route at low temperature (Equation 2.1) (MERKX et al., 2001):

$$CH4 + NADH + H^+ + O_2 \rightarrow CH_3OH + NAD^+ + H_2O \quad (2.1)$$

Due to the capability to consume CH_4 in its metabolic route, methanotrophic bacteria are really important to the global carbon cycle, helping to reduce methane levels and contributing to atmosphere health (MERKX et al., 2001). Deep characterization of these bacteria and monooxygenase enzyme allowed to discover its composition. Basically, the methanotrophs are composed by a membrane-bound that could be a particulate or soluble form of MMO, the pMMO and sMMO, respectively (Figure 2.2) (ITO et al., 2014) .

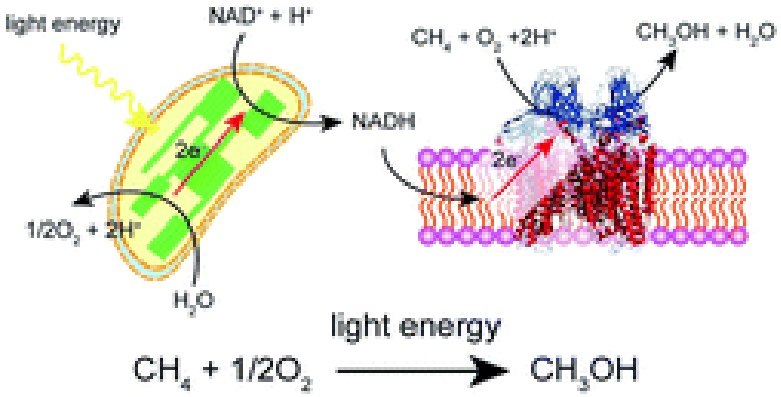

Figure 2. 2 Schematic diagram of the photoinduced methane oxidation system using methane monooxygenase by the combination of photosynthetic system. Adapted from (ITO et al., 2014).

In the case of pMMO, the structure is composed of two different sites with 12-15 copper atoms and one of these sites could be the active site for methane hydroxylation and the other one responsible by carrying an electron (ITO et al., 2014; NGUYEN et al., 1998). In contrast to pMMO, the active site of sMMO contains a *diiron center* and it is gaining attention due to its stability to endure characterization and purification procedures (ITO et al., 2014).

Since advanced characterization on these enzymes was made, a huge advance on methane conversion technology was reached, allowing the inorganic synthesis of copper- and iron centers ion-exchanged with zeolites actives for MMet reaction(LUNSFORD, 2000).

MMet over metal-exchanged zeolites at low temperatures has been considered as a *holy grail* of modern catalysis for methane conversion (WANG et al., 2017).

The MMet is a reaction thermodynamically possible, however, it is difficult to kinetically prevent overoxidation of methane to carbon dioxide since methanol is more leaning to oxidation than methane (HAMMOND; CONRAD; HERMANS, 2012).

Nevertheless, the metal-centers exchanged with zeolites inspired in the MMO enzymes are capable to stabilize the methanol intermediates avoiding the overoxidation to CO_x (Figure 2.3) (HAMMOND; CONRAD; HERMANS, 2012).

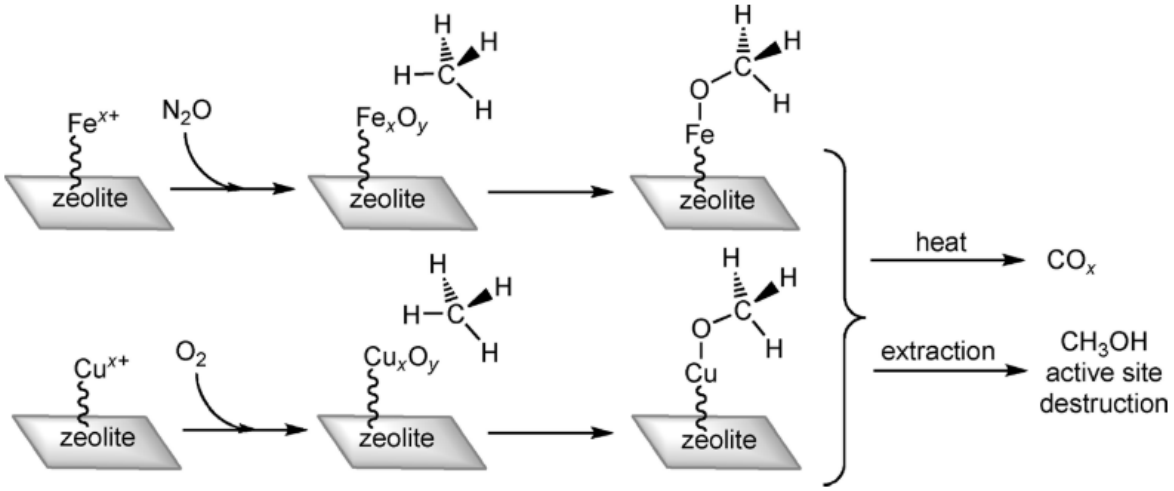

Figure 2. 3 Stoichiometric conversion of methane to surface-bound methoxy species over Fe- or Cu-exchanged zeolites. Adapted from (HAMMOND; CONRAD; HERMANS, 2012).

It can be observed in Figure 2.3 that Fe- and Cu-exchanged zeolites are capable of both activate methane and stabilize the methanol intermediate species. However, the need for low temperature in MMet reaction is because an overheating thermodynamically favor the overoxidation to CO_x (HAMMOND; CONRAD; HERMANS, 2012; KALAMARAS et al., 2016).

On the other hand, the methanol extraction causes the active site deactivation and an additional step for the reactivation of these sites with oxygen is needed, precluding a continuous procedure(HAMMOND; CONRAD; HERMANS, 2012; KALAMARAS et al., 2016) .

Therefore, MMet reaction relies on three steps cyclic process carried out at various temperatures and hours: (i) material activation under oxygen; (ii) methane activation leading into methanol formation; (iii) methanol desorption under steam flow (on-line extraction) or by water solution (off-line extraction) (TOMKINS et al., 2016a). These steps are summarized in Equations 2.2-2.4 (PAPPAS et al., 2017; SUSHKEVICH et al., 2017a) :

Activation step:

$$xCu^{+}(H_2O) + xO_2 \rightarrow x[Cu_xO_x]^{2+} + H_2O \quad (2.2)$$

Reaction:

$$x[Cu_xO_x]^{2+} + CH_4 \rightarrow xCu_x^{+}(CH_3O^{-}) + H^{+} \text{ (zeolite)} \quad (2.3)$$

Hydrolysis (methanol extraction):

$$xCu_x^{+}(CH_3O^{-}) + H^{+} \text{ (zeolite)} + H_2O \rightarrow xCu^{+}(H_2O) + CH_3OH \quad (2.4)$$

The MMet reaction is usually performed under the so-called 'conventional' procedure (Figure 2.4a): activation in oxygen at usually 450 °C, followed by reaction in a pure or diluted stream of methane at a lower temperature, typically between 150 and 200 °C, and methanol extraction at room temperature in the liquid phase (off-line extraction) or at 150-200°C using water steam (On-line extraction) (PAPPAS et al., 2017; SUSHKEVICH et al., 2017a; WANG et al., 2017). Newly, it has been reported an alternative approach: the isothermal procedure (Figure 2.4b). Using high methane pressures but activating the material and desorbing methanol at the same temperature, typically 200 to 300 °C(KNORPP et al., 2018a; PARK et al., 2017; SUSHKEVICH; VAN BOKHOVEN, 2019).

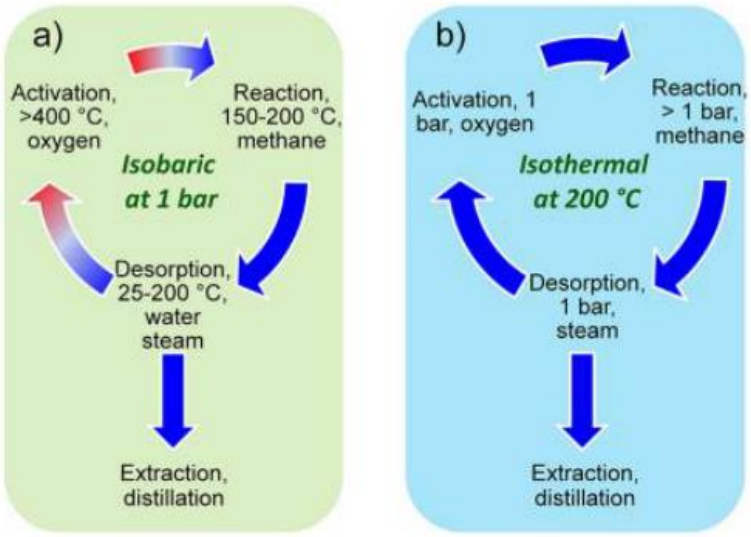

Figure 2. 4 Cyclograms for (a) isobaric (conventional) and (b) isothermal methanol-to-methanol processes. Adapted from (LANGE et al., 2019).

Since its discovery, a reasonable number of different cation-exchanged zeolites have been tested for MMet reaction in both approaches, conventional and isothermal (RAVI et al., 2019). Its performance is compared basically for the methanol yields both by grams of material or moles of Cu (RAVI et al., 2019).The next section summarized the main results for different Cu-exchanged zeolites and justified the relevance of the zeolites chosen for this study.

2.2 Cu-exchanged zeolites for MMet reaction

Figure 2.5 presents the improvements in the performance of Cu-exchanged zeolites for MMet reaction.

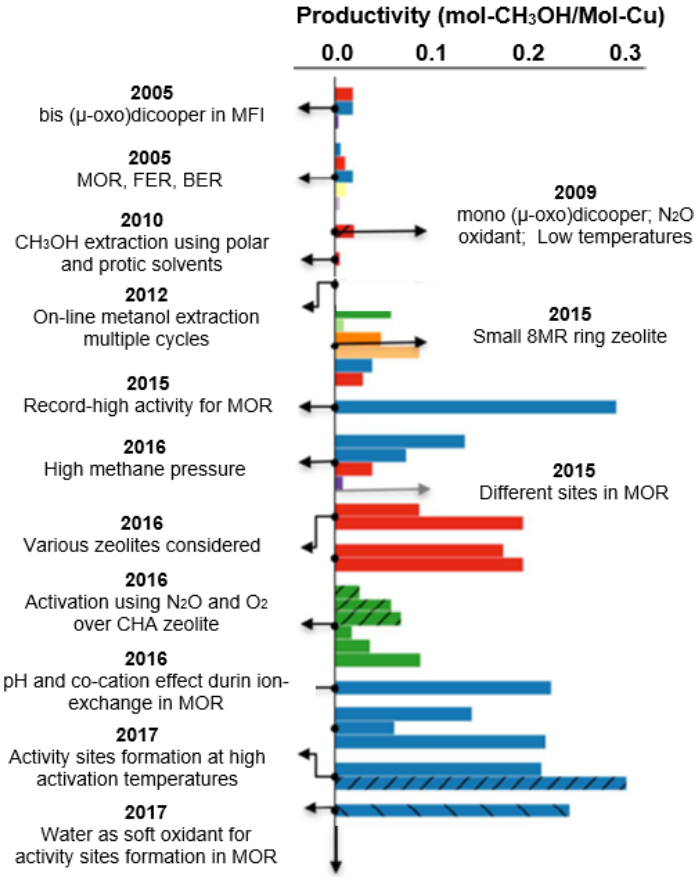

Figure 2. 5 Improvements in the performance of Cu-exchanged zeolites (mol CH_3OH/ mol-Cu)(ALAYON et al., 2012b; BEZNIS; WECKHUYSEN; BITTER, 2010a; BOZBAG et al., 2016; GROOTHAERT et al., 2005a;

GRUNDNER et al., 2016, 2015; IPEK; LOBO, 2016; KIM et al., 2017; NARSIMHAN et al., 2016; SMEETS; GROOTHAERT; SCHOONHEYDT, 2005; SUSHKEVICH et al., 2017b; VANELDEREN et al., 2015; WOERTINK et al., 2009; WULFERS et al., 2015b). Color schemes: MFI (red), MOR (blue), CHA (green), SAPO-34 (light green), AFX (orange), AEI (light orange), FAU (purple), EMT (brown), BEA (light purple). Source: Adapted from (KULKARNI et al., 2017).

As noted in Figure 2.5 the activity of copper ion-exchanged zeolites for MMet reaction is highly dependent on the type of zeolite, but also of the size of the channels and cages, Si/Al ratio, charge and distribution of the charge balancing cations (SMEETS et al., 2010b). Zeolites of pentasil family such as Mordenite (MOR) and ZSM-5 presents large- and medium-pore, respectively, and are able to stabilize Cu sites (bi- or trinuclear) structurally analogous to MMO enzyme (ALAYON et al., 2015a; LI et al., 2016). On the other hand, zeolites that presented small-pore such as chabazite (CHA) and ferrierite FER were not suitable for high methanol yields (ALAYON et al., 2015a; LI et al., 2016).

The achievements in the optimization of the MMet reaction process since 2015 were impressive and clear evidenced by the increase of methanol yields, especially for Cu-exchanged Mordenite zeolite (Figure 2.5).

Mordenite zeolite (MOR) (Figure 2.6) has shown an appropriate environment to host Cu sites inside the 8-membered-ring side pocket, while the Brønsted acids in the larger cages (12-member-ring aperture) are not exchanged and it could help in the first step of methane activation allowing high methanol yields (ZHANG et al., 2015).

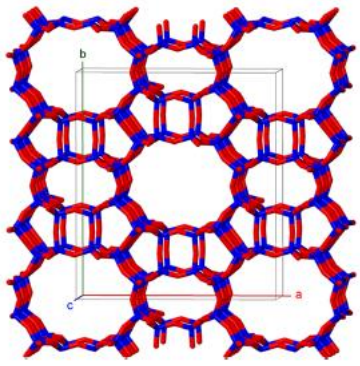

Figure 2. 6 MOR zeolite framework. Red and blue sticks represent O and T (Si or Al) atoms, respectively. The unit cell is depicted. Source: Adapted from (MAHYUDDIN et al., 2018).

For its structural properties, copper-exchanged with MOR (Cu-MOR) zeolite has been widely studied showing notable results on MMet reaction. Some authors suggest that the 12-rings pores of MOR (Figure 2.6) facilitate the methanol extraction rather than the 10-rings pores of ZSM-5 zeolites (ALAYON et al., 2012a).

Vanelderen et al. (VANELDEREN et al., 2015) claimed that the two windows of the 8 membered ringside pocket in MOR are appealing candidates to host the Cu structures being similar to the Cu-O-O sites in ZSM-5. Other authors claimed that the variation in the Si/Al ratio in zeolite MOR enables the control of copper speciation and redox properties of the final material (SUSHKEVICH; VAN BOKHOVEN, 2019).

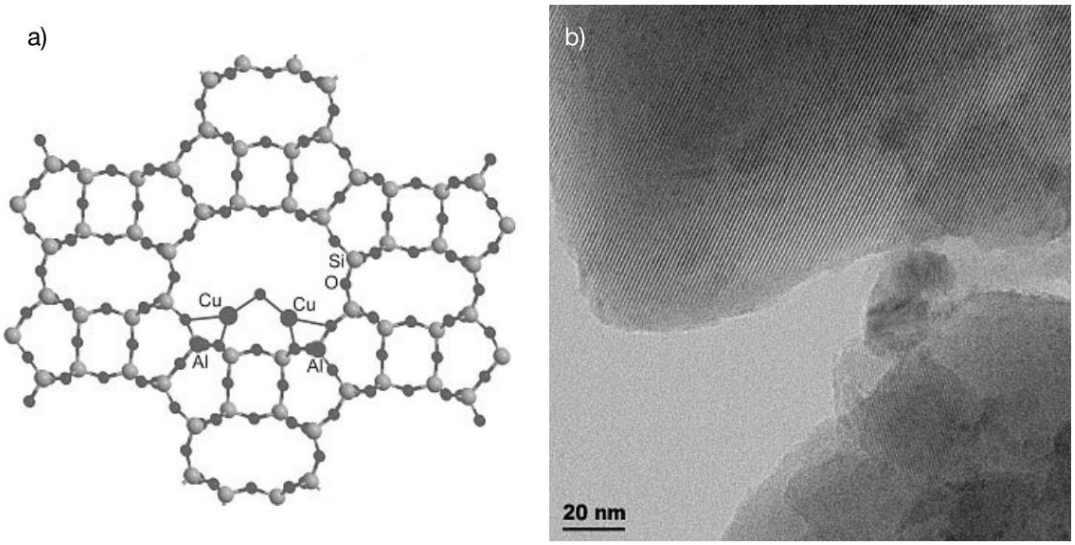

Figure 2. 7 (a) Mordenite zeolite framework with a schematic representation of impregnated Cu species at the main channel and (b) TEM picture of Cu-exchanged MOR showing uniform zeolite channels with no observable metal particles. Adapted from (ALAYON et al., 2012a).

Grundner et al. (GRUNDNER et al., 2015) claimed by DFT and experimental evidence that the active species for MMet reaction is a single-site trinuclear copper oxygen cluster. They observed that this species is anchored to two framework Al atoms located at the pore of the 8 membered ring (MR) side pocket of Mordenite (Figure 2.8).

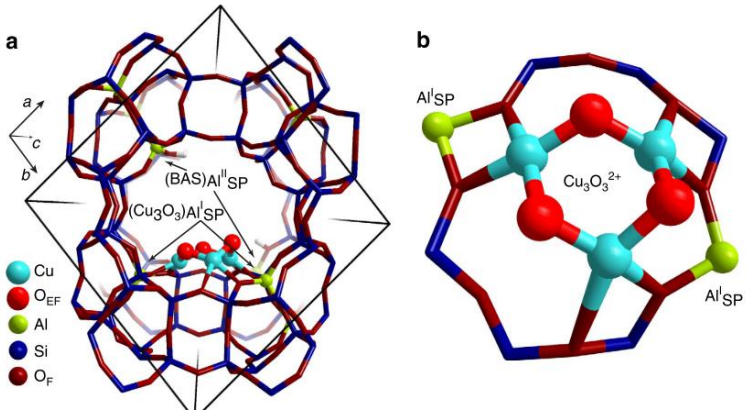

Figure 2. 8 Structure and location of $[Cu_3(\mu\text{-}O)_3]^{2+}$ cluster in mordenite predicted by DFT. The zeolite model contained paired (type I) and isolated (type II) Al atoms located at the pore mouth of the side pocket. The cluster is stabilized by two anionic centers due to Al^{I} SP lattice sites at the entrance of the MOR side pocket (b) so that the extra-framework oxygens responsible for the initial C–H activation are pointing towards the main channel of MOR (a). Adapted from (GRUNDNER et al., 2015).

Palagin et al. (PALAGIN et al., 2017) reported that with the Cu cluster size increase, the cluster stability and also the stability of the methane intermediates increase. With tetra- and pentamer clusters being more stable than dimers and trimmer.

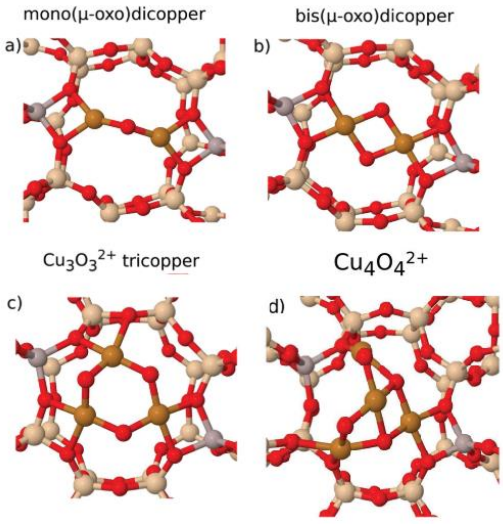

Figure 2. 9 Locally optimized structures of (a) mono (μ-oxo)dicopper, (b) bis (μ-oxo)dicopper, (c) tricopper, and (d) $Cu_4O_2^{2+}$ sites in the 8-ring channel of Cu-MOR. Adapted from (PALAGIN et al., 2017).

And for the cluster formation in the Mordenite pore (Figure 2.9) the authors claimed that there was a relation between the strong interaction of a single aluminum atom and a decreased stability of competing multiple aluminum atoms in the zeolite's pore (PALAGIN et al., 2017).

Despite Mordenite has been extensively studied for MMet reaction, other zeolites have emerged as promising materials. Figure 2.10 shows a comparative study for diverse Cu-exchanged zeolites performance on MMet reaction.

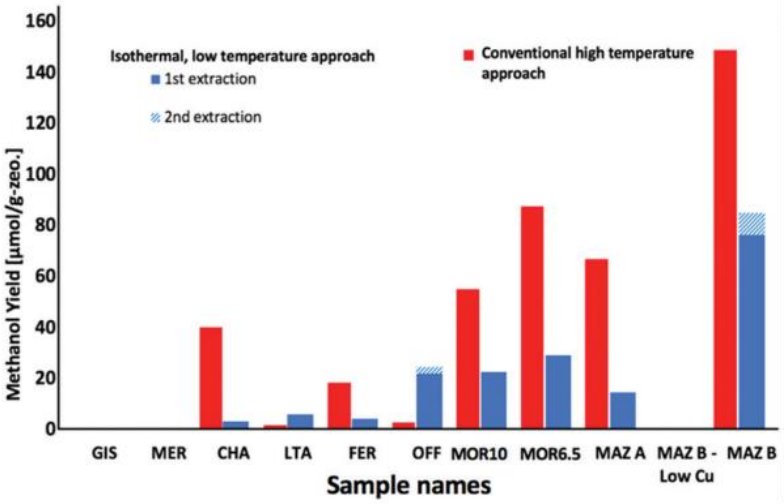

Sample Name	IZA Code	Si/Al	Cu wt.%	Pore size	
GIS	GIS	5.7	5.6	8 MR 8 MR	3.1 x 4.5 [100] 2.8 x 4.8 [010]
MER	MER	2.6	6.4	8 MR 8 MR 8 MR 8 MR	3.1 x 3.5 [100] 2.7 x 3.6 [010] 3.4 x 5.1 [001] 3.3 x 3.3 [001]
CHA	CHA	3.02	4.7	8 MR	3.8 x 3.8 ⊥ [001]
LTA	LTA	1.1	6.3	8 MR	4.1 x 4.1 [100]
FER	FER	15.3	1.6	10 MR 8 MR	4.2 x 5.4 [001] 3.5 x 4.8 [010]
OFF	OFF	4.3	4.0	12 MR 8 MR	6.7 x 6.8 [001] 3.6 x 4.9 ⊥ [001]
MOR10	MOR	9.7	4.7	12 MR	6.5 x 7.0 [001]
MOR6.5	MOR	6.5	4.3	8 MR	2.6 x 5.7 [001]
MAZ A	MAZ	4.32	4.8	12 MR	7.4 x 7.4 [001]
MAZ B-LowCu	MAZ	4.25	1.5	8 MR	3.1 x 3.1 [001]
MAZ B	MAZ	4.25	4.4		

Figure 2. 10 Methanol yields of various zeolites under isothermal conditions (200ºC activation and CH_4) and conventional high-temperature activation conditions (450ºC activation and 200ºC CH_4). Chemical analysis and typical structure features, pore and channel sizes are included. Adapted from (KNORPP et al., 2019a).

It can be observed in Fig. 2.10 that Cu-exchanged Mazzite (Cu-MAZ) zeolite presented highlighted performance on MMet reaction with higher methanol yields than Cu-MOR, in both approaches, isothermal and conventional.

MAZ (Figure 2.11) presents a one-dimensional framework with 12MR, 8MR and a gmelinite (GME) cage that is relatively simple when compared with MOR framework, which presents a threedimensional structure with different channels (MAHYUDDIN et al., 2018).

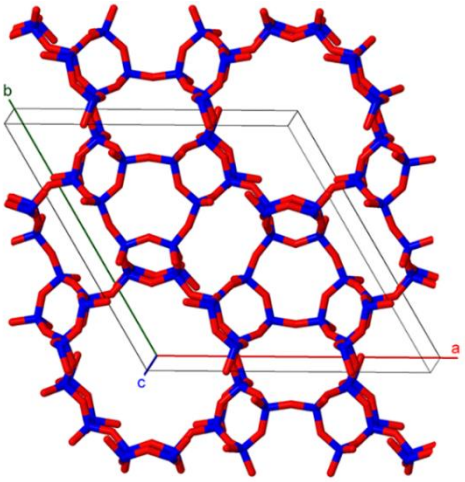

Figure 2. 11 MAZ zeolite framework. Red and blue sticks represent O and T (Si or Al) atoms, respectively. The unit cell is depicted. Source: Adapted from (MAHYUDDIN et al., 2018).

Nevertheless, it is slightly difficult to synthesize pure MAZ since a co-phase, sodalite (SOD), is constantly present and this can compromise the MAZ performance on a possible application (Figure 2.12) (KNORPP et al., 2018b).

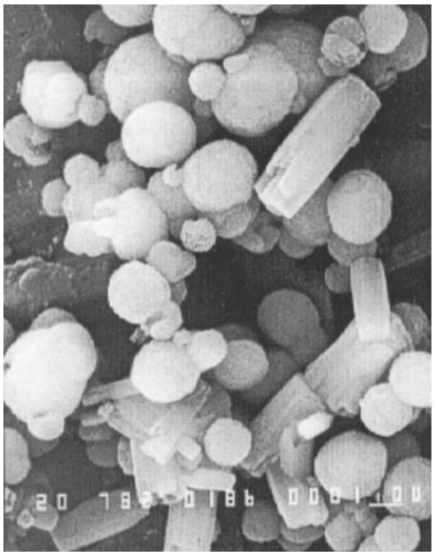

Figure 2. 12 SEM images of mazzite zeolite containing the co-phase sodalite. Mazzite is indicated by the long bundled rods and the sodalite by the spheres. Adapted from (GOOSSENS et al., 2000).

Recently Knorpp et al. (KNORPP et al., 2018b) synthesized pure Mazzite exchanged with Cu and applied on MMet reaction using the ‘conventional procedure’. The authors claimed that Cu-MAZ exhibited a superior performance than Cu- MOR with higher selectivity and methanol yield. They also reported that the copper concentration on the zeolite is directly related to the activity of the samples.

Cu-MAZ has shown highlighted performance also in the MMet reaction using the isothermal procedure. At 6 bar methane pressure, Cu-MAZ presented almost 100 micromols methanol per gram of zeolite at 200ºC, the same yield presented by Cu-MOR sample using the high-temperature procedure (KNORPP et al., 2019a).

As presented in this subchapter, Cu-MOR and Cu-MAZ are promising materials to study in MMet reaction. Both present interesting characteristics related to its framework that allows a better comprehension of MMet reaction.

CHAPTER 3 - ON HOW THE COUNTER IONS AFFECT THE PERFORMANCE ON STEP-WISE METHANE TO METHANOL REACTION: THE CASE OF COPPER EXCHANGED Na- AND NH_4-OMEGA (MAZ) ZEOLITE*

Stefanie C. M. Mizuno[1,2], Amy J. Knorpp[3], Vitaly L. Sushkevish[2], Jie Zhu[3], Jose M. C. Bueno[1], and Jeroen A. van Bokhoven[2,3*]

[1] Federal University of São Carlos, P.O. Box 676, 13565-905, São Carlos, Brazil

[2]Paul Scherrer Institute, Villigen, CH-5232, Switzerland

[3]ETH Zurich, Vladimir-Prelog-Weg 1, Zurich, CH-8093, Switzerland

* This chapter was written using a template for a communication paper.

“In this work, we showed how different counterions (Na- and NH_4) accompanying copper exchanged Omega (MAZ) zeolite affect methanol yield on the step-wise methane to methanol direct conversion (MMet). Extra-framework Aluminum was observed after the reaction cycle and may contribute to material activity. It was also observed that NH_4^+ ions are not completely decomposed during the high-temperature activation procedure.”

Gas flaring is one of the main environmental problems of the world, moreover, it is a billion-dollar waste and it has persisted for decades (AREGBE, 2017). Especially natural gas, composed mainly by methane, has been underestimated due to the troubles associated with its transportation to remote places and it ends up being flared generating harmful waste, re-injected in the crude oil mines, or simply leaked into the atmosphere (ELVIDGE et al., 2018).

Thus, alternative solutions to lessen or extinguish natural gas flaring it become an important issue and converting methane to liquid chemicals (i.e. methanol) can be an interesting way to attenuate the wasting and reinforce hydrocarbon industry (AREGBE, 2017). The industrial conversion of methane to methanol occurs through catalytic processes using gas or liquid phase oxidation reactions that require extreme conditions such as, high pressure and temperature (500ºC; > 30bar) or highly acid medium (ZAKARIA; KAMARUDIN, 2016a).

The step-wise conversion of methane to methanol at low temperatures (MMet) reaction using copper exchanged zeolites has been shown an interesting alternative to conventional processes due to its ‘mild’ operation parameters (DA SILVA, 2016). It has been observed that optimization of reaction conditions and also the preparation of the zeolite is needed before reaching the applicability of this process on an industrial scale, therefore a deep understanding from a fundamental point of view is still required(ALAYON et al., 2014; LANGE et al., 2019).

In the ‘conventional step-wise’ procedure, the Cu-zeolites are activated with oxygen at a high temperature (450°C or above) followed by reaction with methane at a lower temperature (usually 200 °C) and methanol extraction by water solution (off-line extraction) or by steaming (on-line extraction) (GROOTHAERT et al., 2005b; SMEETS; GROOTHAERT; SCHOONHEYDT, 2005). A wide list of zeolite structures has been applied on MMet to evaluate

methanol yield (ALAYON et al., 2012a; NARSIMHAN, 2016; RAVI; RANOCCHIARI; VAN BOKHOVEN, 2017) and outstanding performance can be found for Cu-MAZ with methanol yields about 150 μmols·g $^{-1}$ per reaction cycle at low methane pressure. (KNORPP et al., 2018b) This result shows how Cu-MAZ can be competitive when compared with other widely studied zeolites such as Cu-ZSM-5(AL-SHIHRI; RICHARD; CHADWICK, 2017; GROOTHAERT et al., 2005a; KALAMARAS et al., 2016; WULFERS et al., 2015a) and Cu-MOR (ALAYON et al., 2012a; NARSIMHAN, 2016; RAVI; RANOCCHIARI; VAN BOKHOVEN, 2017).

However, other parameters can affect the performance of Cu-exchanged zeolites on MMet reaction such as sample preparation method. Our group recently demonstrated that different morphologies of Cu-MAZ zeolites originated from different synthesis procedures, perform differently on MMet reaction despite present similar Si/Al ratios (KNORPP et al., 2019b).

Moreover, Dyballa et al. (DYBALLA et al., 2019) observed for Cu-MOR that the exchanged method and also the counter-ion accompanying the zeolite affect the performance on reaction. The solid-state exchange did not show any advantage over aqueous exchange and the highest methanol yield was achieved for H-MOR when compared to Na-MOR form and the authors also claimed that it is not relevant for framework stabilization if the cations are Cu or Na.

In this work, we compare the performance of copper exchanged Mazzite zeolite containing two accompanying cations, Na or NH_4, on the step-wise methane to methanol direct conversion.

We synthesized two samples of high crystalline MAZ (Si/Al=4) (Figure S3.1) containing different counter-ions (Na or NH_4) and copper exchanged varying copper content. The micrographs obtained by SEM (Figure S3.2) revealed that MAZ presented long bundled rods morphology with crystal size about 2-3 μm. The Si/Al and Cu/Al ratios were determined by AAS analysis. The samples were labeled as “Cu-Na-Omega” and “Cu-NH_4-Omega” for Cu-exchanged Mazzite containing Na and NH_4 residual cations, respectively. After the Cu-

exchange procedure, the samples were used without calcination. More details about the experimental procedure can be found in Chapter 3 Supplementary Information (Appendix A).

Screening the samples on “conventional” step-wise methane to methanol procedure (Fig. 3.1) it was observed a linear increase of methanol yield with an increase of Cu/Al ratio. This behavior was previously reported and it was also observed for Cu-exchanged MOR materials (KNORPP et al., 2018b).

The higher methanol yield was observed for the sample with Cu/Al=0.24 containing NH_4 cations achieving the yield of 146 µmols·g $^{-1}$. For the same Cu/Al=0.24, the sample containing Na presented a yield of 101 µmols·g $^{-1}$, based on these results it can be inferred that different charge balancing cation may lead to copper sites which have different redox properties and therefore will require different conditions of operation.

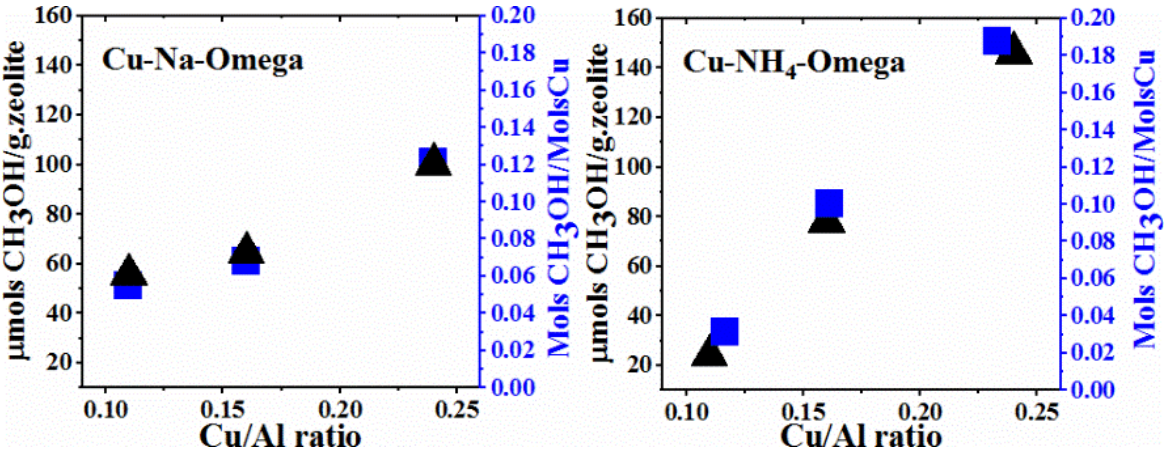

Figure 3. 1 Methanol yield for Cu-Na-Omega (left) and Cu–NH_4-Omega (right) with different Cu/Al ratios. Reaction conditions: activation under O_2 flow at 450ºC; p(CH_4)= 6 bar; reaction temperature: 200ºC.

It was also observed that low Cu/Al brought no benefits, especially for Cu-NH_4-Omega. It might be that higher Al content combined with the formation of the proton after the activation procedure trigger off a dealumination process deactivating the material. Conversely, for high

Cu/Al ratios this effect showed to be positive since the proton can provide Cu species modification with the framework aluminum removal.

We collected the data for Cu reduction profile during methane interaction in several temperatures using Cu K-edge X-ray absorption spectroscopy for the samples with Cu/Al=0.24 and the development of Cu species quantified by Linear Combination Analysis (LCA)[1] are shown in Figure 3.2.

Since the use of bulk Cu_2O to quantify Cu I levels is not reliable(NEWTON et al., 2018) for LCA, we just consider internal standards derived from each sample through treatment at 450ºC in CH_4 and the spectra can be found in the Chapter 3 Supplementary Information (Appendix A). The Cu (II) reduction is highly dependent on temperature and in both samples started above 100 ºC. At 200 ºC a small fraction of Cu(I) was observed and Cu(II) reduction increased rapidly reaching almost 50% on Cu-Na-Omega at 300ºC and for Cu-NH_4-Omega about 30%.

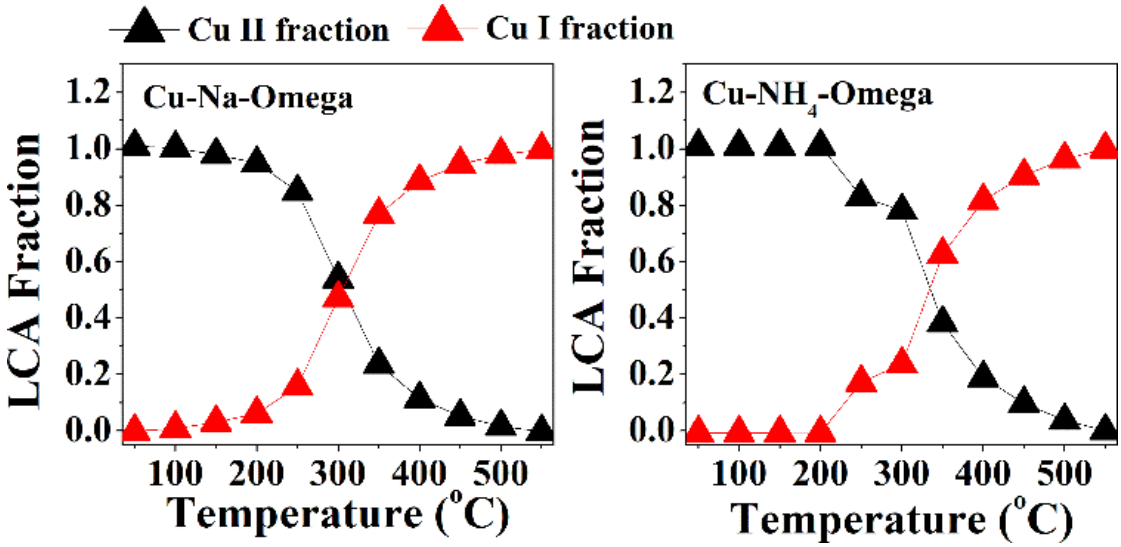

Figure 3. 2 Linear combination analysis (LCA) of the XANES region for Cu I and Cu II fractions for the samples under different temperatures of methane interaction.

[1] Based on the redox mechanism of a Cu pair or dimer that would have a Cu(II) to Cu(I) coupling (ALAYON et al., 2014; KNORPP et al., 2018a).

Despite the higher reduction degree of Cu-Na-Omega until 300ºC its activity in the reaction was lower when compared with Cu-NH_4-Omega. We cannot establish a reliable correlation between the Cu (II) to Cu(I) due to methanol formation since the formation of by-products like CO_x also convert Cu(II) to Cu(I), but we can infer the optimal operation range since that is clear that below 200ºC there was no Cu(II) reduction (KNORPP et al., 2018a).

Therefore, based on the LCA results, we screened the samples with Cu/Al=0.24 varying the reaction temperature and methane pressure and the results are presented in Figure 3.3.

At 1 bar of methane pressure (Fig.3.3a)) the samples presented lower methanol yield, 20 and 69 µmols·g $^{-1}$ for Cu-Na-Omega and Cu-NH_4-Omega respectively when compared to previous data (Fig.3.3b)) collected using a methane pressure of 6 bar. These results are in agreement with earlier works that described that higher methane pressures can be necessary to activate copper sites that were inactive at low pressures(KNORPP et al., 2018b; TOMKINS et al., 2016a).

The highest methanol yield was achieved using 6 bar of methane pressure and reaction temperature of 250ºC, for Cu-NH_4-Omega the yield was 197 µmols·g $^{-1}$ and for Cu-Na-Omega 120 µmols·g $^{-1}$.

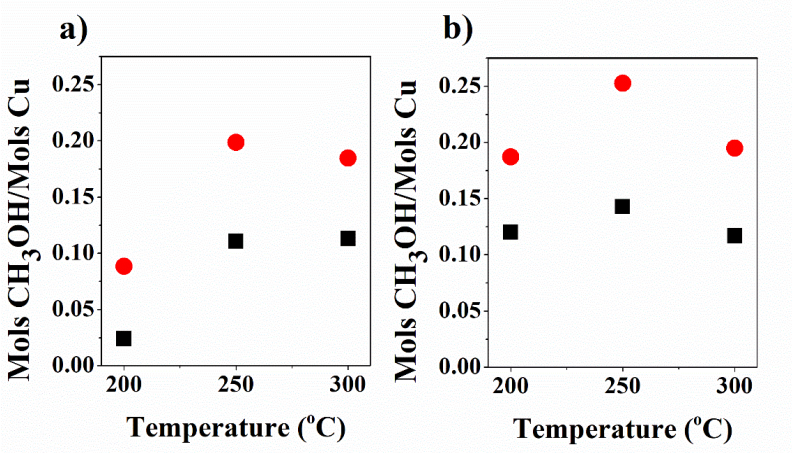

Figure 3. 3 Methanol yield per Mols of Cu versus temperature for Cu-NH_4-Omega (●) and Cu–Na-Omega (■) in different reaction CH_4 pressures: a) 1 bar; b) 6 bar. Activation under O_2 at 450ºC.

At 300ºC a drop in the methanol yield was observed that might to be related to the occurrence of side reactions such as overoxidation to CO_x caused by reaction temperature increase. This assumption is reinforced by the fact that CH_4 pressure is no longer relevant at 300ºC, strongly indicating side reactions domain.

Despite the overoxidation reactions at 300ºC, an expressive difference in methanol yield between samples still observed. For Cu-NH_4-Omega the yield was 152 µmols·g $^{-1}$ and for Cu-Na-Omega 98 µmols·g $^{-1}$, which may indicate that residual Na^+ in Cu-Na-Omega might block active copper sites formation resulting in a kinetic modification that made reaction with CH_4 slower. To check samples selectivity we employed in situ IR technique and results are presented in Figure 3.4.

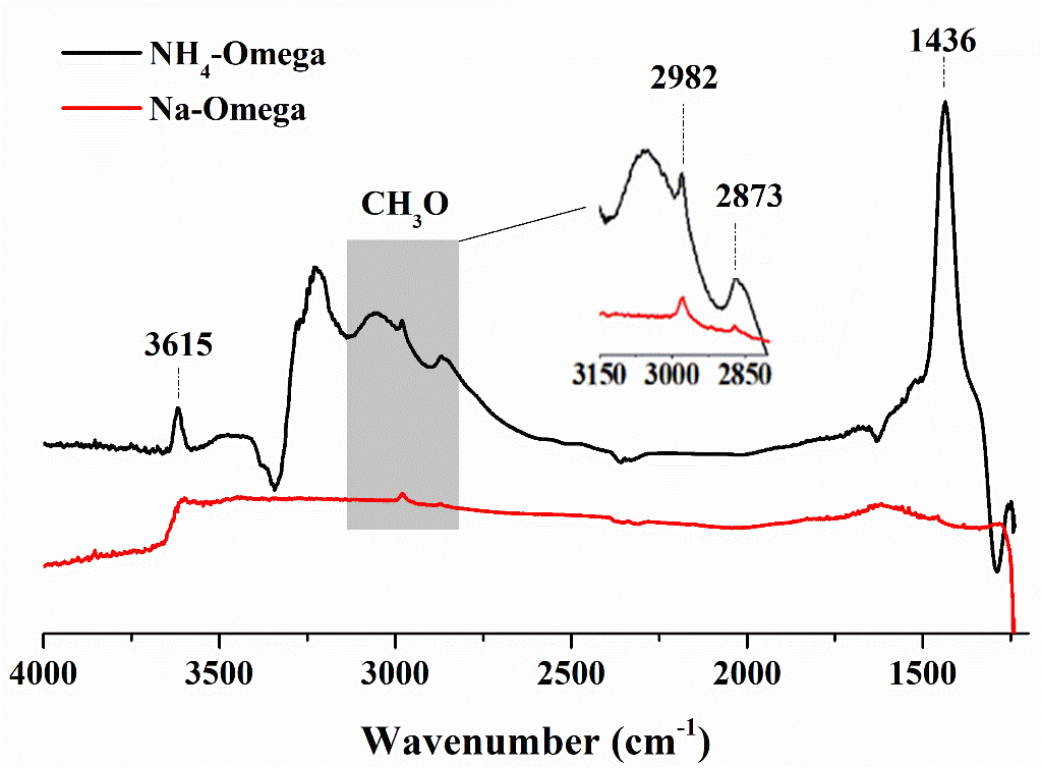

Figure 3. 4 In situ FTIR spectra of surface species formed after reaction with methane (Activation Temperature = 400ºC, p(CH4) = 6 bar at 200 ºC, reaction time 30 min).

Both samples presented surface species formed during reaction with methane. The bands at 2979 cm^{-1} ($\nu_s CH_3$), 2870 cm^{-1} and ($\nu_{as} CH_3$) can be assigned to methoxy species. No bands were observed around 2160 cm^{-1}, related to stretching vibrations of adsorbed CO, indicating samples high selectivity(KNORPP et al., 2018b).

For Cu-NH_4-Omega it was observed two additional bands: at 1436 cm^{-1}, which could be related to residual NH_4^+ ions that were not decomposed during the activation step, and at 3615 cm^{-1} attributed to hydroxyl groups at aluminum deficient sites may be related to the formation of extraframework aluminum due to the instability of MAZ acidic form (MASSIANI, P.; CHAUVIN, B.; FAJULA, 1988; WEEKS; BOLTON, 1976).

Previously, we reported a strong relationship between bronsted sites and selectivity for Cu-MOR. It was observed that the presence of bronsted sites helped to avoid over-oxidation into carbon oxides due to higher stability of surface methoxy intermediates favoring higher methanol yields (SUSHKEVICH; VAN BOKHOVEN, 2018).

^{27}Al MAS NMR was employed in both samples after a reaction cycle at 250 ºC and the results are presented in Figure 3.5.

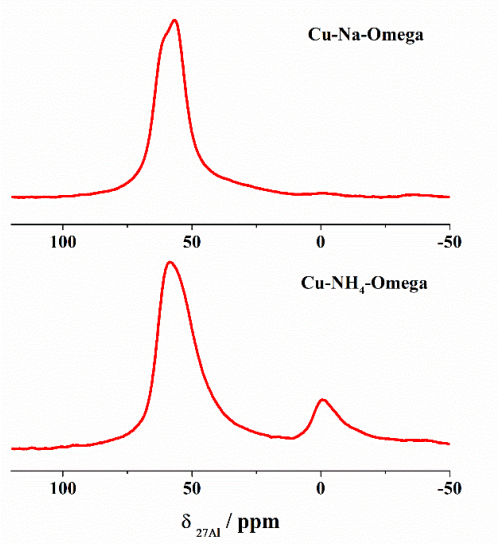

Figure 3. 5 ^{27}Al MAS NMR spectra of Cu-Na-Omega and Cu-NH_4-Omega samples after reaction cycle at 250 ºC (activation temperature = 450 ºC).

Both samples showed a sharp peak around 60 ppm related to framework tetrahedrally coordinated aluminum. However, for Cu-NH_4-Omega it was also observed a peak around 0 ppm related to extraframework aluminum (EFAl) species indicating dealumination after reaction cycle (CHEN et al., 2004; DYBALLA et al., 2019).

Dyballa et al. (DYBALLA et al., 2019) also observed EFAl species on Cu-MOR and the authors claimed that the EFAl species brought benefits to MMet reaction for reasons that remain speculative. In fact, MAZ zeolite is unstable in its protonic form (CHEN et al., 2004), obtained after the calcination procedure leaning to EFAl formation especially after the methanol extraction by liquid water.

Hence, the Cu species contained in the Cu- NH_4-Omega might differ from the contained in Cu-Na-Omega and this could be related to Cu-NH_4-Omega highlighted performance on MMet reaction since the proton can promote framework aluminum removal modifying $(Cu_xO_y\text{-}Al)^{2+}$ species making them accessible and/or active on MMet reaction.

Therefore, the counterion on Omega zeolite plays an important role in the material performance during MMet reaction and has to be carefully considered in a possible design for the scaled-up process.

CHAPTER 4 – STEPWISE METHANE TO METHANOL CONVERSION: EFFECT OF COPPER LOADING ON THE FORMATION OF ACTIVE SPECIES IN COPPER-EXCHANGED MORDENITE

Stefanie C. M. Mizuno,[1] Siriwan Dulnee,[1] Tássia C. P. Pereira,[1] Ricardo J. Passini,[1] Ernesto A. Urquieta-Gonzalez,[1] Jean Marcel R. Gallo,[2] João B. O. Santos,[1] and José M. C. Bueno[1]

[1] Department of Chemical Engineering, Federal University of São Carlos, Rod. Washington Luis, km 235, C.P. 676, São Carlos, SP, 13565-905, Brazil

[2] Renewable Energy, Nanotechnology, and Catalysis Group (GreenCat, www.greencat.ufscar.br), Department of Chemistry, Federal University of São Carlos, Rod. Washington Luis, km 235, C.P. 676, São Carlos, SP, 13565-905, Brazil

4.1 Introduction

Natural gas, consisting mainly of methane (CH_4), is an abundant global resource, with reserves exceeding those of crude oil (HAN et al., 2016). Although CH_4 has potential as a fuel, difficulties related to its transportation and storage rend it an underused feedstock (RAVI; RANOCCHIARI; VAN BOKHOVEN, 2017). Therefore, the conversion of CH_4 to added-value liquid chemicals that are easier to store and transport could be one way to reduce greenhouse gas emissions due to flaring during refining processes (HAN et al., 2016).

The current industrial process applied for CH_4 utilization has high energy consumption and involves several processes leading to the final products. For instance, the production of methanol involves the steam reforming of CH_4 to synthesis gas ($CO + H_2$), followed by CO hydrogenation at high pressure (REDDY; KIM; SONG, 2013). Alternatively, methanol can be obtained by the stepwise Direct Methane To Methanol (DMTM) conversion, which can proceed at relatively low temperature and pressure, avoiding excessive energy consumption (ARUTYUNOV, 2014; HAN et al., 2016). However, despite the attraction of the DMTM reaction, developing an industrial process remains challenging, since the reaction intermediates can undergo overoxidation to carbon dioxide (KNORPP et al., 2018b; LANGE et al., 2019; TAIFAN; BALTRUSAITIS, 2016).

Mono-oxygenase enzymes found naturally in methanotrophic bacteria are active for selective conversion of CH_4 to methanol at low temperatures (LIEBERMAN; ROSENZWEIG, 2005; MERKX et al., 2001). Biomimetic research has enabled the development of inorganic materials inspired by these enzymes, based on ion-exchanged copper zeolites that are capable of highly selective conversion of CH_4 to methanol at low temperatures, as an attractive alternative to the current industrial process (LIEBERMAN; ROSENZWEIG, 2005; SOLOMON et al., 2014; VINCENT et al., 2006).

Early studies of copper-exchanged zeolites reaction proposed that the active sites for DMTM were bis(μ-oxo)dicopper centers $[Cu_2\text{-}(\mu O)_2]^{2+}$ exchanged in the Zeolite anionic sites (GROOTHAERT et al., 2005b). Other species such as isolated Cu trinuclear sites (GRUNDNER

et al., 2015) and a combination of mono(m-oxo) and bis(m-oxo) dicopper species (ALAYON et al., 2015a) have also been proposed to be active. In fact, the structure of the active Cu species in zeolites have been thoroughly explored in the literature (DYBALLA et al., 2019; GRUNDNER et al., 2015; HAMMOND et al., 2012b; IPEK et al., 2017; KULKARNI et al., 2016b; MEYET et al., 2019; NEWTON et al., 2020; PALAGIN et al., 2017; PAPPAS et al., 2017; TOMKINS et al., 2016b; VOGIATZIS et al., 2017; WULFERS et al., 2015a).

Recent studies are converging to the attribution of mono(μ-oxo) dicopper species, $[Cu_2O]^{2+}$ (BREZICKI et al., 2019), as the actual active species for DMTM reaction, as it has been found by resonance Raman and UV-Vis-NIR spectroscopy analyses and DFT calculations for ZSM-5 (WOERTINK et al., 2009). Recent studies of copper-exchanged MOR by high-energy-resolution fluorescence detection technique to the near edge structures identified five types of Cu species and the active species $[Cu_2O]^{2+}$ (PAPPAS et al., 2018; VANELDEREN et al., 2014, 2015) accounted for 47 % of the Cu sites (PAPPAS et al., 2018). Indeed, the amount of the active species can vary based on the zeolite preparation methods, Si/Al ratio, Cu loading, and zeolite treatment (PAPPAS et al., 2018). Mordenite zeolite (MOR) possesses an appropriate environment for hosting Cu sites inside the 8-membered-ring side pocket, while the Brønsted acids in the larger cages (12-membered-ring apertures) are not exchanged and can assist in the first step of CH_4 activation, enabling higher methanol yields (DYBALLA et al., 2019; ZHANG et al., 2015). Different Cu sites can be hosted inside the MOR pores, depending on parameters such as the Si/Al ratio, Cu content, and preparation method (LE et al., 2017; SUSHKEVICH; VEREL; BOKHOVEN, 2020).

Interestingly, two types of $[Cu_2O]^{2+}$ were found in Cu-MOR and their different reactivity was attributed to the typology of Zeolite lattice in which they are hosted in (VANELDEREN et al., 2014, 2015). Furthermore, the type of zeolite appears to affect significantly the reactivity of the material. For instance, the structure of the active sites in Cu-MOR and Cu-ZSM-5 has been showing to be similar (VANELDEREN et al., 2014, 2015) and, still, the reactivity towards the DMTM reaction is significantly different (SUSHKEVICH; VAN BOKHOVEN, 2019; VANELDEREN et al., 2014, 2015). Overall, the activity of the Cu site is drastically affected by

the Zeolite structure, which has been recently shown to be related to the Cu site reduction temperatures as well for the temperature of CH_4 activation in the different materials (SUSHKEVICH; VAN BOKHOVEN, 2019). Indeed, Sushkevich et al. (SUSHKEVICH; VAN BOKHOVEN, 2019) claimed that there is still no clear insight that allows the correlation between material characteristics and activity for DMTM reaction. The authors also suggested that understanding the redox properties of copper-exchanged in zeolites play a major role in designing highly active materials.

Besides the zeolite structure, the reducibility of the Cu active site can be also drastically affected by the reaction conditions and the presence of oxygen or water impurities (BREZICKI et al., 2019). Although it is accepted that there is a plurality of active Cu structures involved in CH_4 activation, the experimental procedures for the *in situ* characterization of these species are still a challenge (PALAGIN et al., 2017).

Herein, we attempted to demonstrate the effect of the copper loading in Cu-exchanged Mordenite (Cu-MOR) in the formation of the active species for CH_4 conversion to methanol at low temperatures. The active species were identified through *in situ* Diffuse Reflectance spectroscopy, which revealed different possible active species and their dynamic behavior as a function of the calcination temperatures under O_2 or under reaction with CH_4.

4.2 Materials and Methods

4.2.1 Mordenite zeolites

Mordenite zeolites (MOR) in the sodium and ammoniacal forms, with Si/Al ratios of 6.5 and 10, respectively, were purchased from Zeolyst International. Na-MOR(6.5) was prepared by two successive exchanges with sodium acetate at 80 °C for 4 h. Na-MOR(10) was obtained from the ammoniacal form of the zeolite by exchange using sodium acetate. For this, 10 g of mordenite in the ammoniacal form were dispersed in 360 mL of 2.44 mol L^{-1} sodium acetate

solution, with stirring for 4 h at 80 °C. The solid was filtered off while hot, rinsed with 120 mL of deionized H_2O, and dried for 4 h at 110 °C. This entire procedure was carried out three times, to ensure that all the NH_4^+ was replaced by Na^+. The sodium form of the zeolite was used to avoid the formation of extraframework aluminum during the sample thermal treatment (PAPPAS et al., 2017).

4.2.2 Cu ion-exchange

The Na-MOR(6.5) and Na-MOR(10) materials were exchanged with Cu ions to yield Cu-MOR(6.5)-(X) and Cu-MOR(10)-(X), respectively, where X is the duration of the exchange procedure (in hours).

In a typical procedure, 4.0 g of sodium mordenite (Na-MOR, with Si/Al ratio of 6.5 or 10) were stirred for 12 or 24 h, at room temperature, in 400 mL of a 0.01 mol L^{-1} solution of copper(II) acetate hydrate ($Cu(COOCH_3)_2 \cdot H_2O$). The solid was then filtered off, washed with 400 mL of water, and dried at 110 °C overnight. This procedure generated the samples denoted Cu-MOR(6.5)-(12h), Cu-MOR(6.5)-(24h), Cu-MOR(10)-(12h), and Cu-MOR(10)-(24h).

Additionally, to increase the Cu loading, the Cu-MOR(6.5)-(24h) and Cu-MOR(10)-(24h) samples underwent one or two extra cycles of ion-exchange, using the same methodology described above. The resulting samples were denoted Cu-MOR(6.5)-(2x24h), Cu-MOR(6.5)-(3x24h), Cu-MOR(10)-(2x24h), and Cu-MOR(10)-(3x24h).

4.2.3 Incipient wetness impregnation

A solution of copper(II) nitrate hemi(pentahydrate) ($Cu(NO_3)_2 \cdot 2.5H_2O$), obtained using 0.24 g of the salt in 30 drops of deionized water, was dripped onto 1.0 g of the Na-MOR(6.5) or Na-MOR(10). The resulting suspension was sonicated for 2 h at room temperature, followed by drying at 110 °C for 12 h.

4.2.4 Characterization methods

X-ray diffractograms were acquired using a Rigaku Miniflex DMAX 2500 PC instrument operating at 30 kV and 10 mA, with Cu Kα radiation. The diffractograms were obtained in the 2θ range between 5 and 60°, at a scan rate of 2° min^{-1}, with a step size of 0.05°. Nitrogen physisorption isotherms at -196 °C were obtained using a Micromeritics ASAP 2000 instrument. The samples were evacuated at 250 °C before the measurements. Elemental analyses were performed using ICP-OES. For this, the mordenite and Cu-mordenite samples were dissolved in 5 mL of aqua regia (fresh 1:3 mixture of concentrated HNO_3 and HCl) and 1 mL of HF, followed by microwave heating at 160 °C for 20 min. The solutions were quantitatively transferred to sample vials and diluted to 40 mL with deionized water, followed by the analysis of Cu, Al, Si, and Na.

4.2.5 Diffuse reflectance infrared Fourier transform spectroscopy (DRIFTS) with CO adsorption

DRIFTS spectra with CO adsorption were recorded using a Thermo Nicolet is110 FT-IR spectrophotometer equipped with a mercury cadmium telluride (MCT) detector and a Harrick DRIFTS cell with CaF_2 windows. In the CO adsorption experiments, the samples (~80 mg) were treated for 3 h at 450 °C (heating rate of 5 °C min^{-1}), under a flow of 5% O_2 in He (30 mL min^{-1}), and the samples were then cooled to room temperature. The samples were then cooled to liquid nitrogen temperature and the analysis cell was fed with CO at 2 mL min^{-1} for 10 min, followed by He at 30 mL min^{-1} for 30 min. FT-IR spectra (obtained using 64 scans at 4 cm^{-1} resolution) were collected during the experiment.

4.2.6 In situ Diffuse Reflectance UV-Visible Spectroscopy

The *in situ* Diffuse Reflectance (DR) UV-Vis spectra were collected on a Thermo Scientific Evolution 300 UV-Vis Spectrophotometer equipped with a Harrick cell and a reaction chamber. Scans were collected over a wavelength range of 190–1100 nm, at a scan rate of 600 nm min^{-1}. Background scans were taken using barium sulfate ($BaSO_4$) and parent MOR zeolite was used as the reference. Around 100 mg of sample was allocated on the reaction cell and heated at 5 °C min^{-1} from room temperature until 450 °C in synthetic airflow (60 mL min^{-1}) and calcination was performed for 1 h. In this step, DR UV-Vis spectra were collected every 10 minutes. Then, the sample was cooled down to 350ºC, 300ºC, 250ºC, 225ºC, and 150ºC, and a spectrum was collected in each of these temperatures. The cell was flushed with Argon flow (60 mL min^{-1}) for 10 minutes and the atmosphere was switched to reaction (8%CH_4/Ar; 30 mL min^{-1}) and the sample was heated from 150ºC to 225ºC, 250ºC, 300ºC, and 350ºC, and after 5 min in each temperature, a spectrum was collected. In order to eliminate the contributions of the Mordenite material, a DR UV–Vis spectrum of all dehydrated zeolite samples used in this study were subtracted from all Cu-MOR samples spectra. The spectra were converted with the Kubelka–Munk function and deconvoluted into sub-bands by applying Gaussian functions.

4.2.7 In situ X-ray absorption spectroscopy

The XAS measurements at the Cu K-edge (8979 eV) were collected at Laboratório Nacional de Luz Síncroton (LNLS) in XAFS2 beamline on transmission mode. Around 15 mg of Cu-MOR was allocated on the tubular reactor and heated at 5 °C min^{-1} from room temperature until 450 °C in 5%O_2/He flow and calcination was performed at 450 °C for 1 h. In this step, X-ray absorption near edge structure (XANES) spectra were collected to evaluate the oxidation states [Cu^+ and Cu^{2+}] of samples during calcination. The reactor was cooled down in 5%O_2/He to 250 °C and the atmosphere switched to reaction (He, 40%CH_4/He, and He/H_2O stream (saturator at 25 ºC) at 250 °C in sequence, 30 min in each condition). XANES spectra were

acquired at 250 °C in each reaction step. The processing of XANES data in the K edge of the Cu was performed using the IFEFFIT software version 1.2.11d with the Horae (Athena and Artemis) package.

4.2.8 Activity tests

The DMTM process involved the following steps: treatment of the zeolite in O2 at high temperature, CH4 activation at 250 ºC, and extraction of the methanol with steam. For the tests, the sample (500 mg) was loaded into the reactor and treated at 150 °C (heating rate of 5 °C min^{-1}) for 30 min, under a flow of He (50 mL min^{-1}). The temperature was then increased to 450 °C (at 5 °C min^{-1}), maintained for 2 h, under a flow of O_2 (50 mL min^{-1}). The reactor was cooled to 250 °C (still under the O_2 flow) and was then flushed with He (50 mL min^{-1}) for about 10 min. Next, the reactor was fed with CH_4 (50 mL min^{-1}) for 30 min, after which the system was switched to a flow of water steam (from a saturator kept at 50 °C and 12.4 kPa). During this step, the desorption of methanol was monitored using a gas chromatograph (GC) coupled to a mass spectrometer (MS). Methanol was quantified considering the signals at m/z 31 and 29, while CO_2 was quantified using the signal at m/z 44.

4.3 Results

4.3.1 Chemical compositions and textural properties

The chemical compositions and textural properties of the samples are provided in Table 4.1. The results showed that the Cu loading depended on the duration and number of cycles of Cu^{2+} ion exchange. Interestingly, for the same number of exchange cycles, the Cu loading was comparable for the MOR(6.5) and MOR(10) sets of samples. For example, Cu loadings of 4.4 and 4.0 wt.% were obtained for the Cu-MOR(6.5)-(3x24h) and Cu-MOR(10)-(3x24h) samples, respectively.

Table 4.1 Results of elemental analyses by ICP-OES and textural properties of the zeolites.

Sample	%Cu	Cu/Na[a]	Si/Al[a]	Cu/Al[a]	Na/Al[a]	S_{BET} ($m^2\ g^{-1}$)	V_{pore} ($cm^3\ g^{-1}$)
Na-MOR(6.5)	-	-	5.9	-	1.01	382	0.23
Cu-MOR(6.5)-(12h)	1.4	0.36	6.6	0.10	0.45	-	-
Cu-MOR(6.5)-(24h)	2.5	0.83	7.3	0.25	0.40	385	0.23
Cu-MOR(6.5)-(2x24h)	4.0	1.09	7.1	0.39	0.29	325	0.21
Cu-MOR(6.5)-(3x24h)	4.4	1.13	7.0	0.43	0.24	373	0.20
Cu-MOR(10)-(12h)	1.3	0.36	10.0	0.14	0.23	-	-
Cu-MOR(10)-(24h)	2.5	0.80	10.5	0.33	0.18	367	0.20
Cu-MOR(10)-(2x24h)	3.5	1.65	11.2	0.51	0.38	300	0.19
Cu-MOR(10)-(3x24h)	4.0	1.32	11.5	0.58	0.13	345	0.20
6%Cu-MOR(6.5)-IWI	5.6	1.72	5.8	0.79	1.06	7	0.08

[a] Molar ratio.

Elemental analyses indicated the presence of Na^+ in the Cu-exchanged samples, suggesting that the exchange was incomplete. The Cu/Na molar ratio (Table 4.1) increased in line with the Cu loading, reaching maxima of 1.13 and 1.32 for Cu-MOR(6.5)-(3x24h) and Cu-MOR(10)-(3x24h), respectively, corresponding to 56 and 66% of Cu, concerning the total amount of counterions.

Assuming that roughly every Al provided an exchangeable site, the Cu/Al molar ratio indicated the fraction of sites occupied by Cu (Table 4.1). For the samples prepared here, the value varied from 10 to 58%, again indicating that ion-exchange was an effective way to control the Cu loading while suggesting that not every site was exchangeable.

A sample prepared by incipient wetness impregnation (IWI), namely 6%Cu-MOR(6.5)-IWI, reached 5.6 wt. % of Cu. This type of preparation did not lead to the exchange of the surface sites with Cu since the Na/Al was similar to the parent zeolite (Table 4.1). Therefore, the Cu particles could be dispersed, but not bonded to the zeolite structure.

4.3.2 Activity testing

The Cu-MOR(6.5) and Cu-MOR(10) samples were tested in the stepwise oxidation of CH_4. As mentioned before, the reaction consisted of three steps: (i) generation of the active sites under a flow of oxygen; (ii) activation of CH_4; (iii) desorption of methanol under a flow of water steam. The activities of the samples in the reaction were tested using three complete cycles of these steps. Figure 4.1 and Table 4.2 presented the results obtained for the yield of methanol, as a function of the Cu/Al molar ratio.

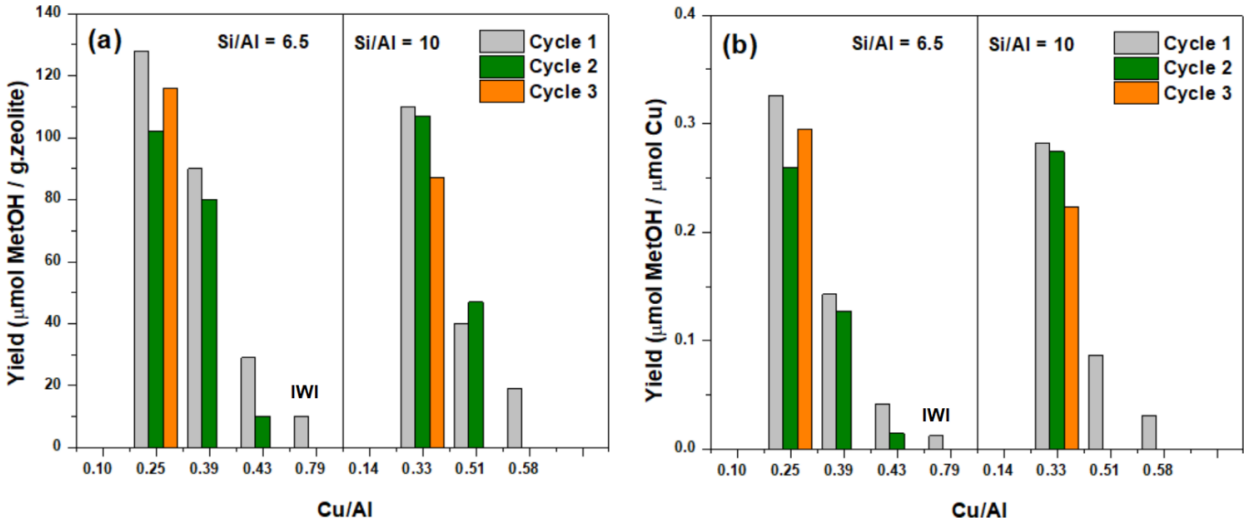

Figure 4. 1 Methanol yields, as a function of Cu/Al molar ratio, in three consecutive reaction cycles: (a) micromol of methanol per gram of zeolite; (b) micromol of methanol per micromol of Cu.

The Cu-MOR(6.5)-(12h) (Cu/Al = 0.10) and Cu-MOR(10)-(12h) (Cu/Al = 0.14) samples showed no activity for methanol formation in the reaction performed at 250 °C, suggesting

inactive Cu species for CH_4 activation. Increasing the duration of Cu exchange led to Cu-MOR(6.5)-(24h) and Cu-MOR(10)-(24h) samples with Cu/Al ratios of 0.25 and 0.33, respectively, which presented higher activity for methanol formation (Figure 4.1).

Table 4.2. CO_2/CH_3OH molar ratios obtained for the zeolite samples during the reaction cycles.

Sample	Cu/Al	CO_2/CH_3OH molar ratio			Yield (μmol CH_3OH/μmol Cu)		
		Cycle 1	Cycle 2	Cycle 3	Cycle 1	Cycle 2	Cycle 3
Cu-MOR(6.5)-(12h)	0.10	0	0	0	0	0	0
Cu-MOR(6.5)-(24h)	0.25	0.79	0.83	0.79	0.33	0.26	0.30
Cu-MOR(6.5)-(3x24h)	0.43	2.73	8.61	1273.70	0.04	0.01	0.00
Cu-MOR(10)-(12h)	0.14	0	0	0	0	0	0
Cu-MOR(10)-(24h)	0.33	0.65	0.62	0.80	0.28	0.27	0.22
Cu-MOR(10)-(3x24h)	0.58	3.26	10.76	1331.59	0.03	0.00	0.00

The activities of the samples towards CH_4 conversion to methanol were higher at lower Cu/Al molar ratios. For example, in the first cycle, the methanol yields were 0.33, 0.14, and 0.04 μmol CH_3OH/μmol Cu for Cu-MOR(6.5)-(24h), Cu-MOR(6.5)-(2x24h), and Cu-MOR(6.5)-(3x24h), respectively (Figure 4.1b).

The Cu-MOR(6.5)-(24h) and Cu-MOR(10)-(24h) samples, with Cu/Al ratios of 0.25 and 0.33, respectively, were the only ones stable during three reaction cycles. Since the Cu loadings in these samples were relatively low (Table 4.1), it was expected that there would be the formation of isolated Cu sites. On the other hand, for the samples with high Cu loadings, the high Cu/Al ratio could favor the formation of polynuclear Cu species, which were not selective towards methanol formation and appeared not to be regenerated after the first reaction cycle, hence explaining the deactivation during the reaction cycles (Figure 1). Furthermore, as shown

in Table 2, the samples with high Cu/Al molar ratios displayed high selectivity towards over-oxidation of methane to CO_2, which increased during progression of the cycles for Cu-MOR(6.5)-(2x24h), Cu-MOR(6.5)-(3x24h), Cu-MOR(10)-(2x24h), and Cu-MOR(10)-(3x24h).

The 6%Cu-MOR(6.5)-IWI sample prepared by impregnation was the least active (0.012 µmol of methanol per µmol of Cu) and only produced methanol in the first reaction cycle. For this sample, the X-ray diffractograms for the fresh material (data has been not shown) presented reflection peaks at 2θ of 13 and 29°, assigned to Na_2O, and at 32, 36, and 39°, assigned to CuO. This was indicative of the exchange of a fraction of the Na^+ ions in the zeolite cages by Cu^{2+}. However, after the reaction, the intensity of the CuO peaks increased, while the Na_2O peaks disappeared, suggesting that CuO migrated out of the zeolite channels and segregated in the form of agglomerated large particles, which were inactive for methane activation (BEZNIS et al., 2011; SÁNCHEZ-LÓPEZ et al., 2019).

4.4 Characterization of the Cu-MOR samples

4.4.1 Analysis of the Cu-MOR samples using DRIFTS with adsorbed CO

Figures 4.2 and 4.3 show the FT-IR spectra of adsorbed CO of the Cu-MOR(6.5) and Cu-MOR(10) samples treated in O_2 at 450 ºC for 3 h. The FT-IR spectra for Cu-MOR(6.5)-(2x24h) and Cu-MOR(10)-(3x24h) at lower CO adsorption temperatures of -127 and -115 °C, respectively, showed main bands of carbonyl C-O stretching at frequencies of around 2203 and 2170 cm^{-1}, together with a shoulder at 2140 cm^{-1}. The band at 2203 cm^{-1} could be attributed to Cu^{2+}-CO species (HADJIIVANOV; VAYSSILOV, 2002). The band at 2170 cm^{-1} disappeared with slight heating to around -60 °C, indicative of a highly basic surface with the presence of CuO and the formation of polymeric species (SUSHKEVICH; VAN BOKHOVEN, 2018). With the heating of the sample between -90 and 0 °C (Figures 4.2 and 4.3), the most intense bands were observed at 2149 and 2177 cm^{-1}, attributed to asymmetric and symmetric Cu^+-$(CO)_2$ species, respectively (HADJIIVANOV; VAYSSILOV, 2002). At lower temperatures, the

coexistence of signals at 2203 and 2170 cm^{-1} indicated the presence of two Cu^{2+} species adsorbing CO, in the forms Cu^{2+}-CO and Cu^{2+}-$(CO)_n$, respectively (HADJIIVANOV; VAYSSILOV, 2002). With continued heating, the signal at 2170 cm^{-1}, assigned to polycarbonyl species on Cu^{2+}, disappeared and bands appeared at 2149 and 2177 cm^{-1}, attributed to Cu^{+}-CO species. These further indicated the high reactivity of the Cu^{2+} species, which adsorbed CO to produce the polymeric species and were easily reduced from Cu^{2+} to Cu^{+} (HADJIIVANOV; VAYSSILOV, 2002).

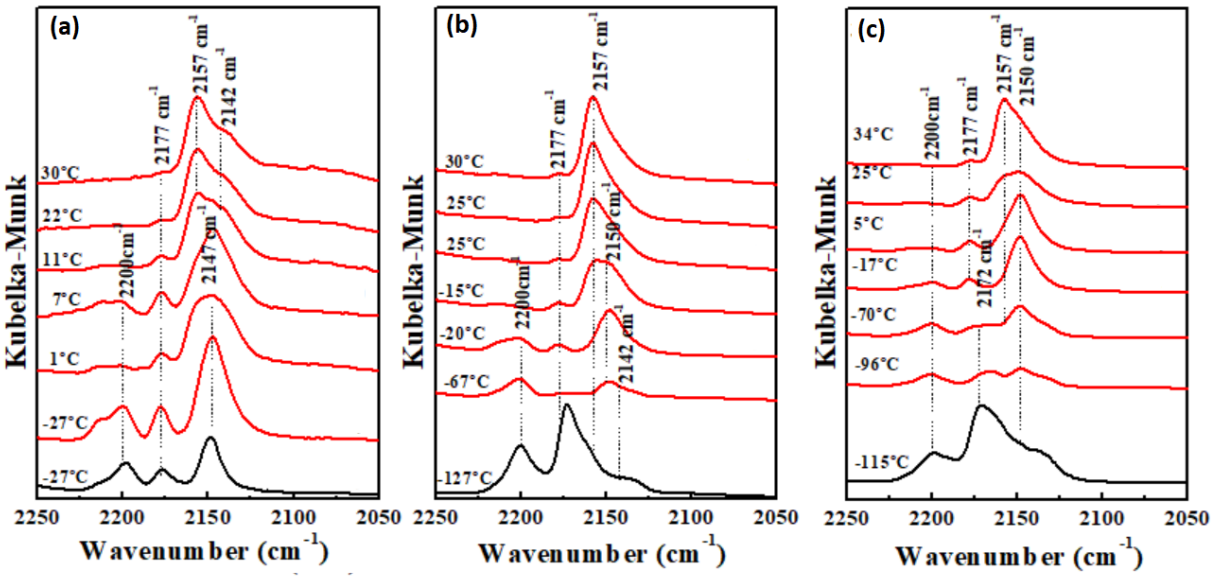

Figure 4. 2 FT-IR spectra of the Cu-MOR samples (Si/Al = 6.5) after CO adsorption for 10 min and heating under a flow of He: (a) Cu-MOR(6.5)-(24h); (b) Cu-MOR(6.5)-(2x24h); (c) Cu-MOR(6.5)-(3x24h).

The Cu^{2+}-CO species (indicated by the band at 2203 cm^{-1}) was not reactive and were present together with the Cu^{+}-$(CO)_2$ species, in the intermediate temperature region. The Cu^{2+}-CO species were desorbed by heating the samples to about -10 °C (Figure 4.3), so this band could be explained by the association of CO with species such as bulk CuO nanoparticles. With the heating of the samples at temperatures higher than 0 °C, the dicarbonyl species Cu^{+}-$(CO)_2$

became decomposed to Cu^{+}-CO, with the appearance of a new band at 2157 cm^{-1} (HADJIIVANOV; VAYSSILOV, 2002).

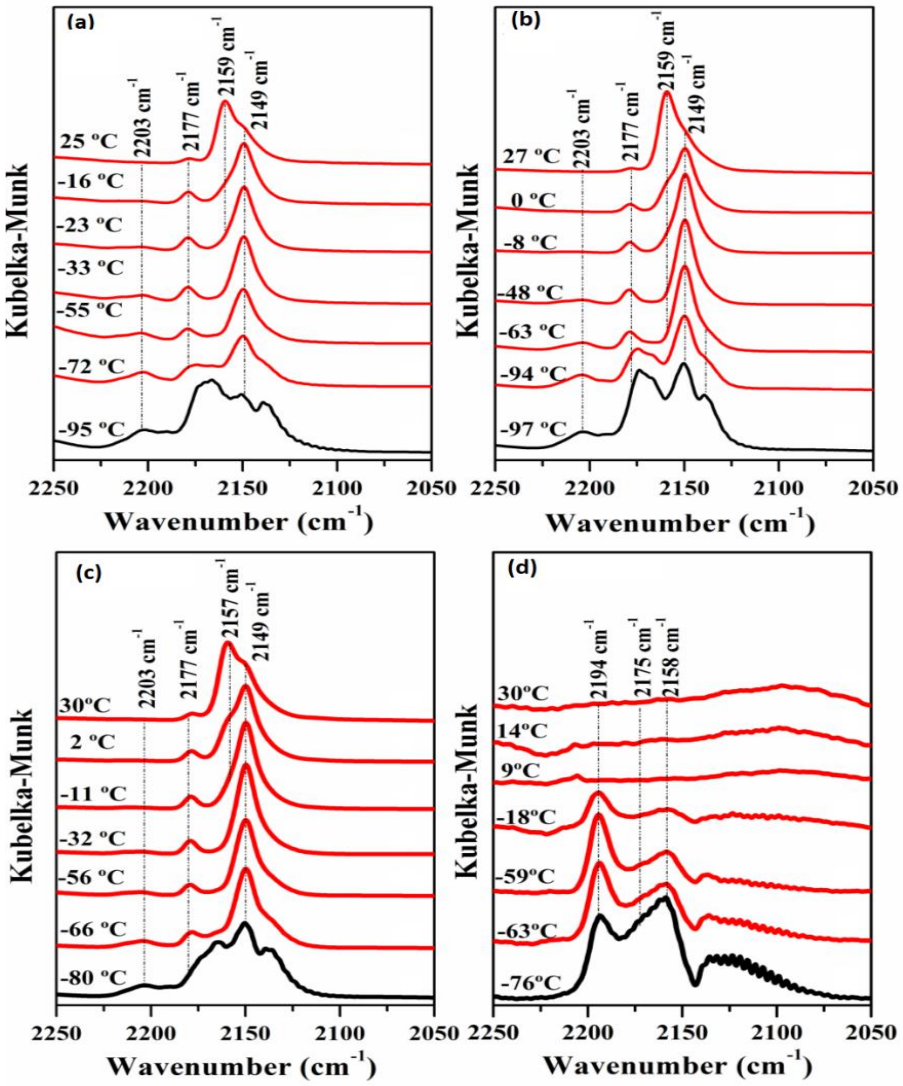

Figure 4. 3 FT-IR spectra of the Cu-MOR samples (Si/Al =10) after CO adsorption for 10 min and heating under a flow of He: (a) Cu-MOR(10)-(24h); (b) Cu-MOR(10)-(2x24h); (c) Cu-MOR(10)-(3x24h); (d) 6%CuMOR(10)-IWI.

The Cu-MOR samples obtained by the impregnation method showed different Cu^{2+} oxi-reduction properties in the presence of CO, compared to the Cu-MOR obtained by Cu-exchange. For example, at low temperatures, the 6%Cu-MOR(10) sample presented carbonyl C-O stretching bands at 2203 and 2170 cm^{-1} (Figure 4.3(d)). Although these species were similar to those observed for Cu-MOR obtained by Cu-exchange, they were only decomposed by sample heating, while the Cu^{2+} species, which adsorbed polymeric CO, was not reduced to Cu^{+}. Therefore, these results suggested that the CuO species obtained by the impregnation method were located outside the zeolite cavity and presented lower reactivity with CO. This was supported by the activity results since the impregnated sample did not show activity in the DMTM reaction.

4.4.2 In situ DR UV-Vis

The *in situ* DR UV-Vis spectra of Cu-MOR(6.5) with various copper contents as prepared (fresh), after thermal treatment under O_2 flow at 450 ^{o}C (calcinated) and its respective Gaussian fitting are shown in Figure 4.4.

For all fresh samples, absorption features with maxima at ca. 12000, 31600-33000, 39000, and 48000 cm^{-1} were observed (Figure 4.4 (a-c)). The absorption feature at ca. 12000 cm^{-1} corresponded to a d–d transition of isolated Cu^{2+} sites and these species were present in both fresh (Figure 4.4 (a-c)) and calcined samples (Figure 4.4 (d-f)). The intense band between ca. 48000 cm^{-1} (Figure 4.4 (a-c)) is typically assigned to the ligand to metal charge transfer transition (LMCT) in Cu(II) octahedral aqua complexes (GIORDANINO et al., 2013; KORHONEN et al., 2011; OORD; SCHMIDT; WECKHUYSEN, 2018). Interestingly, after thermal treatment under oxygen flow, this band significantly reduced its relative intensity (compared to the band at ca. 12000 cm^{-1}), while, concomitantly, the feature at 39000 cm^{-1} increased in intensity. This behavior may suggest that the Cu(II) aqua species (ca. 48000 cm-1) undergo hydrolysis to yield $[CuOH]^{+}$ species (39000 cm^{-1}) (GIORDANINO et al., 2013; KORHONEN et al., 2011; OORD; SCHMIDT; WECKHUYSEN, 2018). Importantly, as the band

at 48000 cm^{-1} (Figure 4.4 (a-c)) reduced in intensity due to the thermal treatment, its center shifted to lower wavenumber (ca. 47000 cm^{-1}) (Figure 4.4 (d-f), suggesting a reduction of the number of water molecules coordinated with Cu(II).

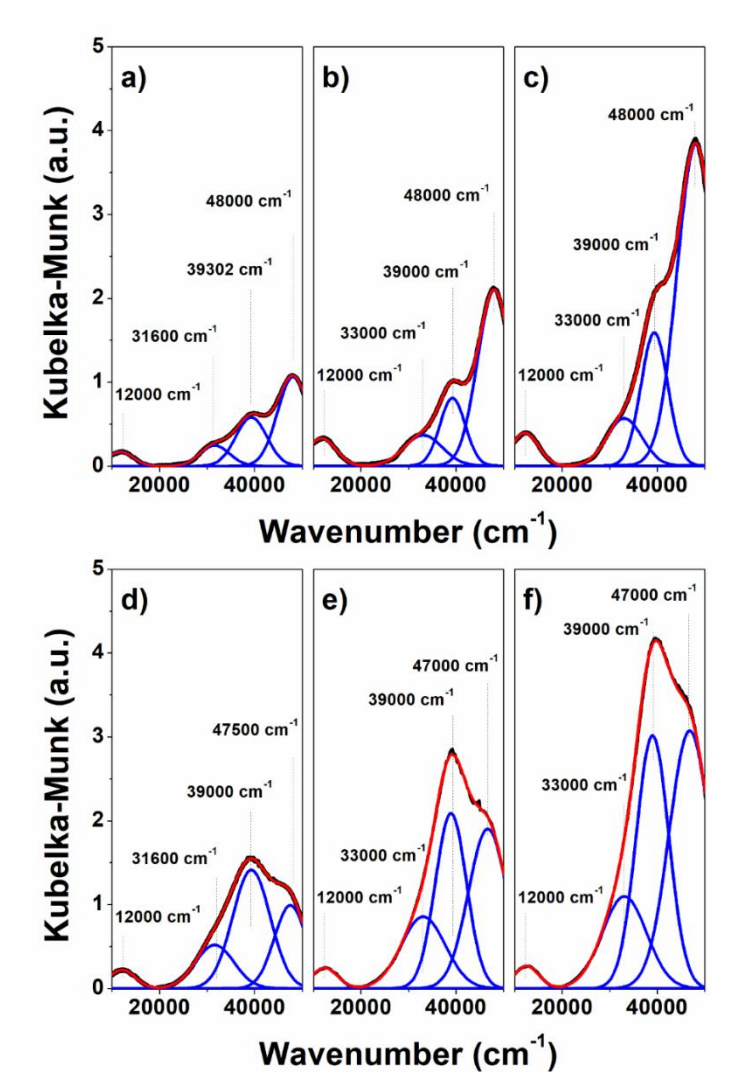

Figure 4. 4 *In situ* DR UV−Vis absorption spectra of Cu-exchanged zeolites and the corresponding Gaussian fitting. Fresh samples: (a) Cu-MOR(6.5)-(12h); (b) Cu-MOR(6.5)-(24h); (c) Cu-MOR(6.5)-(3x24h); and after treatment under O_2 flow at 450 °C: (d) Cu-MOR(6.5)-(12h); (e) Cu-MOR(6.5)-(24h) and (f) Cu-MOR(6.5)-(3x24h). The black solid lines are the sample spectra and the red solid lines represent the sum of the fitting.

The bands at 31000-33000 cm $^{-1}$ were related to the bis(μ-oxo)dicopper $[Cu_2\text{-}(\mu O)_2]^{2+}$ or to single-site trinuclear copper oxygen $[Cu_3(\mu\text{-}O)_3]^{2+}$ sites (GRUNDNER et al., 2015; HALFEN et al., 1996; KIM et al., 2017; LI et al., 2019) and their intensity increased upon calcination (Figure 4.4 (c-e)), indicating that their formation was dependent on the temperature.

Hence, the samples were also studied by DR UV-Vis under methane flow. To evidence the species formed, the spectra obtained under a stream of CH_4 were subtracted from the spectra of the calcined samples. The resulting spectra for Cu-MOR(6.5) samples are shown in Figure 4.5 and revealed Cu species with absorption features at ca. 14000; 22000; 32000-33000; and 40000 cm^{-1}.

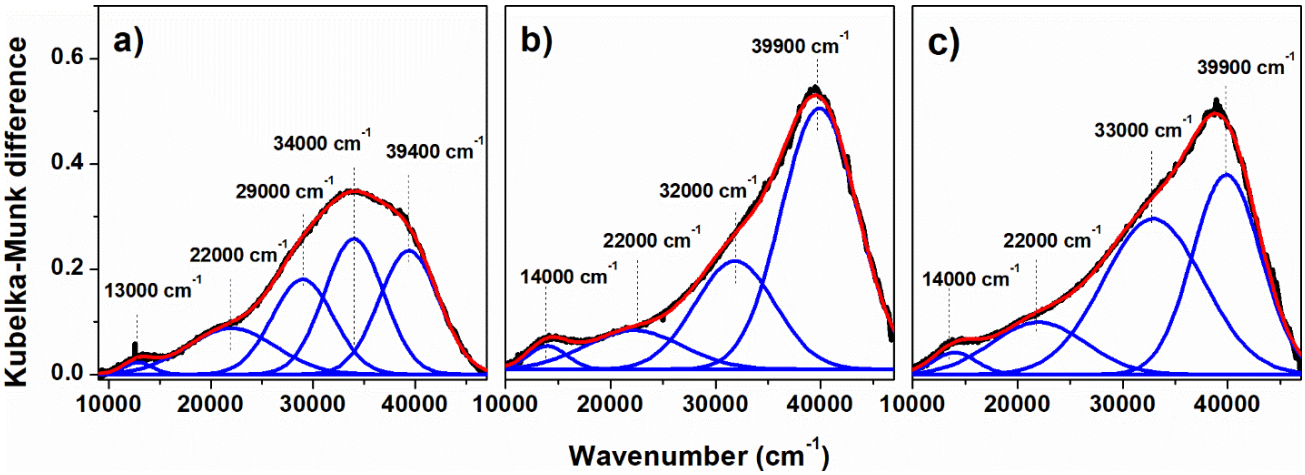

Figure 4. 5 *In situ* DR UV-vis spectra under flow of methane at different temperatures for (a) Cu-MOR(6.5)-(12h) ; (b) Cu-MOR(6.5)-(24h); (c) Cu-MOR(6.5)-(3x24h). Spectra were subtracted from the ones obtained for the samples calcined under O_2 flow at 450^{o}C. Spectra were deconvoluted using a Gaussian fitting and the black solid lines are the sample spectra and the red solid lines represent the sum of the fitting.

Additionally, the species at about 29000 and 34000 cm^{-1} were also present in the sample with the lowest Cu loading [Cu-MOR(6.5)-(12h)] (Figure 4.5 (a)). The absorption feature at about ~22000 cm^{-1} was assigned to the active $[Cu_2O]^{2+}$ species (WOERTINK et al., 2009) which, interestingly, was only formed once the sample was exposed to methane. The other

bands observed in Figure 4.5 were also observed in the spectra in Figure 4.4 and these species appeared to be persistent to CH_4 exposition.

In order to further understand the role of the Cu species, *in situ* DR UV-Vis spectra under CH_4 flow subtracted from the spectra of the calcined sample were also performed for Cu-MOR(6.5)-(24h) and Cu-MOR(6.5)-(3x24h) at different temperatures (150-350°C), as shown in Figure 4.6.

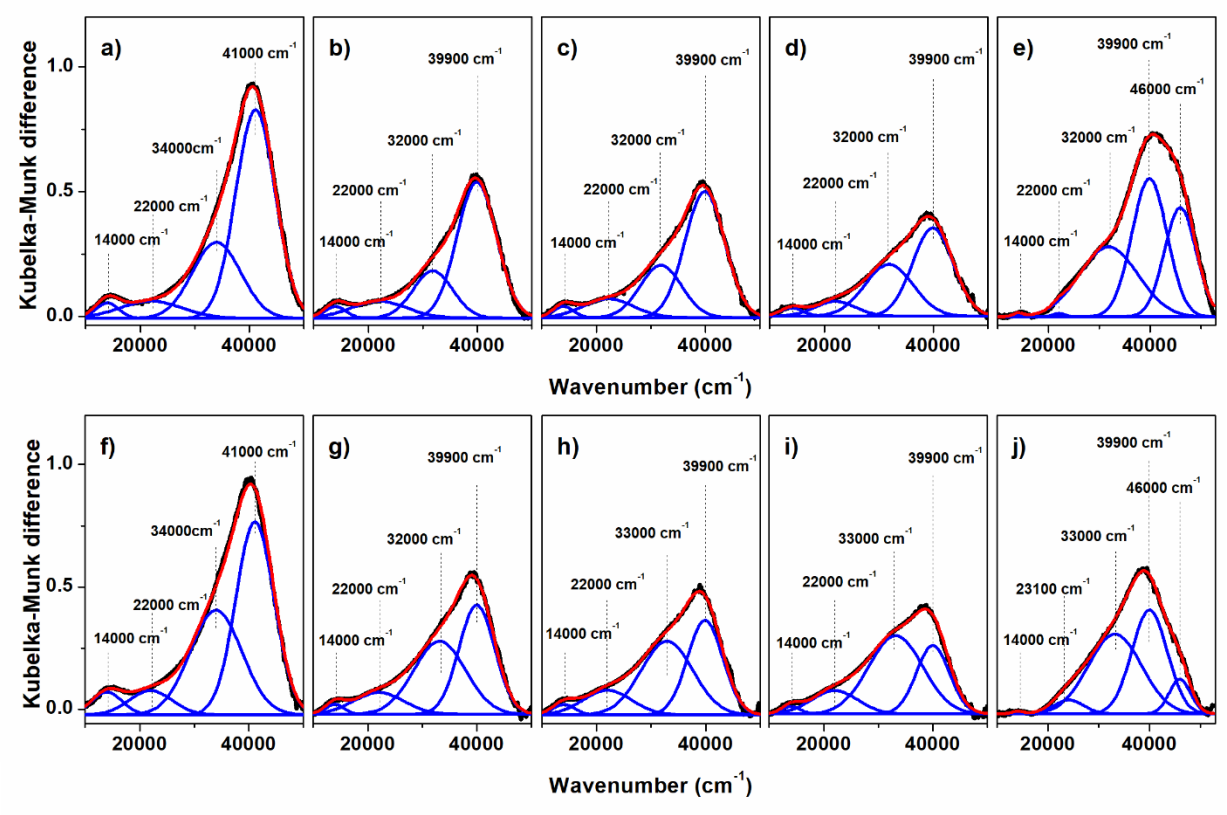

Figure 4. 6 DR UV-vis spectra under a flow of methane at different temperatures for Cu-MOR(6.5)-(24h): (a) 150 ^oC; (b) 225 ^oC; (c) 250^oC; (d) 300 ^oC; (e) 350 ^oC; and for Cu-MOR(6.5)-(3x24h): (f) 150 ^oC; (g) 225 ^oC; (h) 250^oC; (i) 300 ^oC; (j) 350 ^oC. Spectra were subtracted from the ones of the samples calcined under O_2 flow at 450^oC. Spectra were deconvoluted using a Gaussian fitting and the black solid lines are the sample spectra and the red solid lines represent the sum of the fitting.

As mentioned before, the band at ca. 22000 cm^{-1} can be assigned to the $[Cu_2O]^{2+}$ active species (WOERTINK et al., 2009), however, previous studies showed that two different species could be present in Cu-MOR and they should generate bands at 21900 and 23100 cm^{-1} (BEZNIS; WECKHUYSEN; BITTER, 2010b) and both can be active towards the DMTM reaction (VANELDEREN et al., 2015). Cu-MOR(6.5)-(24h) displayed only the species at ca. 22000 cm^{-1} which were stable until 300 °C (Figure 4.6(a-d)) and nearly disappeared only when the temperature reached 350 °C (Figure 4.6(e)). As for Cu-MOR(6.5)-(3x24h), the DR UV-Vis band at ca. 22000 cm^{-1} due to the $[Cu_2O]^{2+}$ species was predominant (Figure 4.6(f-i)), however, as the temperature reached 350 °C, it was possible to identify the second type of $[Cu_2O]^{2+}$ species that presented a DR UV-Vis band at ca. 23000 cm^{-1} (Figure 4.6(j)). These results, along with the ones from Figure 4.5, showed that the formation of the active $[Cu_2O]^{2+}$ species took place in CH_4 presence and it was dependent on the temperature and Cu loading. Hence, only the sample with the highest Cu loading (Cu-MOR(6.5)-(3x24h)) presented both types of $[Cu_2O]^{2+}$ species indicated by the band at ca. 23000 cm^{-1} which appeared to be stable at temperatures higher than 300 °C.

However, we observed a band about ca. 12000 cm^{-1} in the spectra of the samples treated in O_2 (Figure 4.5), a band about ca. 14000 cm^{-1} was observed *in situ* in different temperatures (Figure 4.6) and both of these bands were related with active Cu^{2+} sites. The species associated with these features decreased significantly after CH_4 exposure at 350 ^oC. Indeed, at 350 ^oC (Figure 4.6 (e) and Figure (j)), a new feature was observed at high absorption energy (46000 cm^{-1}) and has been associated with a charge transfer of isolated Cu^{2+} sites coordinated with lattice oxygen (OORD; SCHMIDT; WECKHUYSEN, 2018; PRALIAUD, 1998). This result suggested that these isolated Cu^{2+} species were reduced by CH_4 in high temperatures of about 350 ^oC (Figure 4.6 (e) and (f)).

This absorption feature centered about ca. 32000 cm^{-1} was observed for both Cu-MOR(6.5) samples (Figures 4.6 (b-e) and Figure 4.6 (g-j)). Although this band has been associated to bis(μ-oxo)dicopper cores (HALFEN et al., 1996; KIM et al., 2017; LI et al., 2019) and/or single-site trinuclear copper oxygen $[Cu_3(\mu\text{-}O)_3]^{2+}$ complexes (GRUNDNER et al., 2015)

it would be reasonable to consider this band as a result of various species like copper-oxo clusters. The 29000 and 34000 cm^{-1} absorption features were observed in the low copper loading sample (Cu/Al= 0.10) spectra (Figure 4.5 (a)) and for the other samples with Si/Al = 6.5 interacting with CH_4 at low temperature (150 ^oC) (Figure 4.6(a) and (f)). The feature at 29000 cm^{-1} was assigned to the charge transfer transition from peroxo π^*_σ to Cu^{2+} related to an intermediate Cu–(O_2)–Cu peroxo species which disproportionate to yield the mono-μ-oxo dicopper sites (SMEETS et al., 2010a). Similar species were previously described as a fingerprint for active oxygen species (KIM et al., 2017). With the temperature increase from 225 to 300 ^oC this band (29000 cm^{-1}) was not resolved and the broadband at ca. 32000 cm^{-1} was observed (GRUNDNER et al., 2015; HALFEN et al., 1996; KIM et al., 2017; LI et al., 2019). The band at 34000 cm^{-1} has been ascribed to copper oxide cluster extra zeolite pore, found in Cu-SSZ-13 and Cu-SSZ-39 materials with high copper loading and low Si/Al ratio (IPEK et al., 2017).

4.4.3 In situ XANES

As mentioned above, the CO-DRIFTS analyses revealed Cu^{2+} and Cu^+ species, with a fraction of the Cu^{2+} being strongly reactive and reduced by CO at low temperatures. To obtain a better understanding of the Cu species and the changes in their distribution during the CH_4 oxidation reaction, *in situ* Cu K-edge XANES analyses were performed (Figure 4.7). For the Cu-MOR(6.5) set of samples, after activation in oxygen, a pre-edge was observed at 8977 eV, together with a high-intensity feature at 8986.3 eV, indicative of the bulk CuO and isolated Cu^{2+} species (MILLAR et al., 1999; VELU et al., 2002). Cu^+ species was not observed for these samples during the treatment with oxygen. After the reaction with CH_4, a characteristic cupric feature (Cu^+) was observed at 8983.5 eV, suggesting that a fraction of the Cu^{2+} species was reduced by (KAU et al., 1987; SUSHKEVICH et al., 2017b). Afterward, the CH_4 flow was replaced by water steam, with part of the Cu^+ species being re-oxidized to Cu^{2+} species which decreased with the Cu content increasing. Interestingly, for the samples treated with H_2O, the

CuO feature at 8996.3 eV was suppressed, suggesting the presence of hydrated Cu^{2+}, such as $[Cu(H_2O)_6]^{2+}$ (BATES et al., 2014). However, the CuO feature at 8996.3 eV was maintained in the samples with high Cu contents, such as Cu-MOR(6.5)-(2x24h).

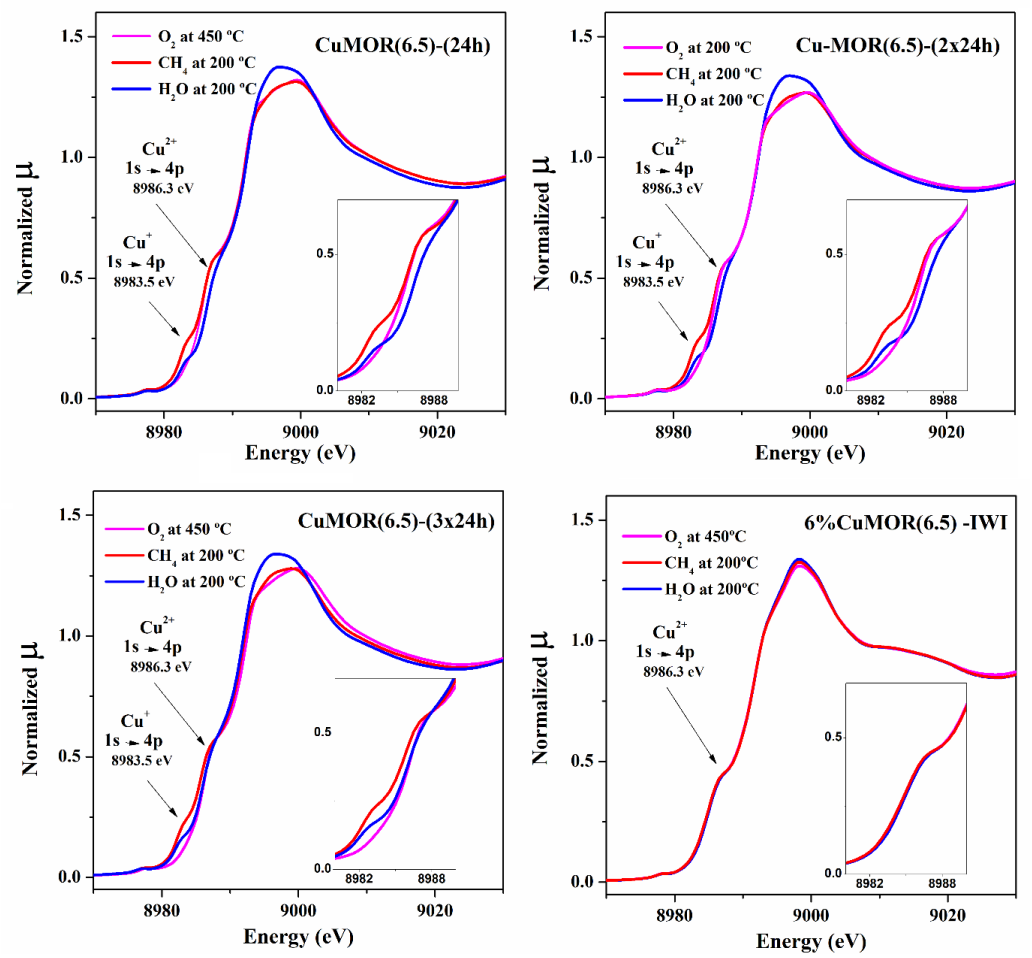

Figure 4. 7 Cu K-edge XANES spectra for the CuMOR6.5 samples treated in O_2, followed by methane activation, and desorption of methanol with water steam.

The impregnated 6%Cu-MOR(6.5)-IWI sample (Figure 4.7) presented a low-intensity feature at 8977 eV and a high-intensity feature at 8986.3 eV, attributed to bulk CuO species.

These features remained unchanged after exposure to CH_4, indicating that the sample was not active for CH_4 activation.

4.5 Discussion

The XRD results for the impregnated 6%Cu-MOR(6.5)-IWI sample before and after use in the reaction (data has been not shown) indicated that a fraction of the Na^+ was initially exchanged by Cu^{2+} ions in the channels of the MOR zeolites. However, during the DMTM reaction, Cu migrated to the outside of the channels, with the formation of bulk CuO oxide. The reaction data and the *in situ* XANES results indicated that the bulk CuO was not active for CH_4 oxidation. In contrast, the X-ray diffractograms for the Cu-MOR samples prepared by ion-exchange (data has been not shown), before and after use, showed no detectable segregation of bulk CuO oxides, suggesting that the Cu^{2+} species were stable and dispersed within the MOR channels.

On the other hand, the CuO_x species formed inside the MOR cavities following ion-exchange presented a fraction of Cu^{2+} that adsorbed CO (Figures 2 and 3), which was desorbed by heating from -95 to 5 °C, and a fraction of Cu^{2+} that was highly reactive with CO, which was easily reduced to Cu^+ at low temperatures of around -60 °C, even for samples with high Cu loadings. In the case of these Cu-MOR samples obtained by ion-exchange, *in situ* XANES indicated that the oxi-reduction of Cu^{2+} species was dependent on the Cu content. When activated in O_2, the spectra for these samples showed a feature at 8996.3 eV that was probably due to the 1s→4p transition of bulk CuO. A fraction of the CuO was reduced to Cu^+ by CH_4 at 250 °C, while a fraction was maintained in the CuO form. However, when these samples were treated underwater steam, the feature due to CuO decreased and was dependent on the Cu content. For the Cu-MOR(6.5)-(24h) sample with low Cu content, the CuO feature at 8996.3 eV was suppressed, indicating the hydration of isolated Cu^{2+} species such as $[Cu(H_2O)_6]^{2+}$. By increasing the Cu content, a fraction was maintained in the form of CuO species, even after treatment under a flow of water steam, indicating that this fraction of CuO had properties similar

to the bulk CuO present in the Cu-MOR prepared by impregnation, which was in the form of segregated bulk CuO particles outside the MOR channels. For the Cu-MOR prepared by ion-exchange, a fraction of stable CuO could be a contribution of inactive $(CuO_x)_n$ species with a high degree of oligomerization, present inside the MOR channels, while bulk CuO crystallites outside the channels were not detectable by XRD.

Interestingly, the XANES and CO-DRIFTS analyses showed that the Cu-MOR(6.5)-(24h) sample (Cu/Al = 0.25), which had the highest activity, displayed the most effective oxi-reduction profile. Consequently, this material showed the highest methanol yield (128 mmol g^{-1}), while the Cu-MOR(6.5)-(48h) material with a higher Cu/Al molar ratio (0.43) presented a much lower methanol yield (29 mmol g^{-1}).

The UV-vis results (Figures 4.4) revealed the presence of isolated Cu^{2+} and different Cu_xO_y species in the samples calcinated in O_2 at 450 ^oC. Considering that isolated Cu^{2+} species, in the as-prepared samples, were obtained in the Cu-MOR by Cu-exchanged, these ions could be partially hydrolyzed to Cu-OH^+ species by O_2 thermal treatment, as confirmed by UV-Vis spectroscopy analysis, and these $[CuOH]^+$ species were converted to $(CuO_x)_n$ oxides (GIORDANINO et al., 2013; SUSHKEVICH; VEREL; BOKHOVEN, 2020). Furthermore, *in situ* UV-Vis spectra (Figure 4.5-4.6) strongly indicated that the isolated Cu^{2+} species present in Cu-MOR were not involved in CH_4 oxidation at temperatures lower than 300 ^oC, evidenced by the absence of the features at high wavenumber (~46000 cm^{-1}) in the difference of samples spectra activated in O_2 and exposed to CH_4 (Figure 4.6). This suggests that isolated Cu^{2+} species can be reduced by CH_4 only in higher reaction temperatures (350 ^oC) (Figure 4.6 (e) and (j)).

Although previous works have been indicated that mononuclear species associated with the band at 14000 cm^{-1} were not active for CH_4 activation (BEZNIS; WECKHUYSEN; BITTER, 2010b), our results suggested that these species were involved in CH_4 activation at low temperatures. Interestingly, *ab initio* molecular dynamics and time-dependent density functional theory (DFT) calculations of UV-Vis spectra for Cu-SSZ-13 revealed that bands of low intensity at about ca.14000 cm^{-1} could be the bands associated to species like $[CuOH]^+$, CuOOCu and Cu-O-Cu (LI et al., 2019), which also could present bands at the region between ca. 22000 and

39000 cm^{-1}. Although the band at high frequency (39000 cm^{-1}) could be associated to the same Cu species that also generate the band at 14000 cm^{-1}, they could be both involved in CH_4 activation due to the presence of $[CuOH]^+$ and/or CuOOCu species. Besides, previous DFT calculations concluded that $[CuOH]^+$ species in the 8MR were responsible for the experimental activity of Cu-exchanged SSZ13 (KULKARNI et al., 2016b).

As it regards to the dicopper mono-μ-oxo sites, which in Cu-MOR present two different species yielding DR UV-Vis bands at 21900 and 23100 cm^{-1}, it has been shown that the species have different stabilities to the reaction temperature (VANELDEREN et al., 2015). Nonetheless, the species associated with the band at 23100 cm^{-1} were observed only for the sample with higher Cu content (Cu-MOR(6.5)-(3x24h)) and at a high temperature of CH_4 activation (350^oC) (Figure 4.6 (j)). Considering that these dicopper mono-μ-oxo species could be stabilized in AlT3−O−SiT1−O−SiT1−O−AlT3 and AlT4−O−SiT2−O−SiT2−O−AlT2 (VANELDEREN et al., 2015), it was reasonable to expect that increasing Cu content consequently will increase the Cu occupation degree, also increasing the specific activity that tended to a constant value. However, the specific activity showed a maximum with an optimum Cu/Al ratio and two hypotheses could be considered: i) the active Cu-O-Cu sites initially formed were modified with the Cu content increase; ii) very active sites were initially present in addition to the Cu-O-Cu species.

The absorption at 30000 and 34000 cm^{-1} were resolved for Cu-MOR(6.5)-(12h) with low Cu contents (Figure 4.5 (a)). With the increase of Cu loading and reaction temperature (>150 ^0C), these bands seem enveloped, shifting its maximum to about 31850 cm^{-1}. Considering that species in this region (~31000 cm^{-1}) like peroxo dicopper core and/or single-site trinuclear copper oxygen $[Cu_3(\mu\text{-}O)_3]^{2+}$ complexes were described as active to methanol formation (GRUNDNER et al., 2015; HALFEN et al., 1996; KIM et al., 2017; LI et al., 2019) and the species at 34000 cm^{-1} have been related as copper oxide clusters extra pore (IPEK et al., 2017), our results indicated that species associated with the band of about 34000 cm^{-1} become more important relative to the species at ~30000 cm^{-1} with the increase of Cu content.

Furthermore, the presence of active sites such as trans-(μ1,2-peroxo) dicopper(II) core in 12 MR channels of MOR was not ruled out (PAPPAS et al., 2018). The polynuclear copper oxides could be formed in 12 MR channels or even anchor in exposed T4 Al sites modifying peroxo dicopper species and mono(μ-oxo) dicopper(II) cores.

Although both species related to 30000 and 34000 cm^{-1} bands were involved in CH_4 activation, recent work demonstrated quantitative evidence of the active sites nuclearity, where dicopper sites were active for selective methane oxidation (PAPPAS et al., 2018). Therefore, the formation of polynuclear species in substitution of dicopper would impact the specific activity with the Cu content.

The increased content of $[CuOH]^+$ species increased the proximity of these species, and their abundance was proportional to the $(Cu/Al)^2$ ratio, which favored the subsequent formation of polynuclear species, such as dicopper mono-μ-oxo species and trimeric species, by dehydration (PALAGIN; SUSHKEVICH; VAN BOKHOVEN, 2019; SUSHKEVICH; VEREL; BOKHOVEN, 2020). Hence, it was expected that the degree (n) of polynuclear species $(CuO_x)_n$ should increase with the Cu content, where $[CuOH]^+$ species were the precursors of polynuclear species formed by heating in a flow of oxygen. As shown in Figure 4.8, the methanol yield was strongly dependent on the $(Cu/Al)^2$ ratio, indicating that it was also dependent on the density of precursor neighboring $[CuOH]^+$ species in the MOR channels.

Therefore, it is plausible to consider that: i) Cu^{2+} ions or isolated $[CuOH]^+$ species compensated the charge of the zeolite cage and these species were not able to promote the CH_4 oxidation; ii) the degree of hydrolysis during the treatment in O_2 increased with Cu content as confirmed by UV-Vis, generating new acid sites; iii) the species involved in CH_4 activation were similar in different Cu contents; iv) the inactivity of the Cu-MOR samples with lower Cu contents was associated with the low $(Cu/Al)^2$ ratios (Figure 4.8).

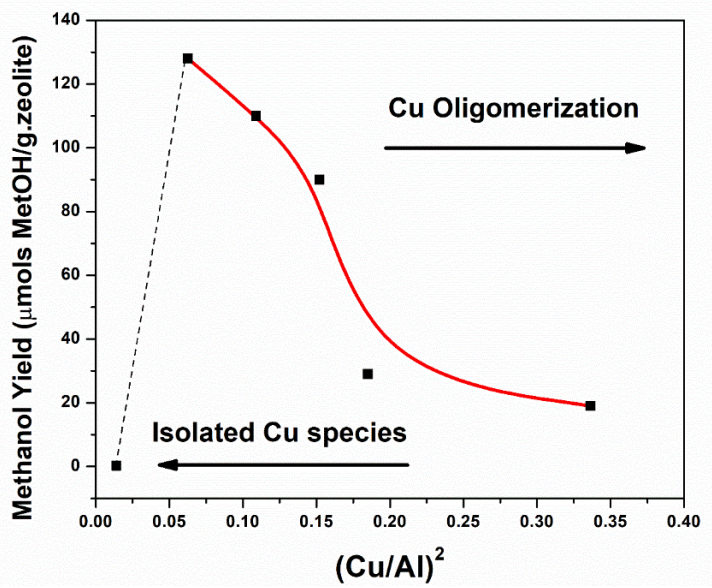

Figure 4. 8 Correlation between $(Cu/Al)^2$ ratio and methanol yield.

Since neighboring $[CuOH]^+$ species and $(CuO_x)_n$ were able to oxidize CH_4, herein, we propose a reaction mechanism in Scheme 4.1 using both Cu-oxo and dicopper mono-μ-oxo species (ALAYON et al., 2015b). According to the CH_4 oxidation pathway shown in Scheme 4.1A, in the presence of H_2O, neighboring Cu^{2+} species could generate active precursors such as $[CuOH]^+$ and acid sites, as previously demonstrated by Sushkevich et al. (SUSHKEVICH; VEREL; BOKHOVEN, 2020). The activation of CH_4 by $2[Cu\text{-}OH]^+$ sites led to the methoxy intermediate, forming Cu^+ species, such as $[Cu\text{-}OCH_3\text{-}Cu]^+$, and Brønsted acid sites with coordinated H_2O, such as $Al\text{-}OH(H_2O)\text{-}Si$ sites.

The conversion of $[CuOH]^+$ by treatment in oxygen at high temperatures could lead to the consecutive formation of dimeric or trimeric copper-oxo oligomer clusters of the type $(CuOx)_n$ (MEYET et al., 2019). The degree of oligomerization (n) was favored by increasing the Cu/Al ratio, which was reflected in an increased density of $[CuOH]^+$ precursors neutralizing charges at nearby sites (Figure 4.8).

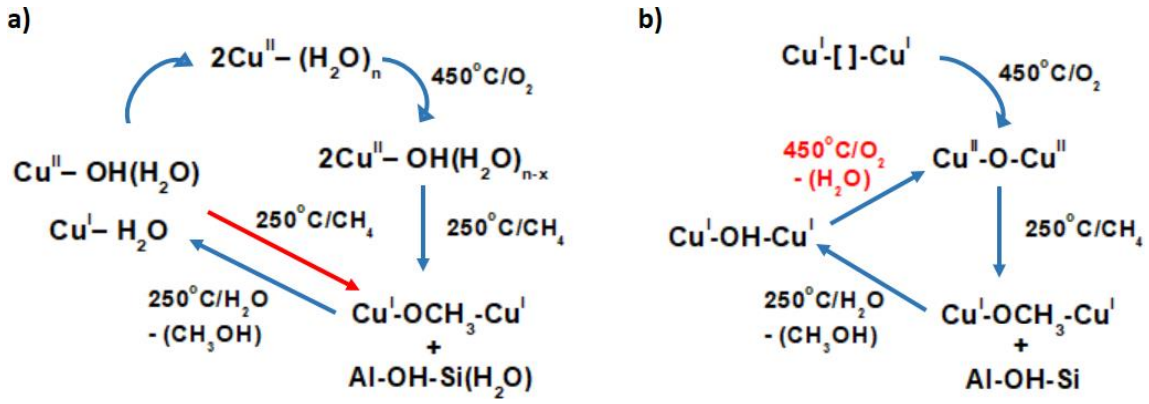

Scheme 1 Pathway for the DMTM reaction over: a) isolated Cu-oxo species and b) dicopper mono-μ-oxo species.

In this case, the $(CuO_x)_n$ clusters were active in CH_4 oxidation. The DMTM could follow the reaction pathway shown in Scheme 4.1B (SUSHKEVICH; VEREL; BOKHOVEN, 2020), where dicopper mono-μ-oxo species reacted with CH_4, forming a methoxy intermediate species adsorbed on a Cu^+ site $[Cu\text{-}OCH_3\text{-}Cu]^+$ and a free Brønsted acid Al-OH-Si site, where Cu^{2+} was reduced to Cu^+. However, the formation of the $[Cu_2O_2]^{2+}$ active sites from the precursor $[CuOH]^+$, as proposed by Lobo and co-workers (IPEK et al., 2017), cannot be discarded.

The DR UV-Vis results suggested that the band of about 32000 cm^{-1} could reflect the presence of species with a high oligomerization degree, formed by successive Cu-exchange procedures, which increased with Cu content and the decreasing of the specific activity.

In both reaction pathways (Schemes 4.1A and 4.1B), intermediates such as $[Cu\text{-}OCH_3\text{-}Cu]^+$ were formed. However, in pathway 1A, the formation of these $[Cu\text{-}OCH_3\text{-}Cu]^+$ intermediates was followed by the formation of Brønsted acid sites with coordinated H_2O, such as Al-OH(H_2O)-Si sites. These groups could react with each other to form $[Cu\text{-}OH\text{-}Cu]^+$ and Al-OH(CH_3OH)-Si, with easy desorption of CH_3OH under a flow of water steam. In pathway 4.1B, the formation of the $[Cu\text{-}OCH_3\text{-}Cu]^+$ intermediate was followed by the formation of the (Al-OH-Si) Brønsted acid site. In the absence of H_2O and dependent on temperature, these groups could react, with the formation of $[Cu\text{-}OH\text{-}Cu]^+$ and Al-(O-CH_3)-Si. These stable methoxy groups

were then difficult to desorb, resulting in decreases in activity and selectivity (SUSHKEVICH; VAN BOKHOVEN, 2018; SUSHKEVICH; VEREL; BOKHOVEN, 2020).

Given that the Cu-MOR samples were activated at high temperature in O_2, it was reasonable to suppose that at low Cu contents, there was the presence of isolated Cu^{2+} and $[CuOH]^+$ (Figure 4.6), which were inactive towards CH_4 activation. By increasing the Cu content, the main species formed could be neighboring 2-$[CuOH]^+$ and O-[Cu-O-Cu]-O sites. Therefore, the higher activity found with the increase of the Cu/Al ratio indicated that these sites were more active for CH_4 conversion to CH_3OH. Further increase of the Cu content favored the formation of polynuclear species such as $(CuO_x)_n$. The strong decrease of activity towards methanol formation, as the Cu/Al ratio was increased, indicated that polynuclear species such as $(Cu\ O_x)_n$ exhibited low activity towards methanol formation.

The XAS results for the Cu-MOR(6.5)-(24h) sample indicated that during CH_3OH desorption, the Cu^+ species were re-oxidized to Cu^{2+}. It could be considered that the main active sites in these materials activated in O_2 were O-[Cu-O-Cu]-O sites, which after CH_3OH desorption resulted in $[Cu\text{-}OH\text{-}Cu]^+$ and Al-OH-Si sites (Scheme 4.1B). Therefore, this re-oxidation was likely to proceed according to Equation 4.1.

$$[Cu\text{-}OH\text{-}Cu]^+ + Al\text{-}OH\text{-}Si \leftrightarrow 2\text{-}[O\text{-}Cu\text{-}]^{2+} \leftrightarrow 2[O\text{-}CuOH]^+ \quad \text{(Equation 4.1)}$$

With the increase of the Cu/Al ratio and under a flow of water steam, the re-oxidation of Cu^+ decreased. The re-oxidation only occurred at high temperatures under a flow of O_2, resulting in changes in the formation of active sites, due to the presence of poly(copper-oxo) oligomers.

The increase of the Si/Al ratio increased the average distance between the Cu^{2+} cations on the zeolite, so a higher Cu content was required to trigger the oligomerization reactions that allowed the formation of copper-oxo active sites.

The selectivity for CO_2 was also strongly related to the active species involved in the reaction. With the increase of the copper content, the selectivity to CO_2 also increased (Table

4.2). Given that oligomerization of the Cu species could occur in the samples with higher Cu contents, it was plausible that these Cu oligomers were not selective to methanol, but were active for the total oxidation of methane. The oligomerization reactions resulted in Cu_n-oxo clusters capable of higher oxygen storage, with this high availability of oxygen atoms favoring the total oxidation of methane to CO_2.

4.5 Conclusions

The findings of this work showed that the active Cu species in mordenite (MOR) depended on the Cu/Al and Si/Al ratios, as well as the sample preparation method. The Cu-exchanged samples were active in the oxidation of CH_4 to methanol, with the Cu/Al ratio strongly affecting their performance.

The activity results showed that there was an optimal Cu/Al ratio. The methodology used for analyses of the *in situ* UV-Vis spectra indicated that various Cu species were active in CH_4 oxidation. Isolated Cu^{2+} species were not involved in CH_4 activation at temperatures lower than 300 ^{0}C. The isolated Cu^{2+} species were partially hydrolyzed by treatment under O_2 flow and species like $[CuOH]^+$ and $[CuO_x]_n$ were formed.

The samples were practically inactive at a low Cu/Al ratio, which was attributed to the presence of isolated Cu^{2+}, which undergoes a low degree of hydrolysis to the formation of $[CuOH]^+$ and the acid sites. The increase of the Cu/Al ratio led to an abrupt increase of activity, due to a higher density of precursor $[CuOH]^+$ species, which increased the probability of these species being located at distances favorable for the formation of polynuclear Cu species. The highly active dicopper mono-μ-oxo sites were formed by the treatment of the precursor 2-Cu-OH^+ species at high temperature under a flow of oxygen.

The increase of the Cu/Al ratio and decrease of the Si/Al ratio favored the formation of polynuclear compounds such as $(CuO_x)_n$, which presented lower specific activity for the oxidation of methane to methanol.

Followed by the spectroscopic pieces of evidence raised on this work, it is clear that there was a multiplicity of the active copper structures on copper-exchanged mordenite zeolite for CH_4 oxidation of at low temperatures. However, the origin of its activity still requires further understanding.

CHAPTER 5: DIRECTING Cu SITES ON MAZZITE ZEOLITE BY ACIDIC DEALUMINATION

Stefanie C. M. Mizuno[1,2], Jose M. C. Bueno[1], and Jeroen A. van Bokhoven[2,3*]

[1] Federal University of São Carlos, P.O. Box 676, 13565-905, São Carlos, Brazil

[2]Paul Scherrer Institute, Villigen, CH-5232, Switzerland

[3]ETH Zurich, Vladimir-Prelog-Weg 1, Zurich, CH-8093, Switzerland

5.1 Introduction

Since its discovery, Cu-exchanged zeolites for MMet reaction are widely studied in terms of how to improve the activity and stability of these materials. Despite the applicability of this process has been hardly studied, the fundamentals involved in this process still not clear and are gaining more and more attention(RAVI; RANOCCHIARI; VAN BOKHOVEN, 2017; ZAKARIA; KAMARUDIN, 2016b).

As discussed in the previous chapters, the active sites for MMet reaction in Cu-exchanged zeolites still in warm discussion on the scientific community (PALAGIN et al., 2017; RAVI; RANOCCHIARI; VAN BOKHOVEN, 2017). Especially for MOR, different active sites have been described by literature, such as mononuclear Cu sites, tri-nuclear, binuclear, isolated or not and others (GRUNDNER et al., 2015; KULKARNI et al., 2016a; MAHYUDDIN et al., 2018; PALAGIN et al., 2017).

In fact, as observed in Chapter 2.2 Figure 2.6 Mordenite presents a relatively complex framework, with a three-dimensional structure with 4 T-Al atoms allowing different Cu distribution in the structure when exchanged (MEIER, 1961). Therefore, fundamental studies about the Cu species on MOR zeolite become challenging. Other zeolites framework both active on MMet reaction and simpler structure could be an alternative for a deep understanding of these active Cu species. MAZ zeolite presents a large-pore structure, which favors MMet reaction, but a simpler framework when compared with MOR with a one-dimensional structure and only 2 T-Al atoms (Figure 5.1) (MARTUCCI et al., 2003).

Another special characteristic of MAZ structure is that its T-atoms can be identified by ^{27}Al Nuclear Magnetic Resonance (^{27}Al NMR), which could facilitate the comprehension of this material (MARTUCCI et al., 2003).

The ^{27}Al NMR technique is vastly employed in the research of zeolite and its properties. For the spectra of zeolites, usually, the signal around 60 ppm is related to tetrahedrally coordinated aluminum on the framework (T-Al) and around 0 ppm octahedrally coordinated Al species not in the framework, the so-called “extra-framework” Al (EFAl) (KLINOWSKI, 1991).

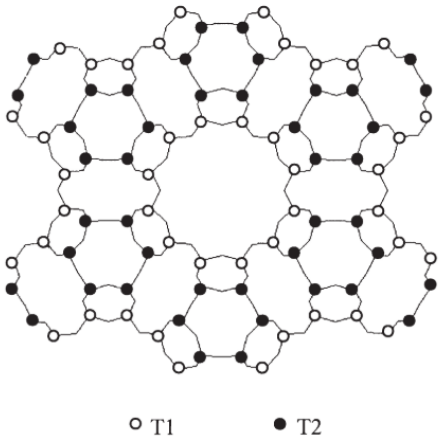

Figure 5. 1 Projection of the MAZ topology over the [001] axis indicating the two crystallographically non-equivalent tetrahedral sites denoted as T1 and T2. Adapted from (GOOSSENS et al., 2000).

Post-synthesis treatments on zeolite are also widely studied and employed to improve the zeolite interested properties and in some cases a crucial step on the zeolite final form for commercialization. Usually, for zeolites, the post-synthesis consists in remove Al or Si aiming to control acid-base properties, besides the increase in its stability by steaming treatments (RAHBARI; KHOSRAVAN; KHARAT, 2017).

In this chapter, we studied MAZ zeolite passing through a post-synthesis treatment trying to control the Al distribution and employed ^{27}Al NMR to identify the changes. Then, by using ion-exchange method, the Cu sites were introduced on the modified MAZ structure and study about how this material performs on MMet reaction was conducted.

5.2 Materials and Methodology

5.2.1 Mazzite hydrothermal synthesis

The MAZ zeolite was synthesized using a hydrothermal method with a molar composition of 10 SiO_2: 1 Al_2O_3: 3.2 Na_2O: 0.8 TMA_2O: 106 H_2O. Sodium aluminate and Ludox AS-30 was used as aluminum and silicon source, respectively. The directing agent was

Tetramethylammonium hydroxide. The gel slurry was transferred to a Teflon autoclave and placed in a static oven at 100ºC for 13 days. The samples were then rinsed with ethanol and water and dried at 80ºC overnight. The dried powder was then calcined at 550º for 8 hours with a rate of 1°C/min.

5.2.2 NH_4- Cation exchange

The sample was stirred in a 2M solution of ammonium nitrate for 24hr at room temperature (100 mL solution per gram of zeolite). The sample was filtered, rinsed with deionized water and dried overnight at 80ºC.

5.2.3 Cu- cation exchange

The zeolite (Na- and NH_4- form) was cation-exchanged with 0.025M or 0.0125M of aqueous copper nitrate solution (100 mL solution per gram of zeolite). Each sample was exchanged from one to three times. Between each exchange, a fresh solution was prepared, and the sample filtered.

5.2.4 Acidic post-treatment

Nitric acid (70% pure, Merck) was used as a dealuminating agent. The MAZ zeolite was submitted to an acid attack using 1 M nitric acid solution at 70 °C for 1 hour. The volume V of the nitric acid solution used (in mL) was equal to 10 times the weight P (in grams) of dry zeolite (V/P = 10). After the acid leaching, the zeolite was washed with water. Next, the zeolite was dried overnight at 100 °C. The dealuminated samples were labeled as DEA-X, where X= Na-MAZ or H-MAZ.

5.2.5 NMR, XRD, SEM and AAS

^{27}Al Magic Angle Spinning Nuclear Magnetic Resonance (MAS NMR) measurements were performed on a Bruker 400 UltraShield spectrometer at a resonance frequency of 104.29 MHz. A 4 mm MAS probe was filled with each sample and spun at 10 kHz. Chemical shifts were referenced to $(NH_4)Al(SO_4)_2 \cdot 12H_2O$ for aluminum.

The powder XRD patterns were collected in a Bruker D8 diffractometer using Cu-Kα radiation (λ = 1.5418 Å, 40 kV, 40 mA). Data were recorded from 5 to 60 2θ range with a step size of 0.02° and a counting time of 0.068s per step.

SEM images of the calcined sample were obtained with a Zeiss Gemini 1530 instrument that was operated at 5 keV.

The chemical composition was determined by Atomic Absorption Spectroscopy (AAS). Copper (Cu), aluminum (Al), and silicon (Si) content were determined using SpectraAA 220FS atomic absorption spectrometer. Approximately 10 mg of dried sample was digested in 2 ml of concentrated hydrofluoric acid and 3 ml of concentrated nitric acid overnight and then diluted to 50ml with deionized water. Copper, aluminum, and silicon calibration curves were prepared from standard solutions.

5.2.6 Activity testing

Zeolite samples were sieved to 150-250μm. Approximately 0.3 grams of samples were loaded into stainless steel autoclave (Premex Reactor Ag). Samples were activated at 450ºC under pure O_2 flow (~25mL/min) for 1 hour. The reactors were cooled down to the selected temperature (200ºC, 250ºC or 300ºC) and then purged for 15 minutes in pure helium flow. Pure methane was then introduced at 1 bar or 6 bar into the reactor and kept at the chosen temperature for 30 minutes. The reactor was then cooled down to room temperature under pure Helium flow and methanol was extracted by off-line method using liquid water solution and the product were analyzed by GC.

5.3 Partial results and discussion

Table 5.1 presents the chemical composition of parent MAZ and dealuminated samples. For the Na-MAZ the Si/Al of 4.04 increased to 12.25 and for H-MAZ the Si/Al ratio increased from Si/Al=4.03 to 17.02.

Table 5.1 - Chemical composition of MAZ samples.

SAMPLE	Si/Al
Na-MAZ	4.04
NH_4-MAZ	4.03
H-MAZ	3.34
DEA Na-MAZ	12.25
DEA H-MAZ	17.02

It is plausible that the H-MAZ form presented a higher dealumination degree since this form of MAZ is more unstable presenting more EFAl species susceptible to leaching by the acidic treatment (MASSIANI; FAJULA; DI RENZO, 1988; WEEKS; BOLTON, 1976).

Figure 5.2 presents the XRD for parent MAZ and the dealuminated samples. The XRD patterns for the as-synthesized Na-MAZ and NH_4-MAZ presented the reflection peaks characteristics of highly pure and crystalline MAZ zeolite (MARTUCCI et al., 2003).

However, the loss of intensity in the peaks of the acidic form of MAZ might indicate a loss of crystallinity due to the H-MAZ form instability. The dealumination procedure clearly affected the zeolite structure indicated by the diffuse background and narrow peaks on the dealuminated samples diffractogram. These results strongly suggested that the acidic treatment partially destroyed the zeolite structure turning the material partially amorphous (CHAUVIN et al., 1990).

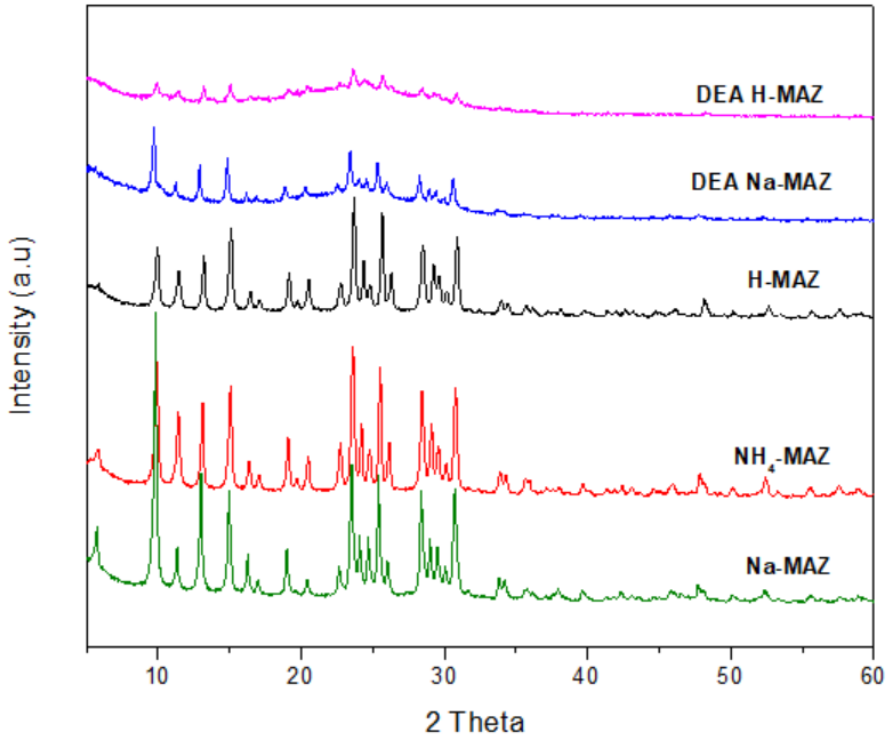

Figure 5. 2 XRD patterns for MAZ zeolite samples.

Despite the dealuminated materials displayed an amorphous phase, a MAZ phase was still present evidenced by its characteristic structure reflections observed after the acidic treatment (Fig.5.2). After the acid leaching, the samples were submitted to a Cu-exchanged procedure and the chemical composition results are presented in Table 5.2.

Table 5.2 Chemical composition of Cu-exchanged DEA-MAZ samples.

SAMPLE	Si/Al	Cu wt%	Cu/Al
Cu-DEA-Na-MAZ	11.42	1.58	0.27
Cu-DEA-H-MAZ	17.06	2.02	0.35

Both dealuminated samples presented Cu content, for Cu-DEA-Na-MAZ a Cu/Al= 0.27 and for Cu-DEA-H-MAZ a Cu/Al = 0.35, indicating that the Cu-exchange occurred.

These results might indicate that despite the acid leaching, there was still Al coordinated in the framework to be counterbalanced by the cation (H^+ or Na^+) and exchanged with the copper ions. This assumption can be reinforced when we observed the SEM images for the as-synthesized MAZ (Figure 5.3a)) and the Cu-exchanged dealuminated MAZ (Figure 5.3b)).

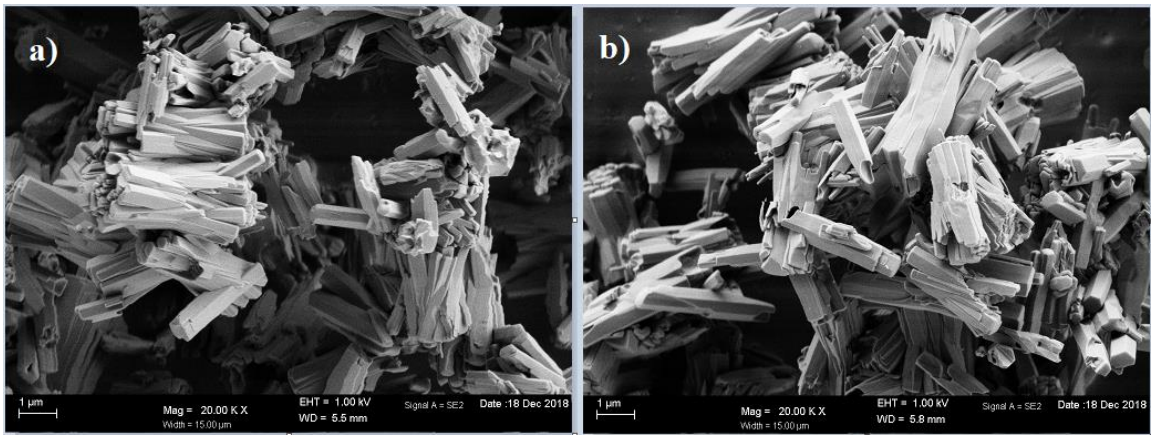

Figure 5. 3 SEM images of a) Na-MAZ; b) Cu-exchanged DEA MAZ.

By observing Fig.5.3 it can be inferred that the structure of dealuminated MAZ visually appeared not to be affected by the acidic treatment, the crystal shape was similar than observed for the parent MAZ zeolite (Fig. 5.3a)) and no segregated CuO was observed after the Cu-exchange (Figure 5.3b)). This further indicated that the dealuminated zeolite still contained exchangeable Al-sites in its framework.

By the XRD patterns for the Cu-exchanged DEA MAZ samples (Figure 5.4) it can be concluded that the Cu was well dispersed since no CuO reflections peaks were observed. Also, no segregated phases of Al or Si were observed despite the amorphous phase was still present(CHAUVIN et al., 1990).

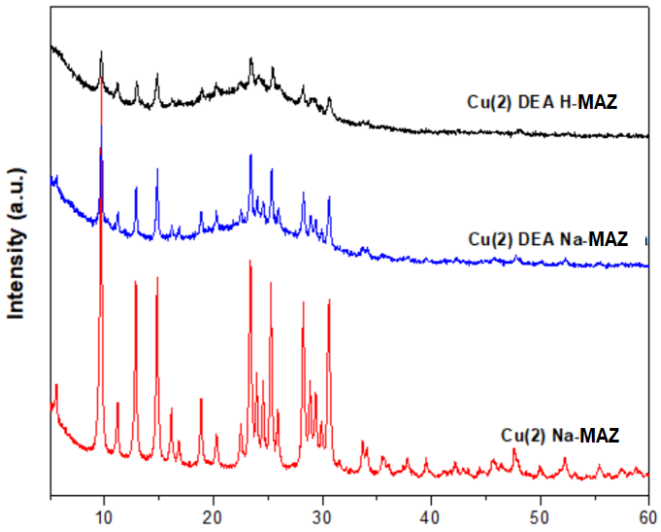

Figure 5. 4 XRD patterns for Cu-exchanged DEA MAZ samples.

^{27}Al NMR was employed to investigate the Al on the samples and the results and respective fit (using the Gaussian method) firstly for parent Na-MAZ zeolite are presented in Figure 5.5.

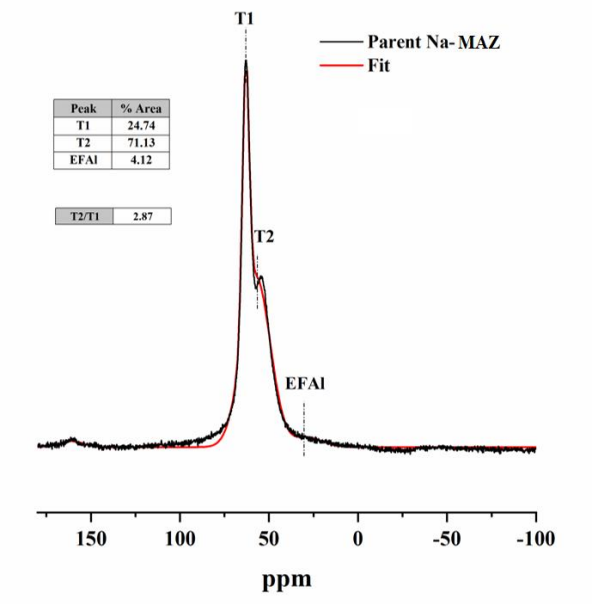

Figure 5. 5 ^{27}Al NMR spectrum for parent Na-MAZ zeolite and the respective Gaussian fitting.

As mentioned above, MAZ zeolite presents a special characteristic that its two T-sites (T1 and T2) can be easily distinguished by ^{27}Al NMR spectroscopy. Hence, through the parent MAZ NMR spectrum, it was possible to estimate the relative percentage of T1 and T2 sites.

The signal in about 60 ppm on the parent Na-omega spectrum (Fig. 5.5) can be assigned to the framework tetrahedrally coordinated Al atoms T1 (left) and T2 (right), and the signal at 0 ppm was attributed to EFAl atoms in an octahedral environment(BARRAS; KLINOWSKI; MCCOMB, 1994; CHEN et al., 2004).

The fitting results indicated that about 71 % of the T-sites of Na-MAZ zeolite were the T1 type, about 25% T2 site and 4% of the aluminum was extra-framework. The relative ratio of T2/T1 was about 2.9, indicating an Al disordered distribution (MARTUCCI et al., 2003; MASSIANI; FAJULA; DI RENZO, 1988). Figure 5.6 presented the ^{27}Al NMR spectra of the dealuminated Na-MAZ and H-MAZ samples.

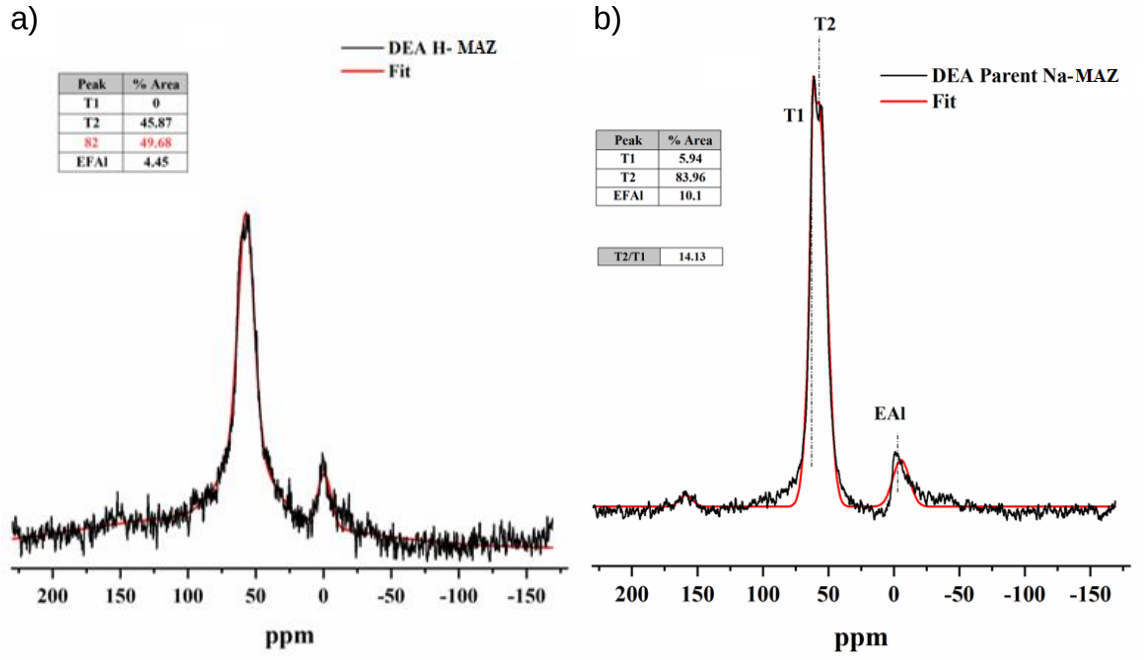

Figure 5. 6 ^{27}Al NMR spectra for dealuminated H-MAZ (a) and Na-MAZ (b) zeolites and the respective Gaussian fitting.

After the acid leaching, there was an increase in the Si/Al for both dealuminated samples (Table 5.1), hence, an increase in the T2/T1 ratio was observed, since majorly the T1 site was removed by the treatment. For the DEA Na-MAZ sample (Fig. 5.6 a)), the T2/T1 ratio increased to about 14 and the fitting results appointed to about 84 % of T-sites being T2 sites and 6% T1 sites. In fact, the acid leaching procedure caused a formation of EFAl species, about 10 % in the DEA Na-MAZ as estimated by fitting the peak around 0 ppm.

For the DEA H-MAZ (Fig. 5.6 b)), despite the Gaussian fit was performed in the spectrum, the signal-to-noise ratio was not favorable to a reliable fitting. But by the spectrum analysis, it can be inferred that almost all T1 aluminum was leached from the sample with a formation of EFAl evidenced by the peak around 0 ppm.

The Cu-exchanged DEA samples were submitted to MMet reaction and the results were presented in Table 5.3. A non-dealuminated Cu-Na-MAZ sample was also added for comparison.

Table 5.3 - Methanol yield after one reaction cycle for MAZ samples.

Sample	**Si/Al**	**Cu wt%**	**Cu/Al**	**μmol CH_3OH/g.zeo**	**μmol CH_3OH/ Mol Cu**
Cu-Na-Omega	3.99	4.90	0.24	101.00	0.12
Cu-DEA-Na-MAZ	11.42	1.58	0.27	9.00	0.04
Cu-DEA-H-MAZ	17.06	2.02	0.35	0.00	0.00

The non-dealuminated Cu-Na-MAZ sample presented 101 micromoles of methanol per gram of zeolite. In contrast, the Cu-DEA-Na-MAZ sample presented 9 micromoles methanol per gram of zeolite and Cu-DEA-H-MAZ presented no activity on MMet reaction.

These results suggested that the copper species contained in the dealuminated samples were not active for MMet reaction or that the harsh conditions of the acid leaching destroyed the MAZ structure preventing the Cu sites formation.

Nevertheless, based on the evidence presented above by the XRD and NMR results, it can be inferred that the dealuminated MAZ samples still presented framework integrity. Thus, the hypothesis that the copper species contained in the dealuminated samples were not active for MMet reaction is still relevant.

By comparing the activity results for the Cu-Na-MAZ (Si/Al = 3.99) and DEA-Cu-Na-MAZ (Si/Al=11.43) in terms of micromoles of methanol per mols of Cu it can be observed a result of 0.12 for Cu-Na-MAZ and 0.04 for DEA-Cu-H-MAZ (Table 5.3). The activity per mols of Cu decreased by about 3 times for the dealuminated sample while the T2/T1 ratio observed by NMR (Fig.5.6) increased.

Mahyuddin et al. (MAHYUDDIN et al., 2018) studied by DFT calculations the possible active species for MMet reaction founded in the MAZ zeolite (Figure 5.7).

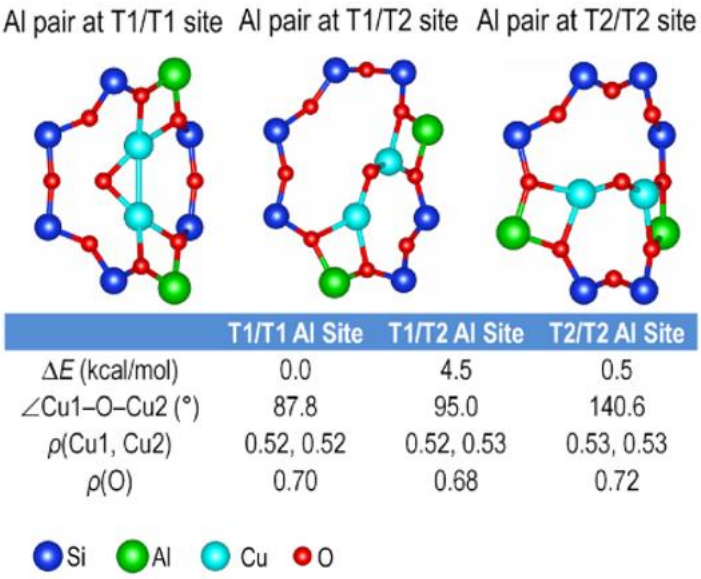

	T1/T1 Al Site	T1/T2 Al Site	T2/T2 Al Site
ΔE (kcal/mol)	0.0	4.5	0.5
∠Cu1–O–Cu2 (°)	87.8	95.0	140.6
ρ(Cu1, Cu2)	0.52, 0.52	0.52, 0.53	0.53, 0.53
ρ(O)	0.70	0.68	0.72

Figure 5. 7 - Optimized triplet-state structures of $[Cu_2(\mu\text{-}O)]^{2+}$ hosted on different Al pair sites of MAZ zeolite. Adapted from (MAHYUDDIN et al., 2018).

According to the authors, the T1/T1 Al site was the energetically most preferable site to host the $[Cu_2(\mu\text{-}O)]^{2+}$ species(MAHYUDDIN et al., 2018). In our case, as shown by NMR results

(Fig.5.6), the dealuminated samples had almost their T1 sites completely removed. Therefore, since the Cu-exchange still occurred it was plausible to infer that Cu species in MAZ was possible not hosted at T1/T1 Al site but hosted in minority in the T1/T2 Al site, and majorly on the T2/T2 Al sites.

Interestingly, despite the diminished activity for the DEA-Cu-Na-MAZ, the sample still presented one-third of the activity presented by the Cu-Na-MAZ (Table 5.3). This might indicate that the Cu species hosted in the T1/T2 Al site might be active for MMet reaction, since not al the T1 Al site could be removed from this sample remaining about 6% being the minority in the sample explaining the low but existent activity. On the other hand, the Cu species hosted on the T2/T2 Al sites seemed not to be active on MMet reaction.

5.4 Partial conclusions

We were able to dealuminate MAZ zeolite samples maintaining the zeolite framework. It was possible to remove in about 75% the T1 Al site increasing the T2/T1 ratio from 2.9 to 14.

Through the XRD and SEM images were possible to confirm that after the acid leaching, the MAZ zeolite still preserved its framework and exchangeable Al sites.

With the most T1 Al site removal, the Cu species preferably will be hosted in the T2/T2 sites and these species possibly were not active for MMet reaction.

CHAPTER 6: GENERAL CONCLUSIONS AND PERSPECTIVE

We were able to prepare active materials based on zeolites for MMet reaction by ion-exchange method and some observations can be made.

The zeolite counterion clearly affected the activity on MMet reaction and residual NH_4^+ cations showed to be benefic helping to protect the reaction intermediate species avoiding overoxidation to CO_x. EFAl species, generated after calcination of Cu-NH_4-Omega (MAZ), were beneficial may be for allowed the Cu species modification making them more accessible or active for MMet reaction.

The Cu content impacted the material properties as well as Si/Al ratio allowing different $(Cu_xO_y)^{2+}$ species formation with different reactivity toward MMet reaction. Our results for Cu-exchanged MOR suggested that high Cu content and low Si/Al ratio were unfavorable, especially for stability over the reaction cycles.

The FTIR results of adsorbed CO in Cu-MOR suggested that all the samples prepared by ion-exchange presented high active copper centers for CO total oxidation to CO_2 but maybe they were not active and/or selective for MMet reaction. While the sample prepared by the impregnation method presented CuO species that were outside of the zeolite cavity and showed lower reactivity with CO. The Cu-MOR samples prepared by multiple copper-exchange procedures showed an optimum Cu/Al ratio for the formation of the most active species for methanol production.

XANES spectra indicated that isolated Cu^+ species were formed after CH_4 interaction and were re-oxidized under a flow of water steam. The Cu-MOR samples obtained by the ion-exchange method presented well-dispersed CuO in the zeolite pores, while samples obtained by the impregnation method presented segregated CuO and were inactive for CH_4 activation.

The Cu-MOR prepared by multiple copper-exchange procedures showed an optimum Cu/Al ratio for the formation of the most active species for methanol production. XANES spectra also indicated that isolated Cu^+ species were formed after CH_4 interaction and were re-oxidized under a flow of water steam.

The methodology used for analyses of the *in situ* UV-Vis spectra indicated that various Cu species were active in CH_4 oxidation. Isolated Cu^{2+} species were not involved in CH_4

activation at temperatures lower than 300 ^{0}C. The isolated Cu^{2+} species were partially hydrolyzed by thermal treatment under O_2 flow and species like $[CuOH]^{+}$ and $[CuO_x]_n$ are formed. The formation of polynuclear species in substitution of dicopper species would impact the specific activity with the Cu content and decreasing the activity to methanol production.

The reoxidation step of the materials for possible reuse on a second reaction cycle could be the key to understand why the loss of activity and stability in reaction occurs in some cases, i.e. for Cu-MOR. Thus, we proposed to continue employing the XAS technique to characterize the materials after multiple MMet reaction cycles that allows following the structural changes of Cu species and its connection with the reaction activity and stability.

It was possible to direct the Cu sites in MAZ zeolite by preferably eliminate a Cu hosting T-Al site through an acidic post-treatment. Further investigation still needed may be employing DFT calculations to simulate the possible Al hosts for Cu species.

The use of other metal-exchanged materials like iron is also proposed since, in the opposite of Cu-exchanged zeolites material reports, the research about iron-exchanged zeolites for MMet reaction still not extense.

The methodology used for analyses of the *in situ* UV-Vis spectra indicated that various Cu species were active in CH_4 oxidation. Isolated Cu^{2+} species were not involved in CH_4 activation at temperatures lower than 300 ^{0}C. The isolated Cu^{2+} species were partially hydrolyzed by thermal treatment under O_2 flow and species like $[CuOH]^{+}$ and $[CuO_x]_n$ are formed. The formation of polynuclear species in substitution of dicopper species would impact the specific activity with the Cu content and decreasing the activity to methanol production.

REFERENCES

AL-SHIHRI, Saeed; RICHARD, Christian J.; CHADWICK, David. Selective Oxidation of Methane to Methanol over ZSM-5 Catalysts in Aqueous Hydrogen Peroxide: Role of Formaldehyde. **ChemCatChem**, *[S. l.]*, v. 9, n. 7, p. 1276–1283, 2017. DOI: 10.1002/cctc.201601563.

ALAYON, Evalyn Mae C.; NACHTEGAAL, Maarten; BODI, Andras; RANOCCHIARI, Marco; VAN BOKHOVEN, Jeroen. Bis(μ-oxo) versus mono(μ-oxo)dicopper cores in a zeolite for converting methane to methanol: an in situ XAS and DFT investigation. **Phys. Chem. Chem. Phys.**, *[S. l.]*, v. 17, n. 12, p. 7681–7693, 2015. a. DOI: 10.1039/C4CP03226H.

ALAYON, Evalyn Mae C.; NACHTEGAAL, Maarten; BODI, Andras; RANOCCHIARI, Marco; VAN BOKHOVEN, Jeroen A. Bis(μ-oxo) versus mono(μ-oxo)dicopper cores in a zeolite for converting methane to methanol: An in situ XAS and DFT investigation. **Physical Chemistry Chemical Physics**, *[S. l.]*, v. 17, n. 12, p. 7681–7693, 2015. b. DOI: 10.1039/c4cp03226h. Disponível em: http://dx.doi.org/10.1039/C4CP03226H.

ALAYON, Evalyn Mae C.; NACHTEGAAL, Maarten; BODI, Andras; VAN BOKHOVEN, Jeroen A. Reaction conditions of methane-to-methanol conversion affect the structure of active copper sites. **ACS Catalysis**, *[S. l.]*, v. 4, n. 1, p. 16–22, 2014. DOI: 10.1021/cs400713c.

ALAYON, Evalyn Mae C.; NACHTEGAAL, Maarten; RANOCCHIARI, Marco; VAN BOKHOVEN, Jeroen A. Catalytic Conversion of Methane to Methanol Using Cu-Zeolites. **CHIMIA International Journal for Chemistry**, *[S. l.]*, v. 66, n. 9, p. 668–674, 2012. a. DOI: 10.2533/chimia.2012.668. Disponível em: http://www.ingentaconnect.com/content/10.2533/chimia.2012.668.

ALAYON, Evalyn Mae; NACHTEGAAL, Maarten; RANOCCHIARI, Marco; VAN BOKHOVEN, Jeroen A. Catalytic conversion of methane to methanol over Cu-mordenite. **Chemical**

Communications, *[S. l.]*, v. 48, n. 3, p. 404–406, 2012. b. DOI: 10.1039/c1cc15840f.

ANDERSON, R. B.; STEIN, K. C.; FEENAN, J. J.; HOFER, L. J. E. Catalytic oxidation of methane. **Industrial and Engineering Chemistry**, *[S. l.]*, v. 53, n. 10, p. 809–812, 161.AD.

AREGBE, Azeez G. Natural Gas Flaring—Alternative Solutions. **World Journal of Engineering and Technology**, *[S. l.]*, v. 05, n. 01, p. 139–153, 2017. DOI: 10.4236/wjet.2017.51012.

ARUTYUNOV, Vladimir. Direct Methane to Methanol: Foundations and Prospects of the Process. **Direct Methane to Methanol: Foundations and Prospects of the Process**, *[S. l.]*, p. 1–309, 2014. DOI: 10.1016/C2012-0-06330-2.

BALASUBRAMANIAN, Ramakrishnan; SMITH, Stephen M.; RAWAT, Swati; YATSUNYK, Liliya A.; STEMMLER, Timothy L.; ROSENZWEIG, Amy C. Oxidation of methane by a biological dicopper centre. **Nature**, *[S. l.]*, v. 465, n. 7294, p. 115–119, 2010. DOI: 10.1038/nature08992. Disponível em: http://dx.doi.org/10.1038/nature08992.

BAÑARES, M. A.; FIERRO, J. L. G.; MOFFAT, J. B. **The partial oxidation of methane on MoO3/SiO2 catalysts: Influence of the molybdenum content and type of oxidantJournal of Catalysis**, 1993. DOI: 10.1006/jcat.1993.1218.

BARBAUX, Y.; ELAMRANI, A. R.; PAYEN, E.; GENGEMBRE, L.; BONNELLE, J. P.; GRZYBOWSKA, B. Silica supported molybdena catalysts. Characterization and methane oxidation. **Applied Catalysis**, *[S. l.]*, v. 44, n. C, p. 117–132, 1988. DOI: 10.1016/S0166-9834(00)80048-2.

BARRAS, Jamie; KLINOWSKI, Jacek; MCCOMB, David W. 27Al and 29Si solid-state NMR studies of dealuminated mordenite. **Journal of the Chemical Society, Faraday Transactions**, *[S. l.]*, v. 90, n. 24, p. 3719–3723, 1994. DOI: 10.1039/FT9949003719.

BATES, Shane A. et al. Identification of the active Cu site in standard selective catalytic reduction with ammonia on Cu-SSZ-13. **Journal of Catalysis**, *[S. l.]*, v. 312, p. 87–97, 2014. DOI: 10.1016/j.jcat.2014.01.004. Disponível em: http://dx.doi.org/10.1016/j.jcat.2014.01.004.

BEZNIS, Nadzeya V.; VAN LAAK, Adri N. C.; WECKHUYSEN, Bert M.; BITTER, Johannes H. Oxidation of methane to methanol and formaldehyde over Co-ZSM-5 molecular sieves: Tuning the reactivity and selectivity by alkaline and acid treatments of the zeolite ZSM-5 agglomerates. **Microporous and Mesoporous Materials**, *[S. l.]*, v. 138, n. 1–3, p. 176–183, 2011. DOI: 10.1016/j.micromeso.2010.09.009. Disponível em: http://dx.doi.org/10.1016/j.micromeso.2010.09.009.

BEZNIS, Nadzeya V.; WECKHUYSEN, Bert M.; BITTER, Johannes H. Partial oxidation of methane over Co-ZSM-5: Tuning the oxygenate selectivity by altering the preparation route. **Catalysis Letters**, *[S. l.]*, v. 136, n. 1–2, p. 52–56, 2010. a. DOI: 10.1007/s10562-009-0206-6.

BEZNIS, Nadzeya V.; WECKHUYSEN, Bert M.; BITTER, Johannes H. Cu-ZSM-5 zeolites for the formation of methanol from methane and oxygen: Probing the active sites and spectator species. **Catalysis Letters**, *[S. l.]*, v. 138, n. 1–2, p. 14–22, 2010. b. DOI: 10.1007/s10562-010-0380-6.

BOOMER, E. H.; NALDRETT, S. N. Oxidation of methane at high pressures IV. **Canadian Journal of Research**, *[S. l.]*, v. 25, p. 494–501, 1947.

BOOMER, E. H.; THOMAS, V. Oxidation of methane at high pressures III. **Canadian Journal of Research**, *[S. l.]*, v. 15, p. 401–413, 1937.

BOZBAG, Selmi E.; ALAYON, Evalyn Mae C.; PECHÁČEK, Jan; NACHTEGAAL, Maarten; RANOCCHIARI, Marco; VAN BOKHOVEN, Jeroen A. Methane to methanol over copper mordenite: Yield improvement through multiple cycles and different synthesis techniques. **Catalysis Science and Technology**, *[S. l.]*, v. 6, n. 13, p. 5011–5022, 2016. DOI:

10.1039/c6cy00041j.

BREZICKI, Gordon; KAMMERT, James D.; GUNNOE, T. Brent; PAOLUCCI, Christopher; DAVIS, Robert J. Insights into the Speciation of Cu in the Cu-H-Mordenite Catalyst for the Oxidation of Methane to Methanol. **ACS Catalysis**, *[S. l.]*, v. 9, n. 6, p. 5308–5319, 2019. DOI: 10.1021/acscatal.9b00852.

CHAN, Sunney I. et al. Efficient oxidation of methane to methanol by dioxygen mediated by tricopper clusters. **Angewandte Chemie - International Edition**, *[S. l.]*, v. 52, n. 13, p. 3731–3735, 2013. DOI: 10.1002/anie.201209846.

CHAUVIN, B.; MASSIANI, P.; DUTARTRE, R.; FIGUERAS, F.; FAJULA, F.; DES COURIERES, T. Factors affecting the steam dealumination of zeolite omega. **Zeolites**, *[S. l.]*, v. 10, n. 3, p. 174–182, 1990. DOI: 10.1016/0144-2449(90)90042-P.

CHEN, Jixin; CHEN, Tiehong; GUAN, Naijia; WANG, Jingzhong. Dealumination process of zeolite omega monitored by27Al 3QMAS NMR spectroscopy. **Catalysis Today**, *[S. l.]*, v. 93–95, p. 627–630, 2004. DOI: 10.1016/j.cattod.2004.06.019.

CULLIS, C. F.; KEENE, D. E.; TRIMM, D. L. Studies of the partial oxidation of methane over heterogeneous catalysts. **Journal of Catalysis**, *[S. l.]*, v. 19, n. 3, p. 378–385, 1970. DOI: 10.1016/0021-9517(70)90262-9.

DA SILVA, Marcio Jose. Synthesis of methanol from methane: Challenges and advances on the multi-step (syngas) and one-step routes (DMTM). **Fuel Processing Technology**, *[S. l.]*, v. 145, p. 42–61, 2016. DOI: 10.1016/j.fuproc.2016.01.023. Disponível em: http://dx.doi.org/10.1016/j.fuproc.2016.01.023.

DYBALLA, Michael; PAPPAS, Dimitrios K.; KVANDE, Karoline; BORFECCHIA, Elisa; ARSTAD, Bjørnar; BEATO, Pablo; OLSBYE, Unni; SVELLE, Stian. On How Copper Mordenite Properties Govern the Framework Stability and Activity in the Methane-to-Methanol

Conversion. **ACS Catalysis**, *[S. l.]*, v. 9, n. 1, p. 365–375, 2019. DOI: 10.1021/acscatal.8b04437.

ELVIDGE, Christopher D.; BAZILIAN, Morgan D.; ZHIZHIN, Mikhail; GHOSH, Tilottama; BAUGH, Kimberly; HSU, Feng Chi. The potential role of natural gas flaring in meeting greenhouse gas mitigation targets. **Energy Strategy Reviews**, *[S. l.]*, v. 20, p. 156–162, 2018. DOI: 10.1016/j.esr.2017.12.012. Disponível em: https://doi.org/10.1016/j.esr.2017.12.012.

GIORDANINO, Filippo; VENNESTRØM, Peter N. R.; LUNDEGAARD, Lars F.; STAPPEN, Frederick N.; MOSSIN, Susanne; BEATO, Pablo; BORDIGA, Silvia; LAMBERTI, Carlo. Characterization of Cu-exchanged SSZ-13: A comparative FTIR, UV-Vis, and EPR study with Cu-ZSM-5 and Cu-β with similar Si/Al and Cu/Al ratios. **Dalton Transactions**, *[S. l.]*, v. 42, n. 35, p. 12741–12761, 2013. DOI: 10.1039/c3dt50732g.

GOOSSENS, Ann M.; FEIJEN, Eddy J. P.; VERHOEVEN, Guy; WOUTERS, Bart H.; GROBET, Piet J.; JACOBS, Pierre A.; MARTENS, Johan A. Crystallization of MAZ-type zeolites using tetramethylammonium, sodium and n-hexane derivatives as structure- and composition-directing agents. **Microporous and Mesoporous Materials**, *[S. l.]*, v. 35–36, p. 555–572, 2000. DOI: 10.1016/S1387-1811(99)00250-4.

GROOTHAERT, Marijke H.; SMEETS, Pieter J.; SELS, Bert F.; JACOBS, Pierre A.; SCHOONHEYDT, Robert A. Selective Oxidation of Methane by the Bis (u-oxo) dicopper Core Stabilized on ZSM-5 and Mordenite Zeolites. **J. Am. Chem. Soc.**, *[S. l.]*, v. 127, p. 1394–1395, 2005. a. DOI: 10.1021/ja047158u.

GROOTHAERT, Marijke H.; SMEETS, Pieter J.; SELS, Bert F.; JACOBS, Pierre A.; SCHOONHEYDT, Robert A. Selective oxidation of methane by the bis(μ-oxo)dicopper core stabilized on ZSM-5 and mordenite zeolites. **Journal of the American Chemical Society**, *[S. l.]*, v. 127, n. 5, p. 1394–1395, 2005. b. DOI: 10.1021/ja047158u.

GRUNDNER, S.; LUO, W.; SANCHEZ-SANCHEZ, M.; LERCHER, J. A. Synthesis of single-site copper catalysts for methane partial oxidation. **Chemical Communications**, *[S. l.]*, v. 52, n. 12, p. 2553–2556, 2016. DOI: 10.1039/c5cc08371k.

GRUNDNER, Sebastian; MARKOVITS, Monica A. C.; LI, Guanna; TROMP, Moniek; PIDKO, Evgeny A.; HENSEN, Emiel J. M.; JENTYS, Andreas; SANCHEZ-SANCHEZ, Maricruz; LERCHER, Johannes A. Single-site trinuclear copper oxygen clusters in mordenite for selective conversion of methane to methanol. **Nature Communications**, *[S. l.]*, v. 6, n. May, p. 1–9, 2015. DOI: 10.1038/ncomms8546. Disponível em: http://dx.doi.org/10.1038/ncomms8546.

H. J. F. STROUD. **England Patent**, Number 1398395, 1975.

HADJIIVANOV, Konstantin I.; VAYSSILOV, Georgi N. Characterization of oxide surfaces and zeolites by carbon monoxide as an IR probe molecule. *In*: **Advances in Catalysis**. Cambridge, USA: Academic Press, 2002. v. 47p. 307–511. DOI: 10.1016/S0360-0564(02)47008-3.

HALFEN, Jason A.; MAHAPATRA, Samiran; WILKINSON, Elizabeth C.; KADERLI, Susan; YOUNG, Victor G.; QUE, Lawrence; ZUBERBUHLER, A. D.; TOLMAN, William B. Reversible Cleavage and Formation of the Dioxygen O-O Bond Within a Dicopper Complex. **Science**, *[S. l.]*, v. 271, n. 5254, p. 1397–1400, 1996. DOI: 10.1126/science.271.5254.1397. Disponível em: https://www.sciencemag.org/lookup/doi/10.1126/science.271.5254.1397.

HAMMOND, Ceri et al. Direct catalytic conversion of methane to methanol in an aqueous medium by using copper-promoted Fe-ZSM-5. **Angewandte Chemie - International Edition**, *[S. l.]*, v. 51, n. 21, p. 5129–5133, 2012. a. DOI: 10.1002/anie.201108706.

HAMMOND, Ceri et al. Direct catalytic conversion of methane to methanol in an aqueous medium by using copper-promoted Fe-ZSM-5. **Angewandte Chemie - International Edition**, *[S. l.]*, v. 51, n. 21, p. 5129–5133, 2012. b. DOI: 10.1002/anie.201108706.

HAMMOND, Ceri; CONRAD, Sabrina; HERMANS, Ive. Oxidative methane upgrading.

ChemSusChem, *[S. l.]*, v. 5, n. 9, p. 1668–1686, 2012. DOI: 10.1002/cssc.201200299.

HAN BAOZHAI, YANG, YANG, XU, YANYAN, U. J. ETIM, QIAO, KE, XU, BENJING, YAN, Zifeng. A review of the direct oxidation of methane to methanol. **Chinese Journal of Catalysis**, *[S. l.]*, v. 37, n. 8, p. 1206–1215, 2016. DOI: 10.1016/S1872-2067(15)61097-X.

HAN, Baozhai; YANG, Yang; XU, Yanyan; ETIM, U. J.; QIAO, Ke; XU, Benjing; YAN, Zifeng. A review of the direct oxidation of methane to methanol. **Chinese Journal of Catalysis**, *[S. l.]*, v. 37, n. 8, p. 1206–1215, 2016. DOI: 10.1016/S1872-2067(15)61097-X. Disponível em: http://dx.doi.org/10.1016/S1872-2067(15)61097-X.

HOLMEN, Anders. Direct conversion of methane to fuels and chemicals. **Catalysis Today**, *[S. l.]*, v. 142, n. 1–2, p. 2–8, 2009. DOI: 10.1016/j.cattod.2009.01.004.

HUERTAS-MIRANDA, J. A.; MARTINEZ-IÑESTA, M. Monte Carlo Studies of the Effect of Temperature, Si/Al, and Metal Loading on the Templated Synthesis of Pt Nanowires in MOR-type Zeolites. **Nano Science and Technology Institute**, *[S. l.]*, v. 2, n. March, p. 633–636, 2010. Disponível em: https://www.researchgate.net/publication/267787485.

IPEK, B.; LOBO, R. F. Catalytic conversion of methane to methanol on Cu-SSZ-13 using N_2O as oxidant. **Chem. Commun.**, *[S. l.]*, v. 52, n. 91, p. 13401–13404, 2016. DOI: 10.1039/C6CC07893A.

IPEK, Bahar; WULFERS, Matthew J.; KIM, Hacksung; GÖLTL, Florian; HERMANS, Ive; SMITH, Joseph P.; BOOKSH, Karl S.; BROWN, Craig M.; LOBO, Raul F. Formation of $[Cu_2O_2]^{2+}$ and $[Cu_2O]^{2+}$ toward C–H Bond Activation in Cu-SSZ-13 and Cu-SSZ-39. **ACS Catalysis**, *[S. l.]*, v. 7, n. 7, p. 4291–4303, 2017. DOI: 10.1021/acscatal.6b03005. Disponível em: http://pubs.acs.org/doi/10.1021/acscatal.6b03005.

ITO, Hidehiro; MORI, Fumiya; TABATA, Kenji; OKURA, Ichiro; KAMACHI, Toshiaki. Methane hydroxylation using light energy by the combination of thylakoid and methane monooxygenase.

RSC Advances, *[S. l.]*, v. 4, n. 17, p. 8645–8648, 2014. DOI: 10.1039/c3ra46870d.

KALAMARAS, Christos; PALOMAS, David; BOS, Rene; HORTON, Andrew; CRIMMIN, Mark; HELLGARDT, Klaus. Selective Oxidation of Methane to Methanol over Cu- And Fe-Exchanged Zeolites: The Effect of Si/Al Molar Ratio. **Catalysis Letters**, *[S. l.]*, v. 146, n. 2, p. 483–492, 2016. DOI: 10.1007/s10562-015-1664-7.

KAU, Lung Shan; SPIRA-SOLOMON, Darlene J.; PENNER-HAHN, James E.; HODGSON, Keith O.; SOLOMON, Edward I. X-ray absorption edge determination of the oxidation state and coordination number of copper. Application to the type 3 site in Rhus vernicifera laccase and its reaction with oxygen. **Journal of the American Chemical Society**, *[S. l.]*, v. 109, n. 21, p. 6433–6442, 1987. DOI: 10.1021/ja00255a032. Disponível em: https://pubs.acs.org/doi/abs/10.1021/ja00255a032.

KIM, Younhwa; KIM, Tae Yong; LEE, Hyunjoo; YI, Jongheop. Distinct activation of Cu-MOR for direct oxidation of methane to methanol. **Chemical Communications**, *[S. l.]*, v. 53, n. 29, p. 4116–4119, 2017. DOI: 10.1039/c7cc00467b. Disponível em: http://dx.doi.org/10.1039/c7cc00467b.

KLINOWSKI, Jacek. Solid-State NMR Studies of Molecular Sieve Catalysts. **Chemical Reviews**, *[S. l.]*, v. 91, n. 7, p. 1459–1479, 1991. DOI: 10.1021/cr00007a010.

KNORPP, Amy J.; NEWTON, Mark A.; MIZUNO, Stefanie C. M.; MEBRATE, Hiwote; PINAR, B.; BOKHOVEN, Jeroen A. Van. ChemComm Comparative performance of Cu-zeolites in the isothermal conversion of methane to methanol †. *[S. l.]*, 2019. a. DOI: 10.1039/c9cc05659a.

KNORPP, Amy J.; NEWTON, Mark A.; PINAR, Ana B.; VAN BOKHOVEN, Jeroen A. Conversion of methane to methanol on copper mordenite: redox mechanism of isothermal and high temperature activation procedures. **Industrial & Engineering Chemistry Research**, *[S. l.]*, v. 57, n. 54, p. 12036−12039, 2018. a. DOI: 10.1021/acs.iecr.8b01183. Disponível em:

http://pubs.acs.org/doi/10.1021/acs.iecr.8b01183.

KNORPP, Amy J.; NEWTON, Mark A.; SUSHKEVICH, Vitaly L.; ZIMMERMANN, Patrik P.; PINAR, Ana B.; VAN BOKHOVEN, Jeroen A. The influence of zeolite morphology on the conversion of methane to methanol on copper-exchanged omega zeolite (MAZ). **Catalysis Science & Technology**, *[S. l.]*, v. 9, p. 2806–2811, 2019. b. DOI: 10.1039/c9cy00013e.

KNORPP, Amy Jenelle; PINAR, Ana Belen; NEWTON, Mark; SUSHKEVICH, Vitaly; VAN BOKHOVEN, Jeroen A. Copper-exchanged omega (MAZ) zeolite: copper-concentration dependent active sites and its unprecedented methane to methanol conversion. **ChemCatChem**, *[S. l.]*, v. 5232, p. 5593–5596, 2018. b. DOI: 10.1002/cctc.201801809. Disponível em: http://doi.wiley.com/10.1002/cctc.201801809.

KORHONEN, Satu T.; FICKEL, Dustin W.; LOBO, Raul F.; WECKHUYSEN, Bert M.; BEALE, Andrew M. Isolated Cu2+ ions: Active sites for selective catalytic reduction of NO. **Chemical Communications**, *[S. l.]*, v. 47, n. 2, p. 800–802, 2011. DOI: 10.1039/c0cc04218h.

KULKARNI, Ambarish R.; ZHAO, Zhi Jian; SIAHROSTAMI, Samira; NØRSKOV, Jens K.; STUDT, Felix. Monocopper Active Site for Partial Methane Oxidation in Cu-Exchanged 8MR Zeolites. **ACS Catalysis**, *[S. l.]*, v. 6, n. 10, p. 6531–6536, 2016. a. DOI: 10.1021/acscatal.6b01895.

KULKARNI, Ambarish R.; ZHAO, Zhi Jian; SIAHROSTAMI, Samira; NØRSKOV, Jens K.; STUDT, Felix. Monocopper Active Site for Partial Methane Oxidation in Cu-Exchanged 8MR Zeolites. **ACS Catalysis**, *[S. l.]*, v. 6, n. 10, p. 6531–6536, 2016. b. DOI: 10.1021/acscatal.6b01895.

KULKARNI, Ambarish R.; ZHAO, Zhijian; SIAHROSTAMI, Samira; NØRSKOV, Jens Kehlet; STUDT, Felix. Cation-Exchanged Zeolites for the Selective Oxidation of Methane to Methanol. **Catal. Sci. Technol.**, *[S. l.]*, v. 8, p. 114–123, 2017. DOI: 10.1039/C7CY01229B. Disponível

em: http://pubs.rsc.org/en/Content/ArticleLanding/2017/CY/C7CY01229B.

LANCE, D.; ELWORTHY, E. G. **French Patent**, Number 352687, 1905.

LANGE, Jean Paul; SUSHKEVICH, Vitaly L.; KNORPP, Amy J.; VAN BOKHOVEN, Jeroen A. Methane-to-Methanol via Chemical Looping: Economic Potential and Guidance for Future Research. **Industrial and Engineering Chemistry Research**, *[S. l.]*, v. 58, p. 8674–8680, 2019. DOI: 10.1021/acs.iecr.9b01407.

LE, Ha V.; PARISHAN, Samira; SAGALTCHIK, Anton; GÖBEL, Caren; SCHLESIGER, Christopher; MALZER, Wolfgang; TRUNSCHKE, Annette; SCHOMÄCKER, Reinhard; THOMAS, Arne. Solid-State Ion-Exchanged Cu/Mordenite Catalysts for the Direct Conversion of Methane to Methanol. **ACS Catalysis**, *[S. l.]*, v. 7, n. 2, p. 1403–1412, 2017. DOI: 10.1021/acscatal.6b02372.

LI, Guanna; VASSILEV, Peter; SANCHEZ-SANCHEZ, Maricruz; LERCHER, Johannes A.; HENSEN, Emiel J. M.; PIDKO, Evgeny A. Stability and reactivity of copper oxo-clusters in ZSM-5 zeolite for selective methane oxidation to methanol. **Journal of Catalysis**, *[S. l.]*, v. 338, p. 305–312, 2016. DOI: 10.1016/j.jcat.2016.03.014.

LI, Hui et al. Consequences of exchange-site heterogeneity and dynamics on the UV-visible spectrum of Cu-exchanged SSZ-13. **Chemical Science**, *[S. l.]*, v. 10, n. 8, p. 2373–2384, 2019. DOI: 10.1039/C8SC05056B. Disponível em: http://xlink.rsc.org/?DOI=C8SC05056B.

LIEBERMAN, R. L.; ROSENZWEIG, A. C. Crystal structure of a membrane-bound metalloenzyme that catalyses the biological oxidation of methane. **Nature**, *[S. l.]*, v. 434, n. 7030, p. 177–182, 2005. DOI: 10.1038/nature03311.

LIU, H. F. ; LIU, R. S. ; JOHNSON, R. E. ; LUNSFORD, J. H. Partial Oxidation of Methane by Nitrous Oxide over Molybdenum on Silica. **Journal of American Chemical Society**, *[S. l.]*, v. 106, p. 4117–4121, 1984. DOI: 10.1021/ef00021a012.

LUNSFORD, Jack H. Catalytic conversion of methane to more useful chemicals and fuels: A challenge for the 21st century. **Catalysis Today**, *[S. l.]*, v. 63, n. 2–4, p. 165–174, 2000. DOI: 10.1016/S0920-5861(00)00456-9.

MAHYUDDIN, M. Haris; STAYKOV, Aleksandar; SHIOTA, Yoshihito; MIYANISHI, Mayuko; YOSHIZAWA, Kazunari. Roles of Zeolite Confinement and Cu–O–Cu Angle on the Direct Conversion of Methane to Methanol by $[Cu_2(\mu\text{-}O)]^{2+}$ -Exchanged AEI, CHA, AFX, and MFI Zeolites. **ACS Catalysis**, *[S. l.]*, v. 2, p. 3741–3751, 2017. DOI: 10.1021/acscatal.7b00588.

MAHYUDDIN, M. Haris; TANAKA, Takahiro; SHIOTA, Yoshihito; STAYKOV, Aleksandar; YOSHIZAWA, Kazunari. Methane Partial Oxidation over $[Cu_2(\mu\text{-}O)]^{2+}$ and $[Cu_3(\mu\text{-}O)_3]^{2+}$ Active Species in Large-Pore Zeolites. **ACS Catalysis**, *[S. l.]*, v. 8, n. 2, p. 1500–1509, 2018. DOI: 10.1021/acscatal.7b03389. Disponível em: http://pubs.acs.org/doi/10.1021/acscatal.7b03389.

MARKOVITS, Monica A. C.; JENTYS, Andreas; TROMP, Moniek; SANCHEZ-SANCHEZ, Maricruz; LERCHER, Johannes A. Effect of Location and Distribution of Al Sites in ZSM-5 on the Formation of Cu-Oxo Clusters Active for Direct Conversion of Methane to Methanol. **Topics in Catalysis**, *[S. l.]*, v. 59, n. 17–18, p. 1554–1563, 2016. DOI: 10.1007/s11244-016-0676-x.

MARTUCCI, Annalisa; ALBERTI, Alberto; DE LOURDES GUZMAN-CASTILLO, Maria; DI RENZO, Francesco; FAJULA, François. Crystal structure of zeolite omega, the synthetic counterpart of the natural zeolite mazzite. **Microporous and Mesoporous Materials**, *[S. l.]*, v. 63, n. 1–3, p. 33–42, 2003. DOI: 10.1016/S1387-1811(03)00429-3.

MASSIANI, P.; CHAUVIN, B.; FAJULA, F. .. Figueras F. Activation of Zeolite Q I . Physicochemical Characterization. **Applied Catalysis**, *[S. l.]*, v. 42, p. 105–120, 1988.

MASSIANI, Pascale; FAJULA, Fraņois; DI RENZO, Francesco. Zoning of aluminium among different crystallographic sites in zeolite omega. **Journal of the Chemical Society, Chemical**

Communications, *[S. l.]*, n. 12, p. 814–815, 1988. DOI: 10.1039/C39880000814.

MEIER, W. M. The crystal structure of mordenite (ptilolite). **Zeitschrift für Kristallographie**, *[S. l.]*, v. 115, p. 439–450, 1961.

MERKX, Maarten; KOPP, Daniel A.; SAZINSKY, Matthew H.; BLAZYK, Jessica L.; MÜLLER, Jens; LIPPARD, Stephen J. Dioxygen Activation and Methane Hydroxylation by Soluble Methane Monooxygenase: A Tale of Two Irons and Three Proteins. **Angewandte Chemie International Edition**, *[S. l.]*, v. 40, n. 15, p. 2782–2807, 2001. DOI: 10.1002/1521-3773(20010803)40:15<2782::AID-ANIE2782>3.0.CO;2-P.

MEYET, Jordan; SEARLES, Keith; NEWTON, Mark A.; WÖRLE, Michael; VAN BAVEL, Alexander P.; HORTON, Andrew D.; VAN BOKHOVEN, Jeroen A.; COPÉRET, Christophe. Monomeric Copper(II) Sites Supported on Alumina Selectively Convert Methane to Methanol. **Angewandte Chemie - International Edition**, *[S. l.]*, v. 58, n. 29, p. 9841–9845, 2019. DOI: 10.1002/anie.201903802.

MILLAR, Graeme J.; CANNING, Arran; ROSE, Graham; WOOD, Barry; TREWARTHA, Lisa; MACKINNON, Ian D. R. Identification of copper species present in Cu-ZSM-5 catalysts for NOxreduction. **Journal of Catalysis**, *[S. l.]*, v. 183, n. 2, p. 169–181, 1999. DOI: 10.1006/jcat.1999.2391.

NARSIMHAN, Karthik. Catalytic oxidation of methane into methanol over copper-exchanged zeolites with oxygen at low temperature. **ACS Central Science**, *[S. l.]*, v. 2, n. 6, p. 424–429, 2016.

NARSIMHAN, Karthik; IYOKI, Kenta; DINH, Kimberly; ROMÁN-LESHKOV, Yuriy. Catalytic oxidation of methane into methanol over copper-exchanged zeolites with oxygen at low temperature. **ACS Central Science**, *[S. l.]*, v. 2, n. 6, p. 424–429, 2016. DOI: 10.1021/acscentsci.6b00139.

NEWTON, Mark A.; KNORPP, Amy J.; PINAR, Ana B.; SUSHKEVICH, Vitaly L.; PALAGIN, Dennis; VAN BOKHOVEN, Jeroen A. On the Mechanism Underlying the Direct Conversion of Methane to Methanol by Copper Hosted in Zeolites; Braiding Cu K-Edge XANES and Reactivity Studies. **Journal of the American Chemical Society**, *[S. l.]*, v. 140, n. 32, p. 10090–10093, 2018. DOI: 10.1021/jacs.8b05139.

NEWTON, Mark A.; KNORPP, Amy J.; SUSHKEVICH, Vitaly L.; PALAGIN, Dennis; VAN BOKHOVEN, Jeroen A. Active sites and mechanisms in the direct conversion of methane to methanol using Cu in zeolitic hosts: A critical examination. **Chemical Society Reviews**, *[S. l.]*, v. 49, n. 5, p. 1449–1486, 2020. DOI: 10.1039/c7cs00709d.

NGUYEN, Hiep Hoa T.; ELLIOTT, Sean J.; YIP, John Hon Kay; CHAN, Sunney I. The particulate methane monooxygenase from Methylococcus capsulatus (Bath) is a novel copper-containing three-subunit enzyme: Isolation and characterization. **Journal of Biological Chemistry**, *[S. l.]*, v. 273, n. 14, p. 7957–7968, 1998. DOI: 10.1074/jbc.273.14.7957.

OLIVOS-SUAREZ, Alma I.; SZÉCSÉNYI, Àgnes; HENSEN, Emiel J. M.; RUIZ-MARTINEZ, Javier; PIDKO, Evgeny A.; GASCON, Jorge. Strategies for the Direct Catalytic Valorization of Methane Using Heterogeneous Catalysis: Challenges and Opportunities. **ACS Catalysis**, *[S. l.]*, v. 6, n. 5, p. 2965–2981, 2016. DOI: 10.1021/acscatal.6b00428. Disponível em: http://pubs.acs.org/doi/10.1021/acscatal.6b00428.

OORD, Ramon; SCHMIDT, Joel E.; WECKHUYSEN, Bert M. Methane-to-methanol conversion over zeolite Cu-SSZ-13, and its comparison with the selective catalytic reduction of NO x with NH 3. **Catalysis Science & Technology**, *[S. l.]*, v. 8, n. 4, p. 1028–1038, 2018. DOI: 10.1039/C7CY02461D. Disponível em: http://xlink.rsc.org/?DOI=C7CY02461D.

PALAGIN, Dennis; KNORPP, Amy J.; PINAR, Ana B.; RANOCCHIARI, Marco; VAN BOKHOVEN, Jeroen A. Assessing the relative stability of copper oxide clusters as active sites of a CuMOR zeolite for methane to methanol conversion: Size matters? **Nanoscale**, *[S. l.]*, v.

9, n. 3, p. 1144–1153, 2017. DOI: 10.1039/c6nr07723d. Disponível em: http://dx.doi.org/10.1039/c6nr07723d.

PALAGIN, Dennis; SUSHKEVICH, Vitaly L.; VAN BOKHOVEN, Jeroen A. Water Molecules Facilitate Hydrogen Release in Anaerobic Oxidation of Methane to Methanol over Cu/Mordenite. **ACS Catalysis**, *[S. l.]*, v. 9, n. 11, p. 10365–10374, 2019. DOI: 10.1021/acscatal.9b02702.

PAPPAS, Dimitrios K. et al. Methane to Methanol: Structure-Activity Relationships for Cu-CHA. **Journal of the American Chemical Society**, *[S. l.]*, v. 139, n. 42, p. 14961–14975, 2017. DOI: 10.1021/jacs.7b06472.

PAPPAS, Dimitrios K. et al. The Nuclearity of the Active Site for Methane to Methanol Conversion in Cu-Mordenite: A Quantitative Assessment. **ACS Catalysis**, *[S. l.]*, v. 140, n. 45, p. 15270–15278, 2018. DOI: 10.1021/jacs.8b08071.

PARK, Min Bum; AHN, Sang Hyun; MANSOURI, Ali; RANOCCHIARI, Marco; VAN BOKHOVEN, Jeroen A. Comparative Study of Diverse Copper Zeolites for the Conversion of Methane into Methanol. **ChemCatChem**, *[S. l.]*, v. 9, n. 19, p. 3705–3713, 2017. DOI: 10.1002/cctc.201700768.

PERIANA, Roy A.; TAUBE, Douglas J.; EVITT, Eric R.; LOFFLER, Daniel G.; WENTRCEK, Paul R.; VOSS, George; MASUDA, Toshihiko. A Mercury-Catalyzed , High-Yield System for the Oxidation of Methane to Methanol. **Science**, *[S. l.]*, v. 259, n. January, p. 340–343, 1993. DOI: 10.1126/science.259.5093.340 ARTICLE.

PRALIAUD, H. Surface and bulk properties of Cu–ZSM-5 and Cu/Al2O3 solids during redox treatments. Correlation with the selective reduction of nitric oxide by hydrocarbons. **Applied Catalysis B: Environmental**, *[S. l.]*, v. 16, n. 4, p. 359–374, 1998. DOI: 10.1016/S0926-3373(97)00093-3. Disponível em:

https://linkinghub.elsevier.com/retrieve/pii/S0926337397000933.

RAHBARI, Zahra Vosoughi; KHOSRAVAN, Mehrji; KHARAT, Ali Nemati. Dealumination of mordenite zeolite and its catalytic performance evaluation in m-Xylene isomerization reaction. **Bulletin of the Chemical Society of Ethiopia**, *[S. l.]*, v. 31, n. 2, p. 281–289, 2017. DOI: 10.4314/bcse.v31i2.9.

RAVEL, B.; NEWVILLE, M. ATHENA, ARTEMIS, HEPHAESTUS: Data analysis for X-ray absorption spectroscopy using IFEFFIT. **Journal of Synchrotron Radiation**, *[S. l.]*, v. 12, n. 4, p. 537–541, 2005. DOI: 10.1107/S0909049505012719.

RAVI, Manoj; RANOCCHIARI, Marco; VAN BOKHOVEN, Jeroen A. The Direct Catalytic Oxidation of Methane to Methanol-A Critical Assessment. **Angewandte Chemie International Edition**, *[S. l.]*, v. 56, n. 52, p. 16464–16483, 2017. DOI: 10.1002/anie.201702550. Disponível em: http://doi.wiley.com/10.1002/anie.201702550.

RAVI, Manoj; SUSHKEVICH, Vitaly L.; KNORPP, Amy J.; NEWTON, Mark A.; PALAGIN, Dennis; PINAR, Ana B.; RANOCCHIARI, Marco; VAN BOKHOVEN, Jeroen A. Misconceptions and challenges in methane-to-methanol over transition-metal-exchanged zeolites. **Nature Catalysis**, *[S. l.]*, v. 2, n. 6, p. 485–494, 2019. DOI: 10.1038/s41929-019-0273-z. Disponível em: http://dx.doi.org/10.1038/s41929-019-0273-z.

REDDY, P. Venkata Laxma; KIM, Ki-Hyun; SONG, Hocheol. Emerging green chemical technologies for the conversion of CH4 to value added products. **Renewable and Sustainable Energy Reviews**, *[S. l.]*, v. 24, p. 578–585, 2013. DOI: 10.1016/j.rser.2013.03.035. Disponível em: http://dx.doi.org/10.1016/j.rser.2013.03.035.

SÁNCHEZ-LÓPEZ, Perla; ANTÚNEZ-GARCÍA, Joel; FUENTES-MOYADO, Sergio; GALVÁN, Donald H.; PETRANOVSKII, Vitalii; CHÁVEZ-RIVAS, Fernando. Analysis of theoretical and experimental X-ray diffraction patterns for distinct mordenite frameworks. **Journal of Materials**

Science, *[S. l.]*, v. 54, n. 10, p. 7745–7757, 2019. DOI: 10.1007/s10853-019-03407-w.

SHILOV, Alexander E.; SHUL, Georgiy B. Activation of C − H Bonds by Metal Complexes. **Chemical Reviews**, *[S. l.]*, v. 97, n. 94, p. 2879–2932, 1997. DOI: 10.1021/cr9411886.

SMEETS, Pieter J.; GROOTHAERT, Marijke H.; SCHOONHEYDT, Robert A. Cu based zeolites: A UV-vis study of the active site in the selective methane oxidation at low temperatures. **Catalysis Today**, *[S. l.]*, v. 110, n. 3–4, p. 303–309, 2005. DOI: 10.1016/j.cattod.2005.09.028.

SMEETS, Pieter J.; HADT, Ryan G.; WOERTINK, Julia S.; VANELDEREN, Pieter; SCHOONHEYDT, Robert A.; SELS, Bert F.; SOLOMON, Edward I. Oxygen precursor to the reactive intermediate in methanol synthesis by Cu-ZSM-5. **Journal of the American Chemical Society**, *[S. l.]*, v. 132, n. 42, p. 14736–14738, 2010. a. DOI: 10.1021/ja106283u.

SMEETS, Pieter J.; WOERTINK, Julia S.; SELS, Bert F.; SOLOMON, Edward I.; SCHOONHEYDT, Robert A. Transition-metal ions in zeolites: Coordination and activation of oxygen. **Inorganic Chemistry**, *[S. l.]*, v. 49, n. 8, p. 3573–3583, 2010. b. DOI: 10.1021/ic901814f.

SOLOMON, Edward I. et al. Copper active sites in biology. **Chemical Reviews**, *[S. l.]*, v. 114, n. 7, p. 3659–3853, 2014. DOI: 10.1021/cr400327t.

SPENCER, Nicholas D. Partial oxidation of methane to formaldehyde by means of molecular oxygen. **Journal of Catalysis**, *[S. l.]*, v. 109, n. 1, p. 187–197, 1988. DOI: 10.1016/0021-9517(88)90197-2.

SUSHKEVICH, Vitaly L.; PALAGIN, Dennis; RANOCCHIARI, Marco; VAN BOKHOVEN, Jeroen A. Selective anaerobic oxidation of methane enables direct synthesis of methanol. **Science (New York, N.Y.)**, *[S. l.]*, v. 356, n. 6337, p. 523–527, 2017. a. DOI: 10.1126/science.aam9035. Disponível em: http://www.ncbi.nlm.nih.gov/pubmed/28473586.

SUSHKEVICH, Vitaly L.; PALAGIN, Dennis; RANOCCHIARI, Marco; VAN BOKHOVEN, Jeroen A. Selective anaerobic oxidation of methane enables direct synthesis of methanol. **Science**, *[S. l.]*, v. 356, n. 6337, p. 523–527, 2017. b. DOI: 10.1126/science.aam9035. Disponível em: http://www.sciencemag.org/lookup/doi/10.1126/science.aam9035.

SUSHKEVICH, Vitaly L.; VAN BOKHOVEN, Jeroen A. Effect of Brønsted acid sites on the direct conversion of methane into methanol over copper-exchanged mordenite. **Catalysis Science and Technology**, *[S. l.]*, v. 8, n. 16, p. 4141–4150, 2018. DOI: 10.1039/c8cy01055b.

SUSHKEVICH, Vitaly L.; VAN BOKHOVEN, Jeroen A. Methane-to-Methanol: Activity Descriptors in Copper-Exchanged Zeolites for the Rational Design of Materials. **ACS Catalysis**, *[S. l.]*, v. 9, n. 7, p. 6293–6304, 2019. DOI: 10.1021/acscatal.9b01534.

SUSHKEVICH, Vitaly L.; VEREL, René; BOKHOVEN, Jeroen A. Pathways of Methane Transformation over Copper-Exchanged Mordenite as Revealed by In Situ NMR and IR Spectroscopy. **Angewandte Chemie**, *[S. l.]*, v. 132, n. 2, p. 920–928, 2020. DOI: 10.1002/ange.201912668.

TAIFAN, William; BALTRUSAITIS, Jonas. CH 4 conversion to value added products: Potential, limitations and extensions of a single step heterogeneous catalysis. **Applied Catalysis B: Environmental**, *[S. l.]*, v. 198, p. 525–547, 2016. DOI: 10.1016/j.apcatb.2016.05.081. Disponível em: http://linkinghub.elsevier.com/retrieve/pii/S0926337316304386.

TOMKINS, Patrick; MANSOURI, Ali; BOZBAG, Selmi E.; KRUMEICH, Frank; PARK, Min Bum; ALAYON, Evalyn Mae C.; RANOCCHIARI, Marco; VAN BOKHOVEN, Jeroen A. Isothermal Cyclic Conversion of Methane into Methanol over Copper-Exchanged Zeolite at Low Temperature. **Angewandte Chemie - International Edition**, *[S. l.]*, v. 55, n. 18, p. 5467–5471, 2016. a. DOI: 10.1002/anie.201511065.

TOMKINS, Patrick; MANSOURI, Ali; BOZBAG, Selmi E.; KRUMEICH, Frank; PARK, Min Bum;

ALAYON, Evalyn Mae C.; RANOCCHIARI, Marco; VANBOKHOVEN, Jeroen A. Isothermal Cyclic Conversion of Methane into Methanol over Copper- Exchanged Zeolite at Low Temperature. **Angewandte Chemie**, *[S. l.]*, v. 128, p. 5557–5561, 2016. b. DOI: 10.1002/anie.201511065.

VANELDEREN, Pieter; SNYDER, Benjamin E. R.; TSAI, Ming Li; HADT, Ryan G.; VANCAUWENBERGH, Julie; COUSSENS, Olivier; SCHOONHEYDT, Robert A.; SELS, Bert F.; SOLOMON, Edward I. Spectroscopic definition of the copper active sites in mordenite: Selective methane oxidation. **Journal of the American Chemical Society**, *[S. l.]*, v. 137, n. 19, p. 6383–6392, 2015. DOI: 10.1021/jacs.5b02817.

VANELDEREN, Pieter; VANCAUWENBERGH, Julie; TSAI, Ming Li; HADT, Ryan G.; SOLOMON, Edward I.; SCHOONHEYDT, Robert A.; SELS, Bert F. Spectroscopy and redox chemistry of copper in mordenite. **ChemPhysChem**, *[S. l.]*, v. 15, n. 1, p. 91–99, 2014. DOI: 10.1002/cphc.201300730.

VELU, S.; SUZUKI, K.; GOPINATH, Chinnakonda S.; YOSHIDA, H.; HATTORI, T. XPS, XANES and EXAFS investigations of CuO/ZnO/Al2O3/ZrO2 mixed oxide catalysts. **Physical Chemistry Chemical Physics**, *[S. l.]*, v. 4, n. 10, p. 1990–1999, 2002. DOI: 10.1039/b109766k.

VINCENT, Julian F. V; BOGATYREVA, Olga A.; BOGATYREV, Nikolaj R.; BOWYER, Adrian; PAHL, Anja-karina; INTERFACE, J. R. Soc. Biomimetics : its practice and theory Biomimetics : its practice and theory. **J. R. Soc. Interface**, *[S. l.]*, v. 3, n. 3, p. 471–482, 2006. DOI: 10.1098/rsif.2006.0127.

VOGIATZIS, Konstantinos D.; LI, Guanna; HENSEN, Emiel J. M.; GAGLIARDI, Laura; PIDKO, Evgeny A. The Electronic Structure of the [Cu $_3$ (μ-O) $_3$] $^{2+}$ Cluster in Mordenite Zeolite and Its Effects on the Methane to Methanol Oxidation. **The Journal of Physical Chemistry C**, *[S. l.]*, p. acs.jpcc.7b08714, 2017. DOI: 10.1021/acs.jpcc.7b08714. Disponível em: http://pubs.acs.org/doi/abs/10.1021/acs.jpcc.7b08714.

WANG, Bingwen; ALBARRACÍN-SUAZO, Sandra; PAGÁN-TORRES, Yomaira; NIKOLLA, Eranda. Advances in methane conversion processes. **Catalysis Today**, *[S. l.]*, v. 285, p. 147–158, 2017. DOI: 10.1016/j.cattod.2017.01.023. Disponível em: http://dx.doi.org/10.1016/j.cattod.2017.01.023.

WEEKS, J.; BOLTON, P. Thermochemical Properties of Ammonium Exchanged Type Omega Zeolite. **J. Chem. Soc., Faraday Trans. 1**, *[S. l.]*, v. 72, p. 575–582, 1976.

WIEZEVICH, Peter J.; FROLICH, Per K. Direct Oxidation of Saturated Hydrocarbons at High Pressures. **Industrial and Engineering Chemistry**, *[S. l.]*, v. 26, n. 3, p. 268–276, 1934. DOI: 10.1021/ie50291a010.

WOERTINK, J. S.; SMEETS, P. J.; GROOTHAERT, M. H.; VANCE, M. A.; SELS, B. F.; SCHOONHEYDT, R. A.; SOLOMON, E. I. A [Cu2O]2+ core in Cu-ZSM-5, the active site in the oxidation of methane to methanol. **Proceedings of the National Academy of Sciences**, *[S. l.]*, v. 106, n. 45, p. 18908–18913, 2009. DOI: 10.1073/pnas.0910461106.

WULFERS, M. J.; TEKETEL, S.; IPEK, B.; LOBO, R. F. Conversion of methane to methanol on copper-containing small-pore zeolites and zeotypes. **Chemical Communications**, *[S. l.]*, v. 51, n. 21, p. 4447–4450, 2015. a. DOI: 10.1039/c4cc09645b. Disponível em: http://dx.doi.org/10.1039/C4CC09645B.

WULFERS, Matthew J.; LOBO, Raul F.; IPEK, Bahar; TEKETEL, Shewangizaw. Conversion of Methane to Methanol on Copper-Containing Small-Pore Zeolites and Zeotypes. **Chem. Commun.**, *[S. l.]*, v. 51, n. 21, p. 4447–4450, 2015. b. DOI: 10.1039/C4CC09645B.

ZAKARIA, Z.; KAMARUDIN, S. K. Direct conversion technologies of methane to methanol: An overview. **Renewable and Sustainable Energy Reviews**, *[S. l.]*, v. 65, p. 250–261, 2016. a. DOI: 10.1016/j.rser.2016.05.082. Disponível em: http://dx.doi.org/10.1016/j.rser.2016.05.082.

ZAKARIA, Z.; KAMARUDIN, S. K. Direct conversion technologies of methane to methanol: An

overview. **Renewable and Sustainable Energy Reviews**, *[S. l.]*, v. 65, p. 250–261, 2016. b. DOI: 10.1016/j.rser.2016.05.082. Disponível em: http://dx.doi.org/10.1016/j.rser.2016.05.082.

ZHANG, Yiwei; YU, Jing Ye; YEH, Yu Hao; GORTE, Raymond J.; RANGARAJAN, Srinivas; MAVRIKAKIS, Manos. An Adsorption Study of CH4 on ZSM-5, MOR, and ZSM-12 Zeolites. **Journal of Physical Chemistry C**, *[S. l.]*, v. 119, n. 52, p. 28970–28978, 2015. DOI: 10.1021/acs.jpcc.5b09571.

APPENDIX A - CHAPTER 3 SUPPLEMENTARY INFORMATION

List of Figures

Synthesis of Na-Omega (MAZ) zeolite

The Omega zeolite was synthesized using a hydrothermal method with a molar composition of 10 SiO_2: 1 Al_2O_3: 3.2 Na_2O: 0.8 TMA_2O: 106 H_2O. Sodium aluminate and Ludox AS-30 was used as aluminum and silicon source, respectively. The directing agent was Tetramethylammonium hydroxide. The gel slurry was transferred to a Teflon autoclave and placed in a static oven at 100ºC for 13 days. The samples were then rinsed with ethanol and water and dried at 80ºC overnight. The dried powder was then calcined at 550º for 8 hours with a rate of 1°C/min.

NH_4- cation exchange

The omega sample was stirred in a 2M solution of ammonium nitrate for 24hr at room temperature (100 mL solution per gram of zeolite). The sample was filtered, rinsed with deionized water and dried overnight at 80ºC.

Cu- cation exchange

The zeolite (Na- and NH_4- form) was cation-exchanged with 0.025M or 0.0125M of aqueous copper nitrate solution (100 mL solution per gram of zeolite). Each sample was exchanged from one to three times. Between each exchange, a fresh solution was prepared, and the sample filtered.

Powder X-ray diffraction

The powder XRD patterns were collected in a Bruker D8 diffractometer using Cu-Kα radiation (λ = 1.5418 Å, 40 kV, 40 mA). Data were recorded from 5 to 60 2θ range with a step size of 0.02° and a counting time of 0.068s per step.

Scanning electron microscopy

SEM images of the calcined sample were obtained with a Zeiss Gemini 1530 instrument that was operated at 5 keV.

Elemental Analysis

Copper (Cu), aluminum (Al), and silicon (Si) content were determined using SpectraAA 220FS atomic absorption spectrometer. Approximately 10 mg of dried sample was digested in 2 ml of concentrated hydrofluoric acid and 3 ml of concentrated nitric acid overnight and then diluted to 50ml with deionized water. Copper, aluminum, and silicon calibration curves were prepared from standard solutions.

In situ XAS measurements

The XAS measurements at the Cu K-edge (8979 eV) was collected at *Laboratório Nacional de Luz Síncroton (LNLS)* in XAFS2 beamline in transmission geometry. Around 15 mg of sample was allocated on the tubular reactor and heated at 10 °C min^{-1} from room temperature until 450 °C under 35%O_2/He flow and calcination was performed at 450 °C for 1 h. The reactor was cooled down in 35%O_2/He to 50ºC and the reactor was purged under pure He flow an then the reactor was heated under 40%CH_4/He flow from 50ºC to 550ºC with 50ºC step (30 min in each temperature). XANES spectra were acquired during all procedures. The processing of XANES data was performed using the IFEFFIT software version 1.2.11d with the Horae (Athena and Artemis) package. (RAVEL; NEWVILLE, 2005)

In situ FT-IR spectroscopy measurements

FTIR spectroscopy was performed on a Thermo Nicolet iS50 spectrometer equipped with an MCT detector and *operando* cell (LCS, EnsiCaen) with KBr windows. Optical adsorption was measured from 400 to 4000 cm^{-1} with a resolution of 4 cm^{-1} and 128 total scans. Spectra of surface species were obtained by subtraction of the pre-treated Cu-omega spectrum before the reaction. For spectra treatment, the OMNIC 9.1 software was used. The gas outlet from the *operando* cell was connected to back pressure regulator (Bronkhorst, EL-press series) and on-line mass spectrometer (Balzers). All connection gas lines were kept at 200ºC. To conduct in situ methane oxidation reactions, the temperature was controlled using a Lumel RE92 controller. 20 mg of Cu-Omega sample was pressed in a self-supporting disc and loaded into the sample cell. The flow of gases, including helium (6.0, Messer), oxygen (4.8, Messer), and methane (4.8, Messer) were controlled with independent mass flow controllers (Bronkhorst Instruments LLC). Water (typically 3.2 kPa) was introduced into the gas stream using a saturator maintained at 25ºC.

Methane to methanol reaction testing

Zeolite samples were sieved to 150-250µm. Approximately 0.3 grams of samples were loaded into stainless steel autoclave (Premex Reactor Ag). Samples were activated at 450ºC under pure O_2 (~25mL/min) for 1 hour. The reactors were cooled down to the selected temperature (200ºC, 250ºC or 300ºC) and then purged for 15 minutes in pure helium flow. Pure methane was then introduced at 1 bar or 6 bar into the reactor and kept at the chosen temperature for 30 minutes. The reactor was then cooled down to room temperature under pure Helium flow.

Methanol Quantification

Methanol was extracted via the off-line method by adding 2mL of MilliQ water to the reacted sample and the resulting suspension was stirred for 30 minutes. The sample was then

filtered, and analysis was performed with a gas chromatograph (Agilent 6890GC equipped with an FID detector). Butanol was added as an external standard after filtration but prior to GC analysis. The procedure was repeated until no more methanol was observed by GC.

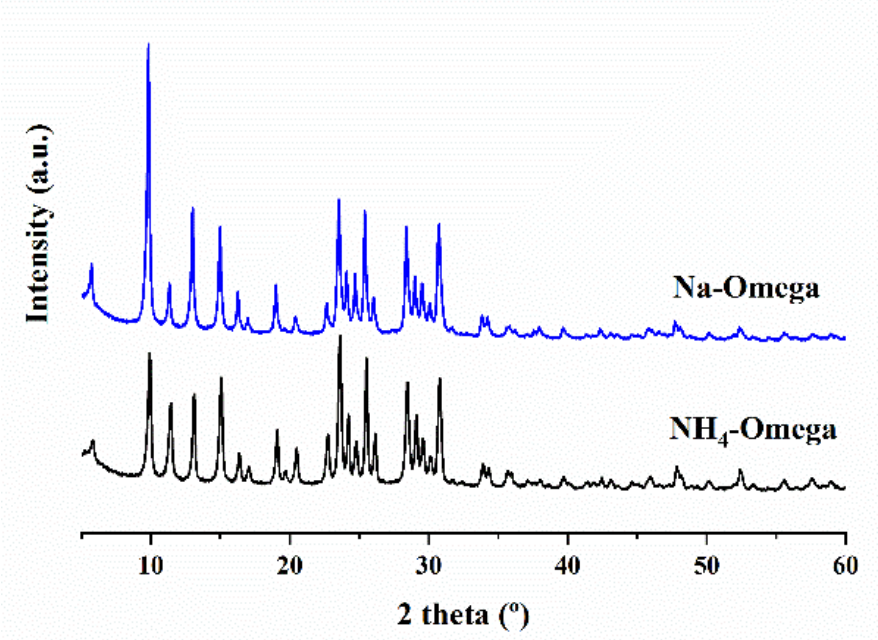

Figure S3.1 - XRD patterns of synthesized parent Omega (MAZ) zeolites.

Figure S3. 2 - SEM images of calcined Na-Omega (MAZ) samples.

Table S3.1. Cu/Al and Na/Al ratios of the samples before and after the reaction.

Sample	Cu/Al ratio				Na/Al ratio			
	Before reaction[a]	Reacted at 200ºC[b]	Reacted at 250ºC[b]	Reacted at 300ºC[b]	Before reaction[a]	Reacted at 200ºC[b]	Reacted at 250ºC[b]	Reacted at 300ºC[b]
Cu-Na-Omega	0.24	0.24	0.22	0.22	0.35	0.33	0.33	0.33
Cu-NH_4-Omega	0.24	0.24	0.24	0.23	0.00	0.00	0.00	0.00

[a] Measured by AAS; [b] Measured by EDS X-Ray microanalysis.

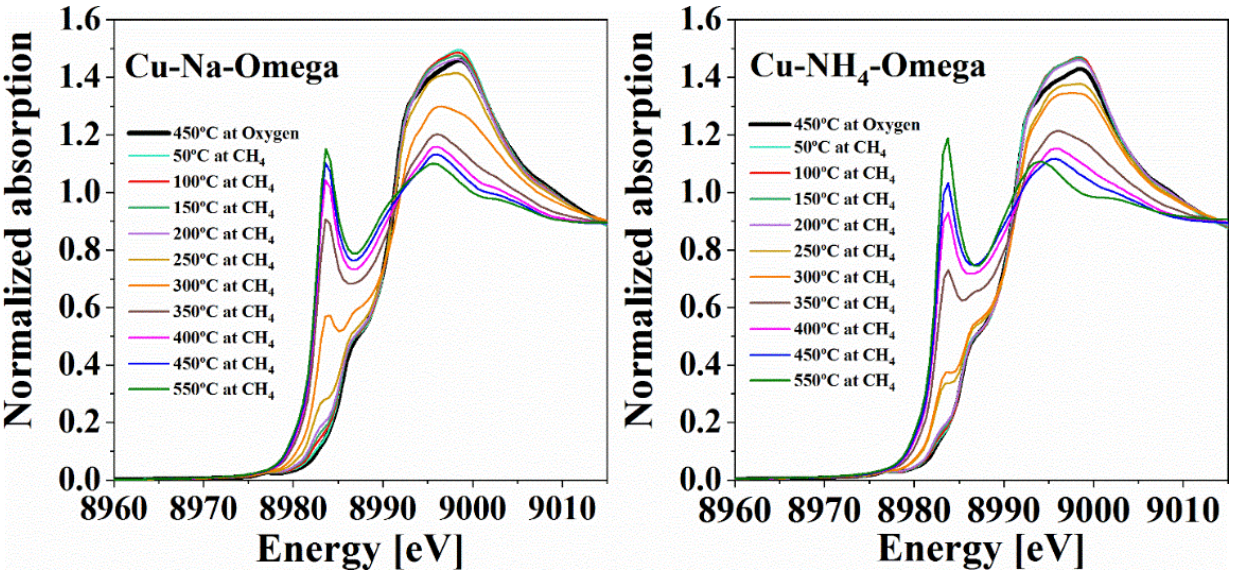

Figure S3.3. Cu K-edge XANES spectra of Cu–Na-Omega and Cu-NH_4-Omega at several temperatures under methane flow. The activated form is after treatment in oxygen at 450 ºC for 1 hour (black line).

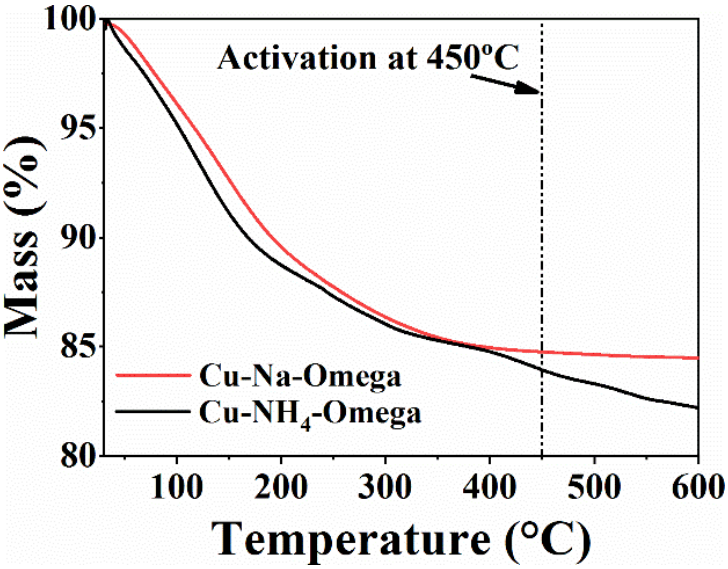

Figure S3.4. TGA data for the samples.